Extended Experimental and Numerical Study to Improve the Blanking Process in Terms of Wear Resistance of the Tool and Product Quality

Ph.D. THESIS

Mahmod Gomah

1303947009

GRADUATE SCHOOL OF AFRONAUTICS AND ASTRONAUTICS

Mechanical and Aeronautical Engineering (English) (Doctorate)

Thesis Supervisor: Assoc. Prof. Dr. Murat DEMIRAL

OF UNIVERSITY OF TURKISH AERONAUTICAL ASSOCIATION

INSTITUTE OF SCIENCE AND TECHNOLOGY

STATEMENT NON-PLAGIARISM

I hereby declare that all information in this study I present as my Ph.D. thesis, entitled: *Extended Experimental and Numerical Study to Improve the Blanking Process in Terms of Wear Resistance of the Tool and Product Quality,* has been presented in accordance with the academic rules and ethical conduct. I also declare and certify with my honor that I have fully cited and referenced all sources utilized in this study.

25 Dec 2018.

Mahmod Saleh Mahmod Gomah

Abstract

Extended Experimental and Numerical Study to Improve the Blanking Process in Terms of Wear Resistance of the Tool and Product Quality

Mahmod Gomah

Ph.D., Department of Mechanical and Aeronautical Engineering

Thesis Supervisor: Assoc. Prof. Dr. Murat DEMIRAL

The shearing processes including sheet metal blanking have been widely used in the industry to manufacture work pieces for industrial, commercial and experimental purposes. In order to understand the underlying physics of the blanking process, specifically the tool wear and the surface finish of the samples with blanked-edge features such as the amount of roll over, and the extent of the burnished zone and the fracture zone various tests were conducted using A36 steel alloy sheet. The experiments are performed for different blanking clearances (2% and 15%), punch tip geometries (flat, concave, shear, concave shear, and Y-shear faces) including the novel flat-face center-point punches with various corner radius values (0.001 mm, 0.01 mm, 0.1 mm, and 0.2 mm), temperatures (25˚C, 100˚C, 160˚C and 270˚C), PVD coating types TiN, TiSiN, AlCrN, CrN and AlTiN, contact conditions ($\mu = 0.1$ to 0.6), and specific tool type: polycrystalline diamond compact punch. Scanning Electron Microscopy (SEM) was used for microanalysis, conducted at the Institute of Materials Science and Nanotechnology (UNAM), Bilkent University.

Prediction of the product quality is important for investigating the blanking process, process development innovation, and optimization. Consequently, a validated numerical model of this process is expected to have great value; therefore, after the experimental study, a detailed finite element model has been developed. The Johnson-Cook material model and its complementary damage model was used to represent the behavior of the sheet material, where the material constants available in the literature were used. The simulations were performed using commercially available Abaqus/Explicit in a quasi-static manner. A reasonably good agreement between the tests and simulations has been obtained. It was found that the clearance between

punch and the die, geometry of the tool tip, corner radius of the punch, initial temperature of the sheet strongly affects the process a clearance of 2%, corner radius between 0.01 mm and 0.02 mm and an initial temperature of 400℃ for the samples, were considered as optimum process values. Experiments show that the novel flat-faced center-point punch was not a promising alternative to the blanking process. It was also observed that the tool with AlCrN coating and the PDC cutter show the best performance to minimize the wear on the tool surface.

Keywords: Blanking process, Wear resistance, Clearance, PVD coating.

ÖZET

Ayırma işleminin kesici takıma ait aşınma direnci ve üretilen numune kalitesi bakımından deneysel ve sayısal çalışma ile geliştirilmesi

Mahmod Gomah

Tez Danışmanı: Doç. Dr. Murat DEMIRAL

Saç metal kesme işlemleri ayırma da dahil olmak üzere sanayi, ticari ve deneysel amaçlar için yaygın olarak kullanılmaktadır. Ayırma işleminin altta yatan fiziğini anlamak için, özellikle kesici uçtaki aşınma ve numunelerin yüzey pürüzlülüğü ayrılan bölgeye ait yuvarlanma bölgesi, perdahlanmis bölge uzunluğu ve kırılma bölgesi 36A çelik alaşımlı levha kullanılarak çeşitli testler aracılığı ile incelenmiştir. Deneyler, farklı ayırma boşlukları (% 2 ve % 15), delgi uç geometrileri (düz, içbükey, kesme, içbükey kesme ve Y-kesme yüzleri) düz yüzlü orta nokta zımbası dahil olmak üzere, delgi köşe yarıçap değerleri (0.001mm, 0.01mm, 0.1mm, and 0.2mm), sıcaklık (25˚C, 100˚C, 160˚C ve 270˚C), PVD kaplama çeşitleri (TiN, TiSiN, AlCrN, CrN ve AlTiN), temas koşulları (μ = 0,1 - 0,6 arası) ve polikristalin elmaslı kompakt zımba kullanılarak yapılmıştır. Mikroanaliz çalışmaları Bilkent Üniversitesi Malzeme Bilimi ve Nanoteknoloji Enstitüsü'nde (UNAM) Taramalı Elektron Mikroskobu (SEM) kullanılarak yapılmıştır.

Ürün özelliklerinin tahmin edilmesi, ayırma sürecini, süreç geliştirmeyi, inovasyon ve optimizasyonu gerçekleştirmek için önemlidir. Sonuç olarak, bu sürecin onaylanmış bir sayısal modelinin büyük bir değere sahip olması beklenir. Dolayısıyla, deneysel çalışmalardan sonra, sayısal araştırma için ayrıntılı bir sonlu eleman modeli geliştirilmiştir. Johnson-Cook malzeme modeli ve tamamlayıcı hasar modeli ile literatürde mevcut olan malzeme sabitleri kullanılarak saç malzemenin davranışı modellenmistir. Simülasyonlar Abaqus / Explicit sonlu elemanlar programı kullanılarak yarı statik bir şekilde gerçekleştirilmiştir. Testler ve simülasyonlar arasında benzerlik elde edilmiştir. Zımba ve kalıp arasındaki boşluk, takım ucunun geometrisi, takım köşe yarıçapı ve tabakanın başlangıç sıcaklığının önemli

parametreler olduğu görülmüştür. %2 ayırma boşluğu, 0.01 mm ile 0.02 mm arası köşe yarıçapı ve 400° numune sıcaklığı optimum proses değerleri olarak görülmüştür. Deneylerde, düz yüzlü merkez noktalı kesici aletin ayırma işlemi için iyi bir alternatif olmadığı sonucuna varılmıştır. AlCrN kaplaması ve PDC kesici takımın takım yüzeyindeki aşınmayı en aza indirerek iyi performans gösterdikleri gözlemlenmiştir.

Anahtar Kelimeler: Ayırma prosesi; Aşınma direnci; Ayırma boşluğu; PVD kaplama; Sonlu elemanlar yöntemi

TABLE OF CONTENTS

LIST OF FIGURES

XI

LIST OF TABLES

ACKNOWLEDGMENTS

I cannot express enough thanks to all of those who continued support and encourage me to complete this thesis. I would like to express my sincere gratitude to my supervisor Assoc. Prof. Dr. Murat Demiral for his intellectual instructions, encouragement, suggestive ideas, constructive criticism and motivation. His patience and understanding I appreciate helped me sail through the hard times. I am very much grateful on this.

I would like to thank the Department of Mechanical Engineering, University of Turkish Aeronautical Association, for financing and sponsoring this research.

My sincere thanks goes to Prof. Dr. Ferhat Kadioglu from Yildirim Beyazit University for providing his lab facilities and the licenses for the FE software used in this thesis.

I would also like to thank the Lab Engineer Mr. Ugur for his patience on my long work and help me to finish it as required.

Finally, I would like to thank my parents, my family and my friends for their encouragement, patience and support during the whole of this research process

NOMENCLATURE

D_P	Punch diameter
D_d	Die diameter
R_P	Punch corner radius
R_d	Die corner radius
T_m	Melting temperature (°C)
T_{room}	Room temperature (°C)
T^*	Homologous temperature
HER	Hole Expansion Ratio
k	Thermal Conductivity
D_1	Fracture parameter (Johnson-Cook fracture equation)
D_2	Fracture parameter (Johnson-Cook fracture equation)
D_3	Fracture parameter (Johnson-Cook fracture equation)
D_4	Fracture parameter (Johnson-Cook fracture equation)
D_5	Fracture parameter (Johnson-Cook fracture equation)
$\Delta\varepsilon$	Increment of the equivalent plastic strain
ε	Equivalent plastic strain (Johnson-Cook constrictive model)
ε^f	Equivalent strain to fracture
ε_{fs}^{exp}	True fracture strain measured from a smooth specimen test
$\bar{\varepsilon}_n$	Void nucleation strain
$\dot{\varepsilon}^*$	Dimensionless plastic strain rate
$\bar{\varepsilon}_f$	Equivalent strain to fracture (Johnson-Cook fracture model)
$\dot{\varepsilon}_\delta$	Discrete value of the strain rate (s-1)

$\dot{\varepsilon}_{\delta}^{*}$	Discrete value of the dimensionless strain rate
η	Stress triaxiality
η_0	Stress triaxiality of the original specimen
η_f	Stress triaxiality of the specimen after fracture
θ	Lode angle
λ	Adjusted variable
ξ	Normalized third stress invariant (MPa)
σ	von Mises flow stress (Johnson-Cook constrictive model)
σ^*	Ratio of the average of the three normal stresses
FEA	Finite element analysis
FEM	Finite element method
2D	Two dimensional
3D	Three dimensional
c_p	Specific heat capacity
ξ	Critical damping
ω_D	State variable in ductile criterion
ω_S	State variable in shear criterion
τ_{max}	Maximum shear stress
σ_{y0}	Yield stress at the onset of damage
θ_S	Shear stress ratio
υ	Passion's ratio
τ	Shear stress
$\boldsymbol{u}$	Displacements
$\boldsymbol{d\varepsilon}$	Element strain increments
k_S	Material parameter
Ω^e	Domain of elements

σ	Stress
ρ	Density
η	Stress triaxiality
δ_f	Effective displacement at complete failure
δ_0	Relative to the effective displacement at damage initiation
δ	Displacement
t	Time increment
q	Von Mises equivalent stress
p	Pressure stress
P	Vector of externally applied force
A	Authentic exterior and outward area
A_D	Defects outward and exterior area
C_d	Current and effective dilatational wave speed of the material
D	Damage evolution variable
ε	Strain
E	Elastic modulus
F	Force
G	Shear modulus
I	Vector of internal element forces
K	Master stiffness matrix
K_e	Eccentricity parameter
L_e	Characteristic length of the element
M	Bulk mass matrix
M^{-1}	Lumping matrix
$\dot{u}^e$	Node degree of freedom velocities
$\dot{\bar{\varepsilon}}^{pl}$	Equivalent plastic strain rate
$\vec{V}^e$	Velocity field
$\bar{u}^{pl}$	Effective plastic displacement
$\bar{u}_f^{pl}$	Effective plastic displacement at failure
$\bar{\varepsilon}^{pl}$	Effective plastic strain

$\bar{\varepsilon}_D^{pl}$	Equivalent plastic strains are at the onset of damage
$\bar{\varepsilon}_S^{pl}$	Equivalent plastic strain in shear criterion
$\bar{\varepsilon}_f^{pl}$	Equivalent plastic strain at failure (when the D=1)
$\bar{\varepsilon}^{pl}$	Equivalent plastic strain in ductile criterion
$\bar{\varepsilon}_0^{pl}$	Equivalent plastic strain at the onset of damage
T_0	Original thickness of the cohesive element
C_d	Current and effective dilatational wave speed of the material
L_e	Dimension of characteristic element
M^e	Element mass matrix
N_v^e	Shape function matrix
T^e	Kinetic energy of elements
$\dot{d}$	Linear form of damage evolution with plastic displacement
$\ddot{u}$	Acceleration of the nodal
$\dot{u}$	Velocities
$\delta_n, \delta_s, \delta_t$	Represents the displacements at damage initiation
ε_f	Failure strain
$\varepsilon_n^0, \varepsilon_s^0, \varepsilon_t^0$	Represents the ultimate values of the nominal strains
ε_p	Plastic strain
σ_p	Plastic stress
σ_u	Ultimate stress
σ_y	Yield stress
τ_u	Ultimate shear stress
$\dot{\varepsilon}$	Strain rate
$\bar{\sigma}$	Effective or undamaged stress
ω_{max}	Maximum eigenvalues
$\omega_{max}^{element}$	Element maximum eigenvalues
Δt	Finite time increment

INTRODUCTION

1.1 Background

Some sheet metal formation processes including stamping, blanking, and bending are generally required for manufacturing metal sheets. These processes are normally combinations of several processes, which are used to make metal sheets or sheet parts. Piercing as well as blanking are shearing procedures, which shear the input sheet materials and convert them into the required shape. During the blanking process, removed material pieces are the desired outcome, and during piercing, removed materials are considered as scrap, and the residual strip part is the product, which is illustrated in Fig.1.1. The current study is significant because it interchangeably uses piercing and blanking processes because both the methods process the material through similar physical procedures. During blanking, a metal sheet severely deforms because the sheet metal shearing/separation results in slug formation.
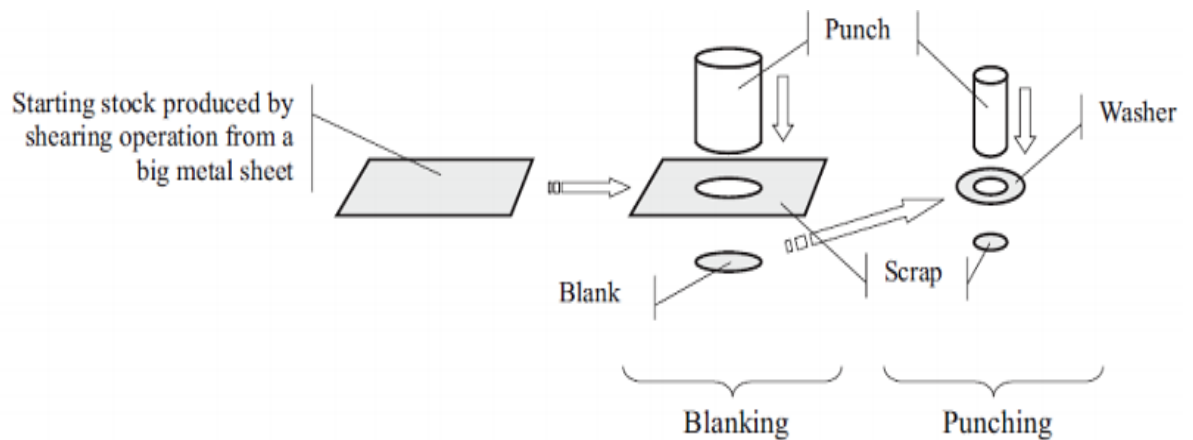
Figure 1.1: Differences between blanking and piercing

The next Fig.1.2 is the schematic diagram of blanking. When the blanking process is carried out, a stripper plate (blank holder) holds the metal sheet applying force denoted as F. The sheet material, which lies between the die and the punch

deforms to a great extent. In this case, the punch penetrates sheet material at a certain velocity denoted as V_P. The mentioned stripper plate removes the slug from the punch when the punch moves upwards.
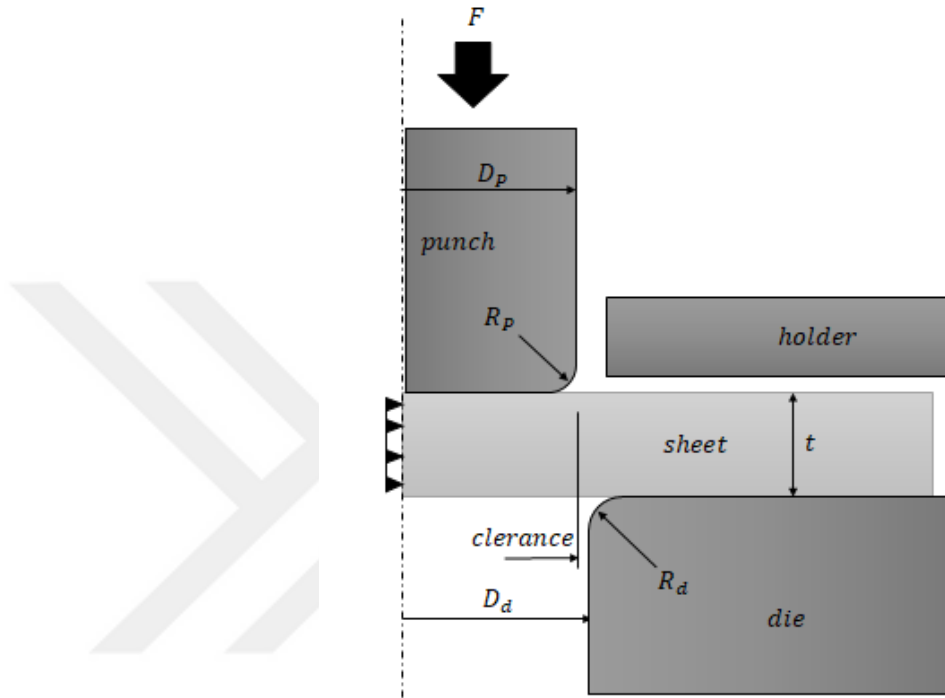
Figure 1.2: Schematic diagram of the blanking tool setup

1.1.1 Blanking Process

Blanking includes many phases, during which, sheet metal becomes deformed and separated, which is illustrated in Fig. 1.3.

Contact with the punch: First, the punch touches fixed sheet. On the point of impact, compressive stress immediately develops, which sends a shock wave.

Plastic and elastic deformation: When the punch penetrates a sheet, it initially causes elasticity and later, it results in plastic deformation.

Crack formation and shearing: The increase in stresses leads to shearing, which results in formation of a fracture. A fracture starts from a sheet's die end and the punch end. When both of them meet, a complete fracture occurs in a metal sheet.

Breakthrough: Whenever a sheet material is either thick or strong, the blanking process needs more force. When the fracture or sheer processes occur, at that time, the tool has compressive forces. A complete fracture means comprehensive forces' instantaneous release, which generates a shock that sometimes breaks the punch.

Stripping: When the punch moves towards the bottom, it rejects the slug/part. On the bottom dead center, the punch motion and direction reverses. Some friction takes place between the punch surface and the stock that lifts the sheet with the punch. A blank holder/stripper strips blank from a punch.
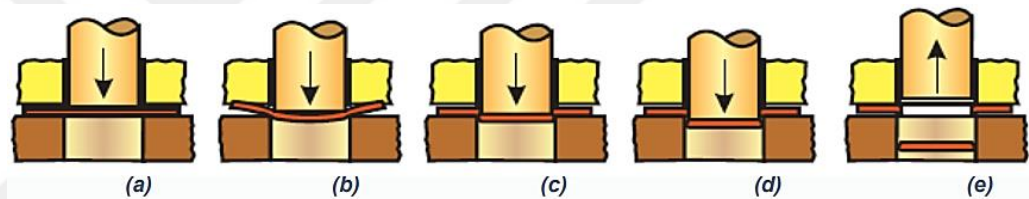
a) Contact between the punch and the sheet b) Slight bending at the early stages of deformation c) Plastic deformation and crack formation d) Breakthrough e) Stripping

Figure 1.3: Phases of the blanking process [Schuler Handbook, 1998]

1.1.2 Forces and stresses

It is a fact that the cutting force is not linearly applied along the cutting edge but horizontal and vertical forces F_H and F_V apply in a small area, which is located closer to the cutting edge. It is illustrated in Fig.1.4. These compressive forces are non-uniformly distributed. The distance between F_V and F_H is l, which means that the bending has to be compensated for through a counter-bending that is generated as a consequence of bending and normal horizontal stresses between the tool and the work piece. The figure depicts that the resulting frictional forces are $\mu . F_V$ and $\mu . F_H$, which increase the overall blanking force. For further investigation of the

blanking process, the changes in the blanking force should be monitored because during the cutting process, this force changes the punch entry time, displacement, or angle of the crack.
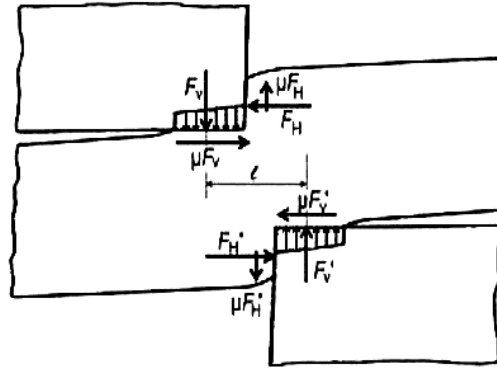
Figure 1.4: Stresses in blanking

1.1.3 Characteristics of the part edge

A blanked/sheared edge has many zones of material deformation. These deformation modes or zones are shown in Fig. 1.5.

• Rollover zone (Z_r): It forms as a consequence of plastic material deformation.

• Shear zone (Z_s): It consists of a shiny and smooth segment that forms because of shearing.

• Rupture/Fracture zone (Z_f): It is a rough area that forms after the formation of material cracks.

• Burr zone (Z_b): It forms after plastic deformation.

• Depth of crack penetration (D_{cp}): It is an angle formed in the fracture zone, and its degree depends on clearance.

• Secondary shear: This situation emerges when the cracks do not move and rupture the sheet in the direction of each other, so, secondary shear takes place.

5

The ratio between different zones is influenced by parameters such as punch-die clearance, punch corner radius and sheet material properties. A large shear zone and small rollover and burr are generally desirable in the blanked part for post-processes like assembly and flanging. Punch/Die Wear affect the quality of blanked edge as it has impact on the die corner radius and punch-die clearance. The punch and die wear are influenced by the blanking of the sheet material, coating, die/punch material, punch geometry and corner radius of the die/punch.
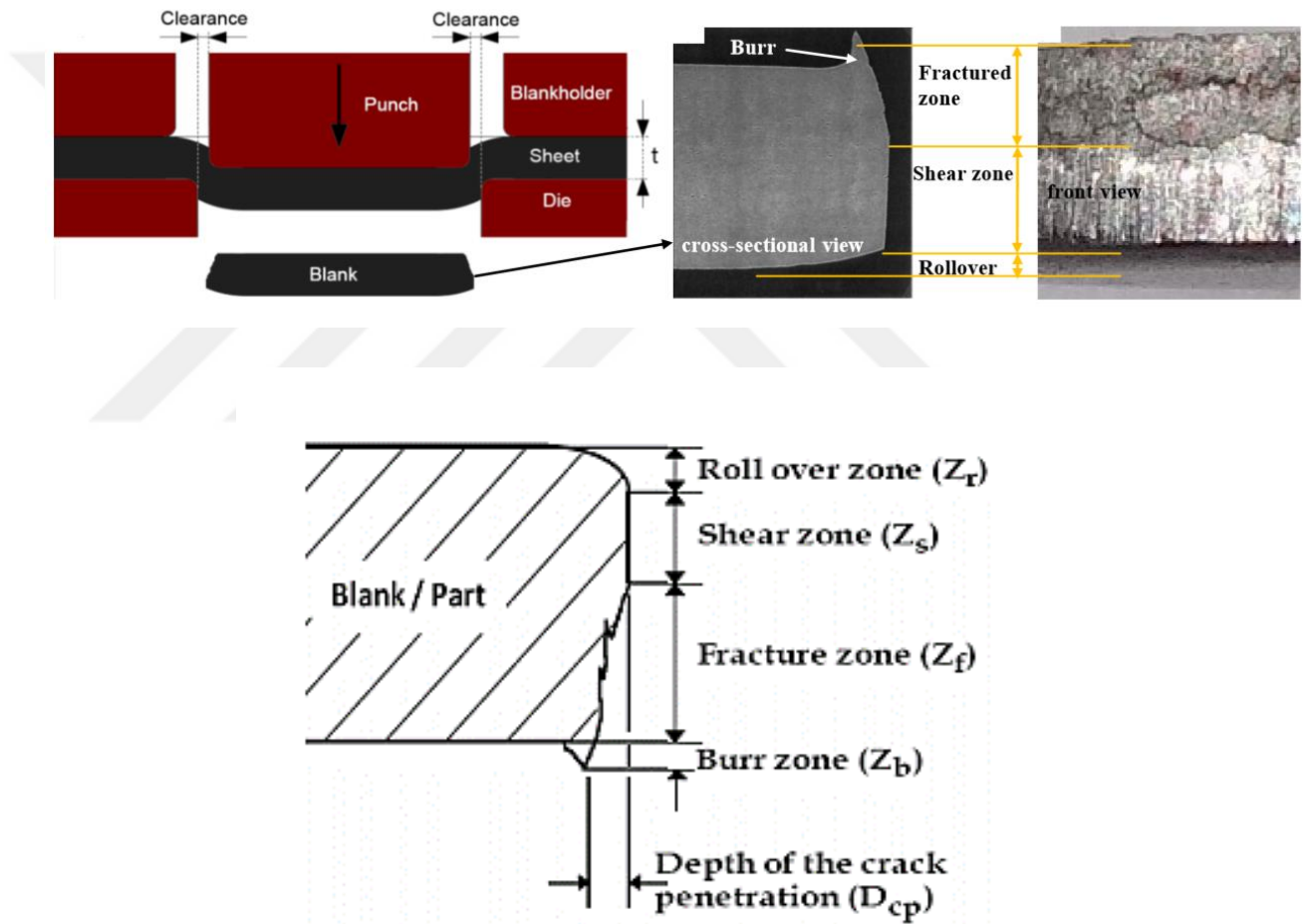
Figure 1.5: Different zones of blanked part edge

1.2 Aims and objectives

There are two fundamental objectives of this study:

1. Improve the punch/die life

2. Improve the blank edge quality of the parts

These objectives can be fulfilled by using two important approaches: (i) design approach (ii) material approach.

The materials used to manufacture die and punch are very significant because they have a definitive impact on the wear; therefore, the most feasible die and punch coating and material help minimizing the wear. Additionally, the researchers applied different process designs, which can help improving the life of the tool, the current study discusses design-focused tool wear minimization. Another aim is to develop a verified and accurate numerical model for predicting the properties of products, which undergo blanking process.

1.3 Methodology

This research presents systematic experimental and numerical analyses of the blanking process. The following methodologies have been implemented throughout the thesis.

- Performing several blanking experiments with different process parameters to identify the significant ones, which have a definitive impact on the die/punch life as well as the quality of the blanked edge. Also, various coatings for the tool tip and different cutters have been used to evaluate their performances.
- Developing the FE model of the blanking process with correct material model and data to accurately represent the experiments. After calibrating and validating the model, the underlying physics of the tool wear and surface finish have been investigated, which could not be performed during the experiments. This is followed by identifying the optimized process values.

This thesis has been organized as follows: Literature survey about the single-lap joint has been presented in Chapter 2. Description of the materials used in the experiments and relevant experimental studies have been given in Chapter 3. Chapter 4 describes the Finite Element Method (FEM) including the explicit time integration scheme and different damage models followed by the details of the developed numerical model. In Chapter 5, the validation of numerical model has been proved after comparing the results with the experimental data. Some critical results are also discussed in this chapter. The thesis ends with some concluding remarks, which are mentioned in Chapter 6.

LITERATURE REVIEW

2.1 Fundamentals of blanking – the impact of various process parameters on quality of blanked edge and punch life

2.1.1 The impact of punch-die clearance

In general, whenever clearance increases between die and punch, the roll over and fracture zones, burr and fracture angle increase, and the shear zone reduces. Insufficient clearance produces secondary shear i.e. the cracks originating at the punch and die do not meet; so, the material is further stressed to its shear limit that uses more energy. Excessive clearance causes large plastic deformation, large burr and high fracture angle. Furthermore, improper clearance reduces the tool life. Some research studies were conducted to study the impact of punch-die clearance on punch life and part edge quality. These studies are mentioned below. Husson et al. [2008] studied blanking simulations by applying them on a 0.58mm thick copper alloy. Later, they obtained the results for comparing them to the experimental outcomes. They studied the impact of punch-die clearance on part edge quality within the range 15µm (2.5%)-110µm (19%) during blanking holes of 3.5mm diameter. The FE simulations show that the shear edge and the rollover boost while fractured edge reduces when blanking clearance is increased. It is shown in Fig.2.1. The fracture angle significantly increases with increasing clearance.
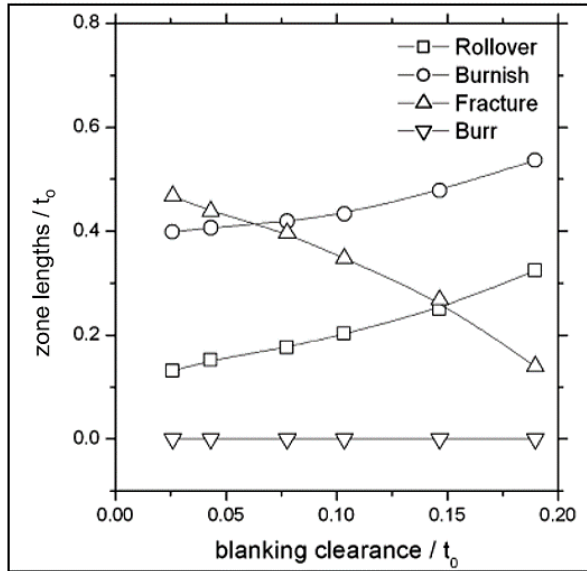
Figure 2.1: Effect of blanking clearance on part edge as predicted using finite element simulations on 0.58mm Cu alloy [Husson et al, 2008]
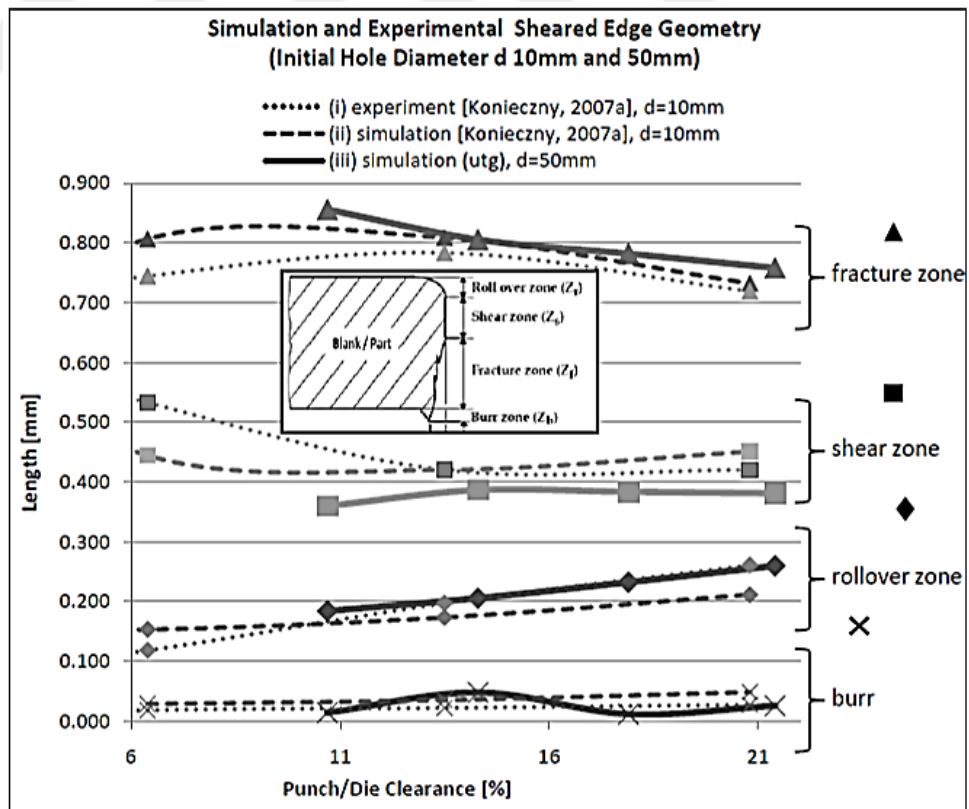
Figure 2.2: Effect of blanking clearance on part edge in DP590 steel having 1.4mm thickness [Wiedenmann et al, 2009]

Wiedenmann et al. [2009] studied blanking process for 1.4 mm thick DP590. They assessed the impact of clearance on the part edge quality (5%-20%) while blanking holes of 10 mm diameter. They found that the fracture and the roll over increase with more clearance and vice versa. It is shown in Figure 3.2. The findings of Grünbaum et al. [1996] endorse the findings of Weidenmann et al. [2009] when they blanked low and high carbon steel alloys and metals such as aluminum, copper, and brass (sheet thickness: 5% - 20%). They blanked 12.7 mm holes. The velocities of blanking ranged from 0.15-3.6 m/s. The shear zone length reduced when clearance increased for all the studied materials mentioned before. The results are illustrated in Fig. 2.3. It was noticed that some materials were more sensitive than others as far as punch-die clearance was concerned. The tests were conducted at different blanking velocities. The shear length increases with rising blanking velocity for all materials, but it significantly increases for copper.
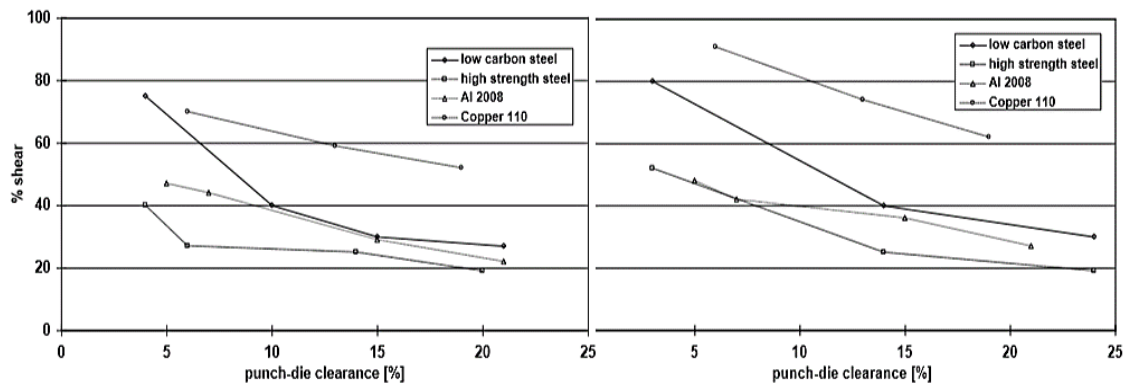
Figure 2.3: Punch-die clearance impact on shear edge length in case of varying blanking velocities [Grünbaum et al, 1996]

Bell [2006], in his investigative study, used 1400MPa sheet with 1 mm thickness, and blanked it with PM 4% V, 60 HRC punch at 6%, 10% and 14% clearances. The measurement of the punch wear was done 200,000 strokes. The experiment showed that the lower clearance resulted in galling and the higher resulted in bending stress of the cutting edge that further increased the danger of edge chipping. In this situation, an optimum clearance point exists between both, at which, tool wear is lower (Fig.2.4).
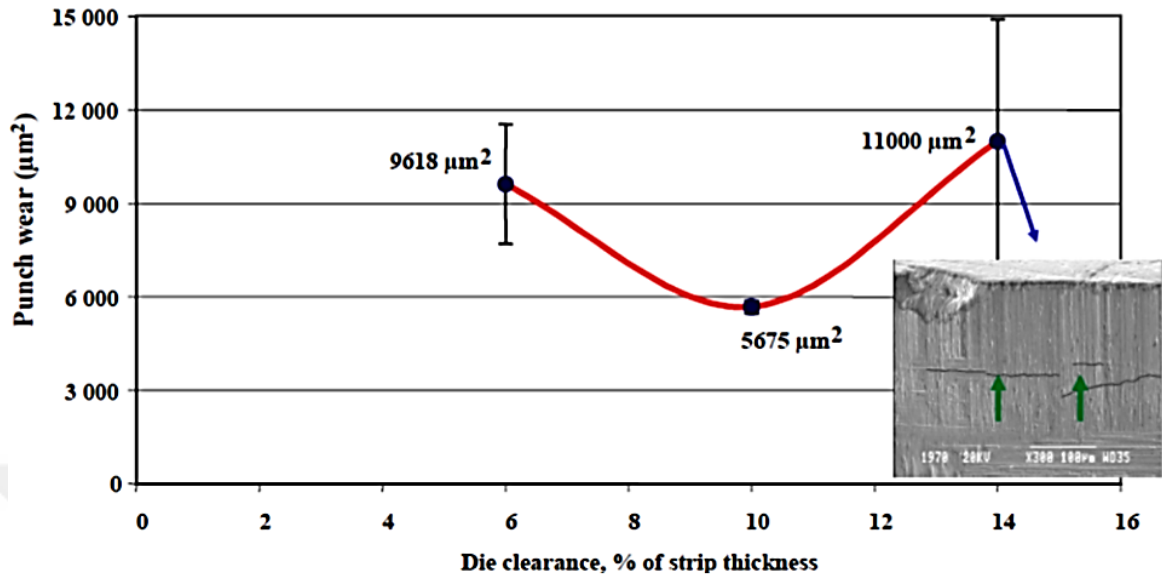
Figure 2.4: The impact of punch-die clearance on the wear of the tool [Bell 2006]

2.1.2 The impact of punch-corner radius [Picas, 2010]

The punch-corner radius as well as clearance has a definitive impact on punch wear and stress. Picas et al. [2010] conducted an experimental study on blank material DP1000 with 2mm thickness. Punch material was cast steel (D2) tempered and hardened to 60-62 HRC. The simulations indicated that the punch corner radius had a dominant impact on Von Mises stress as compared to the impact of clearance. The maximum stresses on the punch show a decrease of 500MPa as corner radius is raised from 0.01 to 0.1mm, while only a reduction of about 50MPa was noticed when the clearance was increased from 10% to 20%. It is illustrated in Fig.2.5a while Fig. 2.5b illustrates the fact that the punching load does not significantly change with change in the corner radius. Experiments show that the punch works only for a few hundred strokes before showing the first signs of wear and 3000 strokes before the fracture while the corner radius was 0.01 mm. The punch with 0.1 mm corner radius that worked for 15,000 strokes without showing any signs of damage whereas 30,000 strokes showed some wear and chipping on the edge.

13
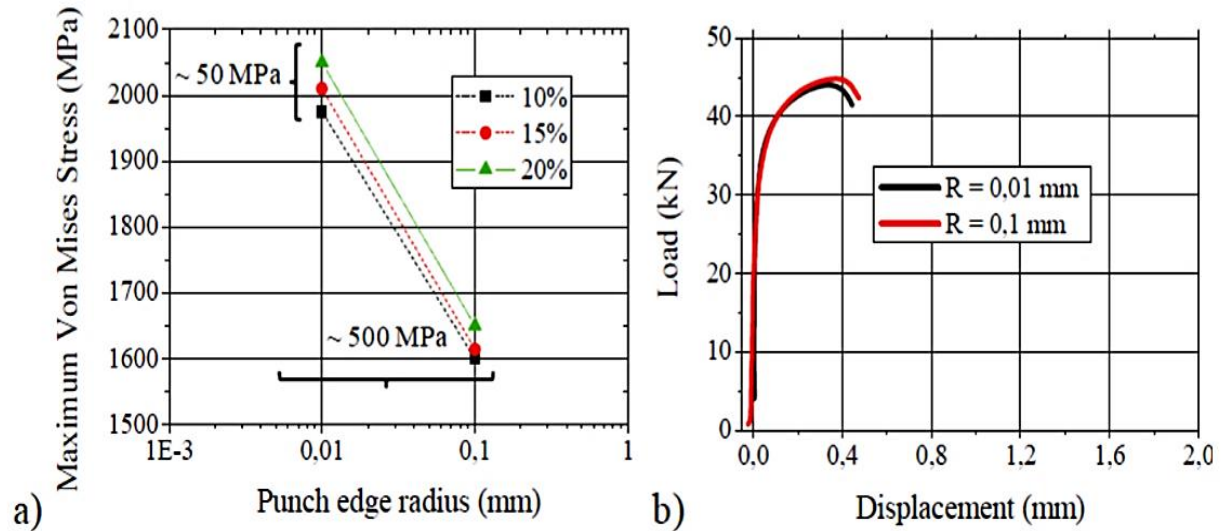
Figure 2.5: (a) Maximum Von Mises stress for 10%, 15% and 20% clearances at 0.1- and 0.01 mm corner radii (b) Experimental load-displacement diagram at corner radius 0.1mm and 0.01 mm [Picas et al, 2010]

The effect of having a very large punch corner radius on the blanked edge quality isn't discussed.

2.1.3 Press stability and reverse loading

Stability of the press, tools and punches plays a very important role for prolonged useful life of a tool and good component quality. There are several reasons that can lead to press and tooling deflections, some of which are (i) uneven blanking loads (ii) inaccurate guiding systems (iii) reverse loading during blanking. Jimma et al. (1990) have looked into the relation between press rigidity and part quality during high-speed blanking. Behrens et al (2010) have considered machine properties for sheet forming simulations to couple with the press performance during the sheet forming process. Groche et al. (2007) have described a process for generating numerical models to make machines, and illustrated processes for experimental machine parameters, which can be utilized for numerical simulations.

Snap-thru or reverse loading is another important factor that contributes to the life of the press, tools and punches. Snap-thru forces are evident while blanking thick

or very strong materials. During blanking, some portion of the material is sheared, and the rest is fractured. The fracturing happens much faster than shearing, and there is a significant reverse tonnage at the end of the fracture on the press. The press components reach their maximum deflection just before fracture.

After fracture, the press components spring back to their original shape at a very high velocity and there is a sudden release of energy. The ram is accelerated to a high speed. The drive train of the press has clearances around every moving component. When the clearances reverse, the ram stops suddenly expending all the energy and sending a shockwave. The press deflects in the opposite direction when the forward tonnage is developed. The snap-thru forces are also called reverse tonnage. The reverse tonnage can go as high as 50% or more in case of very strong materials, which are shown in Fig.2.6.
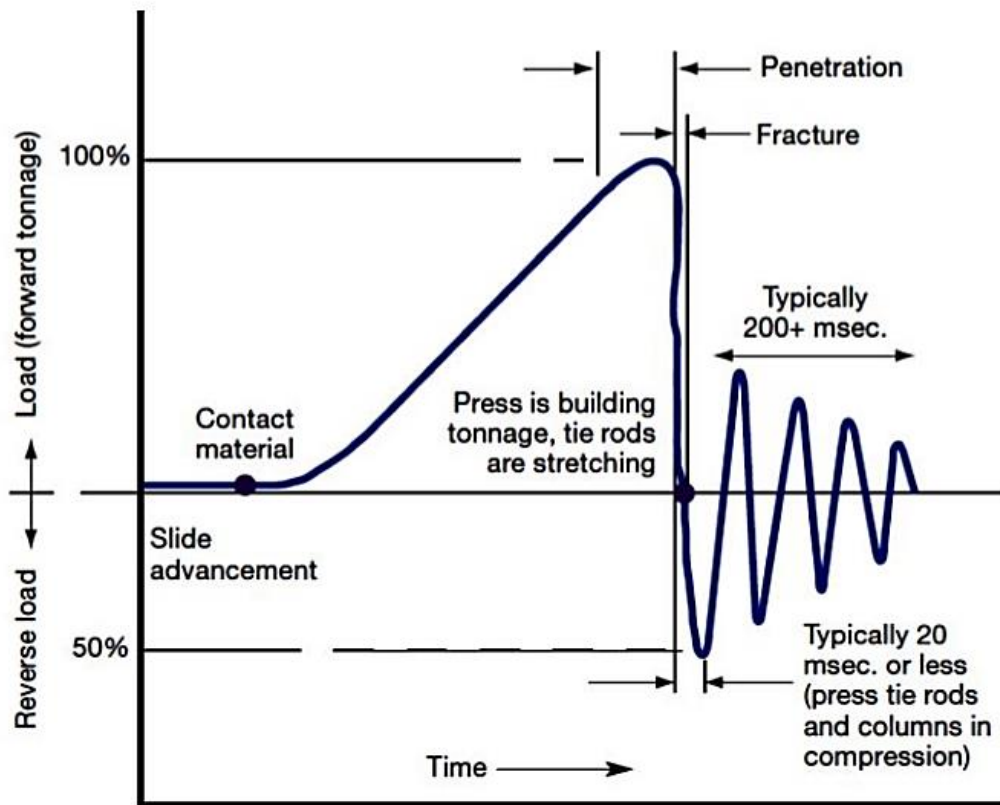
Figure 2.6: Forces during snap-thru [Miles, 2004]

Punch staggering, nitrogen cushion cylinders and hydraulic dampers are some of the commonly used solutions, which are used to address the problem of snap-thru; however, nitrogen cylinders and hydraulic dampers are not viable solutions during high speed blanking, since they cannot operate at high speeds.

2.1.4 Effect of stripper pressure on blanked edge quality of thin parts

Very little data is available in the literature on the effect of stripper pressure on blanked part quality. Stripper plate primarily helps the punch withdrawal from the sheet, and also helps holding thin sheets during the blanking process. It plays an important role for changing the patterns of stress and the fracture path. Using a spring stripper for cutting sheet metal has been experimentally studied by Bing & Wallbank (2008). Their findings are as follows:

1. Utilizing spring stripper lowers the burr height on the cut edge. It reduced by twice in some places and reduced secondary shear on the external edge.

2. This process is managed with the help of sprung stripper holders, and bending prevention devices.

3. Horizontal burr formation is possible on the return stroke, and that happens in case the sprung stripper is utilized. This happens when the strip is pulled from above with a friction from a withdrawing punch while the bulk is kept flat with the help of a stripper. It results in the misalignment of the die, and the emergence of lateral unbalanced force.

4. The average height of burr varies near the hole, and the same applies to the readings of burr height. This does not depend on the stripper type. Jimma et al. (1990) studied various factors that affect the dimensional accuracy of lead frames. Some of them are (i) mechanical properties of the strip (ii) static and dynamic accuracy of press and blanking tools (iii) accuracy of feed (iv) slenderness of punch (v) tool wear (vi) lubricant used (vii) blanking speed (viii) strip-holding

force (ix) order of progression (x) shape of the curved lead frames (xi) ratio of length and width to thickness of leads.

2.1.5 Different Punch Materials and Coatings Used in Blanking.

The punch materials and coatings used in blanking depend largely on the sheet material and the expected tool life.

Steels

According to Sandberg (2004), some of the tool steels are:

AISI D2 – high carbon/chromium tool steel with high quantity of chromium carbides (13%), and a hardness potential of 59-61 HRC after secondary hardening

AISI S7 – shock steel with exceptional impact properties. It is widely used for medium-run cold work tools.

Carmo/Calmax – the first generation of car body die steels with a pure martensitic matrix structure. It has optimized profile in terms of wear, ductility, weldability and induction hardening. 58 HRC is the potential hardness after low temperature tempering.

Diemax – new developed matrix steel with an optimal combination of ductility, hardening and temper resistance at hardness up to 57-58 HRC. Hardening is possible through high temperature tempering, which facilitates surface coating.

Caldie – new car body die steel developed from an old grade Carmo but it has high temperature tempering facilities providing a hardness of 60-62 HRC and still maintaining a very good ductility and temper resistance. It is suitable for surface coating.

Sleipner – the development of AISI A2 and D2 improved ductility as compared to D2 because of less quantity of chromium carbides 6% vs.13% (D2) and higher hardness potential, 64 HRC vs. 61 HRC (A2/D2) after secondary hardening.

Roltec – a spray formed grade in between PM and conventional cold work steels. It is steel that has substantial ductility and abrasive wear resistance, and besides, its hardness potential can be up to 65 HRC.

Some of the other commonly used tool steels for blanking are:

AISI M2 - provides properties such as toughness, compressive strength and wear resistance. These properties make it better than most of the other alloys.

CPM M4 - appropriate choice with greater vanadium content, and HSS, which exhibit improved toughness and wear resistance as compared to M3 as well as M2 for cold-work punch, die insert and lighter high-speed light cutters.

Powder metallurgy (PM), Cermets and Ceramics

PM [Sandberg, 2004]

Vanadis 4 - PM steel sheets assure excellent ductility and wear resistance in tools, which are developed for top performance.

Vanadis 4 Extra – An optimal combination of ductility, wear resistance, mixed abrasiveness and adhesiveness for all PM cold work steels.

Vanadis 6 – PM steel with better abrasive wear resistance than Vanadis 4 Extra.

Vanadis 10 – a high vanadium alloy with PM grade that offers both high ductility and abrasive wear resistance.

Vancron 40 – a nitrogen alloyed PM steel with very good low-friction properties for excellent galling and adhesive wear resistance.

Cermets / Cemented Carbides

They are popular composites, which are added to several wear applications because they offer high strength, toughness and wear resistance [Klassen 2011] TiC - TiCs and their cermets (including Ni alloys/steel binders) are successfully applied in situations requiring strength, more adhesive wear resistance, high weld-ability and high oxidation resistance [Klassen 2011].

When metals such as nickel, copper, and iron are machined, the cemented carbide wear is generally fast because cobalt, nickel or copper, which exist in cemented carbide, result in quick cement carbide deterioration [Misumi Tech Central].

Ceramics

Advanced ceramics need certain properties such as fracture resistance/toughness, strength, appropriategrain size, and minimum porosity because their utilization is mainly in corrosive and damaging environments. Y-TZP (yttria-tetragonal zirconia polycrystal) is a zirconia-alloyed ceramic, which is used for some punching applications. Although it has great wear resistance, it is not very commonly used in metal forming applications because it is very inappropriate for bending. A comparison between the wear characteristics of the tools is conducted by Uddeholm, which has been illustrated in Fig.2.7.
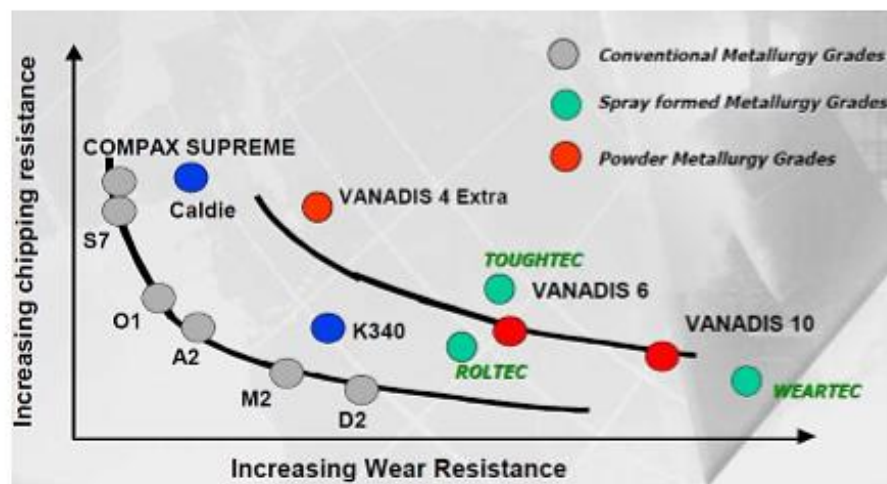
Figure 2.7: Tool Material Characteristics by Böhler Uddeholm [Bell, 2006]

Surface Treatments and Coatings

The common surface treatment processes include:

(i) Nitriding

(ii) Physical Vapor Deposition (PVD)

(iii) Chemical Vapor Deposition (CVD)

(iv) Thermal Diffusion (TD)

CVD and TD are used mainly in those applications, in which, high precision is not needed.

Since the temperature is high during processing, naturally there is a change in size and distortion. PVD has lower processing temperatures; hence it can accommodate more precision during tooling. Some of the coatings, which are commonly used in metal forming tools, are TiN, TiC, TiCN, TiAlN TiCrN, AlCrN, and CrN. MoST™ is a PVD solid lubricant coating. It is composed of sulfur and molybdenum [Dayton Progress]. It should be understood that not all coatings go well with all tool materials in terms of coating adhesion. Similarly, surface treatments are not recommended for all the tool manufacturing materials.

2.2 Environment Friendly Metal Forming Tribo Systems [Bay, 2010]

Many punch manufacturing alloys as well as coatings, which are applied to dry-blank electrical steel sheets, were used for conducting experiments and investigations. It was found that the insulating glass coatings result in extra wear. Moreover, PM High Speed Steel (HSS) and AISI D2 punches were tested using PVD coating using diamond-like carbon, DLC metal containing, Electro-discharge Coating (EDC) and TiC. These coatings increase/increment punch life almost three times. When EDC combines with AISI D2 cryogenic treatment, it can extend the tool life up to nine times. Another relevant blanking investigation on layered steel shows that the PM HSS and TiCN, \AlCrN, \and\ TiAlN + WC/C carbide coating extended the tool life, but the best performance combination was PM\ HSS\ +\ AlCrN. In addition, the results of TiCN punch coating in case of Al sheet perforation extends the life of the tool by 10 times because pick-up reduces, and wear resistance increases. According to a report by Oerlikon Balzers, the

punch coating using AlCrN extends tool life by approximately 3 times as compared to TiCN and TiN coating.

2.3 Improving tool wear resistance for stamping purpose (Straffelini, 2010)

Various tool materials and coatings were evaluated. The correlation between burr height and tool wear was first established in a study conducted by Straffelini (2010). Various tool materials and treatments/coatings are evaluated based on the burr height. The blank is 2.2mm thick, while it is made using cold rolled strip subjected to spheroidisation annealing. Its chemical composition is: 0.7% Mn, 0.7% C, and 0.2% Si. Fig.2.8a and 2.8b show the part's shape and the tools. Fig.2.8 c shows the burr height for various tool materials and hence, their performances as well. S390 is a PM HSS from Uddeholm, QTC and QCT are two different cryogenic treatments on the S390 steel. Hard metals are carbide and Ceratizit H40S.\ AlCrN is PVD coated on S390 steel by Oerlikon Balzers Italy. From this graph, it can be seen than S390 with an AlCrN PVD coating is the best performer followed by the ceramic.
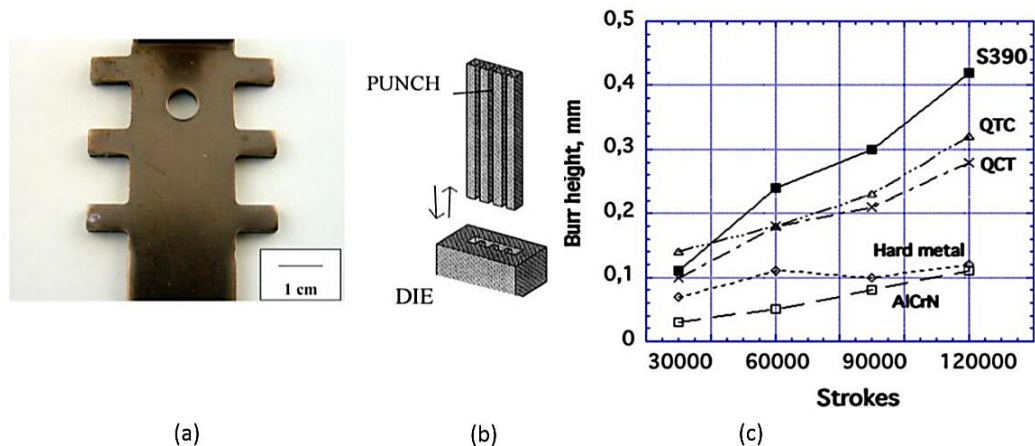
Figure 2.8: (a) Part formed (b) Tools used in the experiment (c) Burr height measured for various tool materials/treatments/coatings (Straffelini, 2010)

2.4 Punch Failure Mechanisms

Punch failure has the following forms:

Wear

Wear means solid surface damage/s, which results in losing material displacement. Wear takes place when a continuous sliding contact occurs between a tool and a work piece. In broader terms, wear has two types [Uddeholm and SSAB 2008; ASTM G40 2005]:

1. Abrasive wear takes place, when tough particles/specs come in contact and cause friction with a solid surface.

2. Adhesive wear takes place when local bonding between any two contacting solids results in transferring material/s, which might result in wear/damage to a single or both the surfaces.

Flank/side wear [Luo, 1999]

This kind of wear takes place on punch sides, which result in partially wearing out the punch. The mentioned side wear generally takes place because adhesive, fatigue, and abrasive wears combine, which further results in reducing the inner diameter of punched holes and increasing the die-punch clearance. Moreover, this kind of deformation does not increase the drawn-in edge of a work-piece while shearing.

Face wear [Luo, 1999]

In this case, the punch face gets worn out that rounds punch edges. Its possible causes include "micro-chipping" and mechanical attrition. It decreases the punch sharpness while shearing and acts as deformation enhancer to a punched work-piece. In addition, it is observed that this form of wear causes larger burrs and raises the noise level in the press. Fig.2.9 illustrates flank and face punch wear.
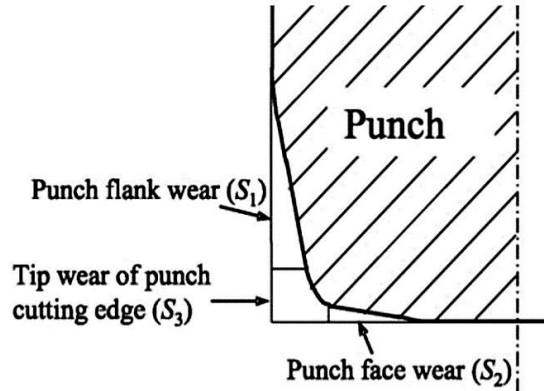
Figure 2.9: Schematic illustration of flank and face wear in punch
[Hernández et al, 2006]

Chipping

This kind of appearance on a punch means existence of micro-crushes, breakages, and segmentation in the edges. Chipping emerges as a consequence of repeated impact load/thermal shock. When there is excessive roughness on the punch surface, chipping takes place quite naturally [Luo, 1999]. Chipping takes place as a direct consequence of stresses, which exceed a tool's fatigue strength [Uddeholm and SSAB 2008]. Fig.2.10 shows images of chipping on the cutting edge of the punch.
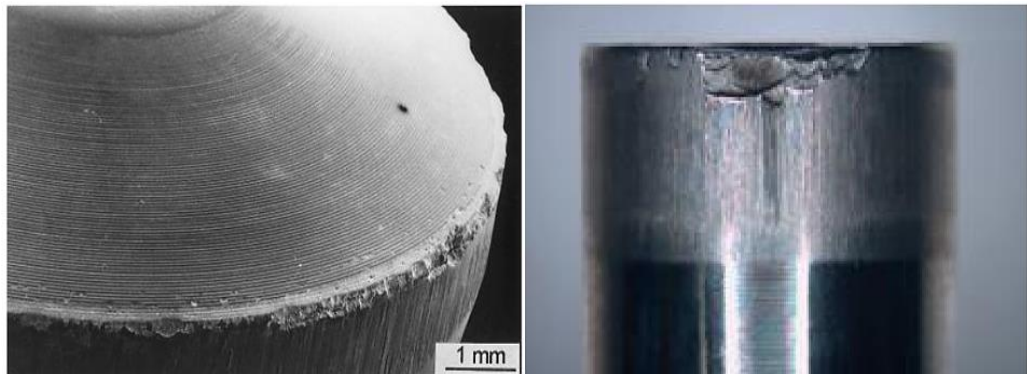
Figure 2.10: Chipping wear seen on punch cutting edge [Luo, 1999],
[Uddeholm and SSAB 2008]

Cracking [Luo, 1999]

It emerges when several micro-cracks appear on the punch edge as illustrated in Fig. 2.11. They appear under excessive mechanical/thermal fatigue while shearing. The cracks continue lengthening if shearing continues, and the edges of the punch show chipping or a major fracture.
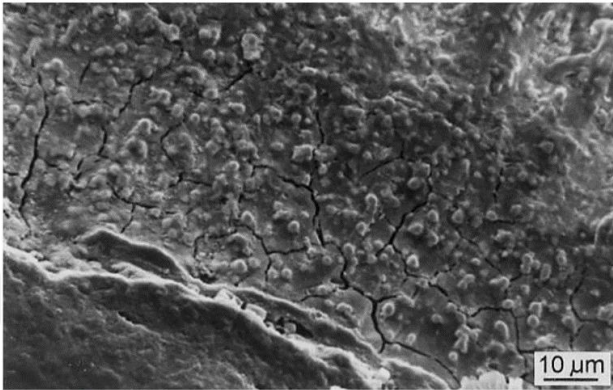
Figure 2.11: Cracking as seen on the punch surface [Luo, 1999]

Gross fracture [Luo, 1999]

Gross/ macro fractures appear on the surface of the punch, which are illustrated in Fig.2.12. It is obvious that the fatigue failure causes beach markings, which grow cyclically. In addition, chipping or cracks might also cause this type of fracture in the shearing process.
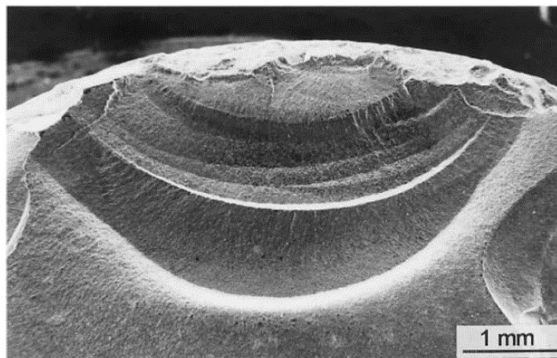
Figure 2.12: Gross Fracture on punch [Luo, 1999]

Galling [Uddeholm and SSAB 2008]

Galling/pick-up is a direct consequence of substantial frictional forces, which cause sliding contact while the work piece is adhesive nature in nature as shown in Fig. 2.13. This process is almost like adhesive wear.

Figure 2.13: Galling on punch face [Uddeholm and SSAB 2008]

2.5 Factors affecting tool wear and galling [Billur, 2009]

Contact Pressure

All failure types can be avoided by reducing the contact pressure. The contact pressure between the punch and the sheet during blanking depends on (i) sheet material (ii) punch-die clearance, (iii) punch corner radii, and (iv) profile blanking.

Surface Quality

Despite the fact that the tool surface is quite smoother as compared to the sheet surface, galling affects the surface quality of a tool. When the tool surface is polished before/coating, it substantially decreases chances of galling. On the other hand, the sheet roughness has minimum impact [Rooij and Schipper 2001].

Tool Material and Coating

When an appropriate material is selected for manufacturing a tool, coating still plays a critical role to help avoiding galling as well as tool wear. Tougher tool manufacturing alloys show higher compressive-yield strength, so, toughness

should be chosen as per requirements. Coatings with lower friction coefficient value should be chosen to coat a tool [Podgornik et al 2006].

<u>Lubrication</u>

Unless there is a solid film lubricant coating, lubrication is needed to reduce wear and galling with traditional coatings (CrN or TD). Lubricants improve the tool performance in processes, which involve high contact pressures and temperatures. Extreme pressure (EP) additives might be required while manufacturing tools [Rooij and Schipper 2001; Janoss 2008; Kim et al 2006].

2.6 The impact of tool wear on the quality of edge

Tool wear has a definitive impact on the quality of the part edge because it results in burr formation and lengthening the burr. Length of burr is in fact a parameter, through which, managers of the manufacturing industries judge part or surface quality. Higher burr lengths mean that the tool needs reprocessing for a sharper die/punch radius. Generally, the impact of tool wear is clear when the burr length is higher.

Makich et al. (2008) have mentioned a process for quantifying the burr volume after the research. This process was utilized for measuring the impact of the tool wear on burr volume. It is evident from Fig.2.14 that the volume of burr initially increased at a higher pace with large number of strokes. It was followed a constant increase in burr, and when the strokes were increased, burr again increased. The pattern of burr formation depends on the kind of sheet material.
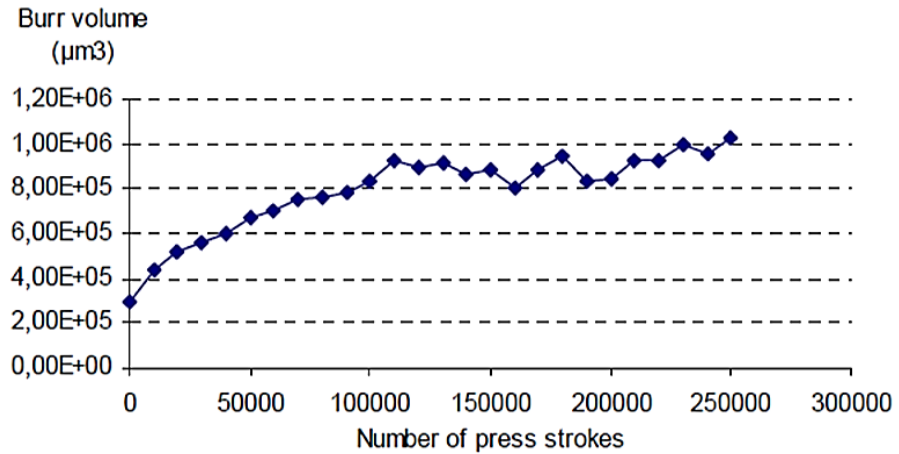
Figure 2.14: Increase in burr volume with strokes as a consequence of tool wear [Makich et al, 2008]
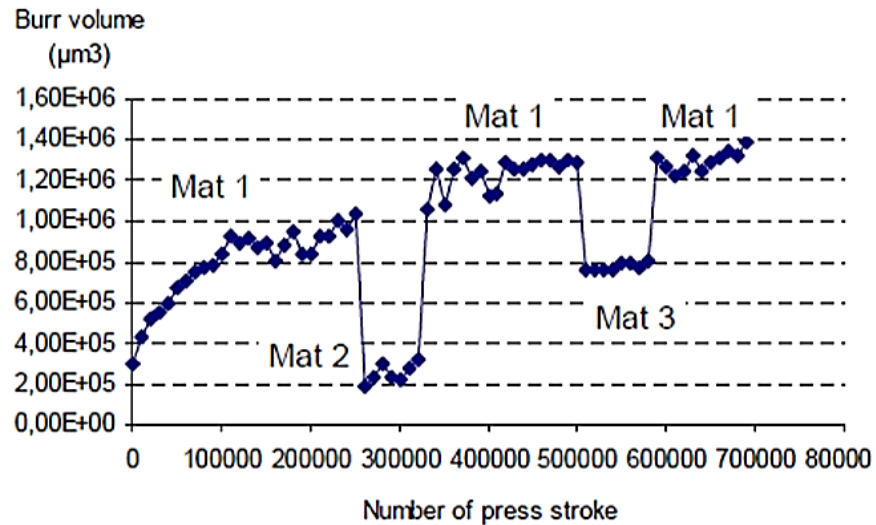
Figure 2.15: Effect of sheet material on the burr volume [Makich et al, 2008]

The volume of burr depends on the sheet material, which is blanked. Fig.2.15 shows that some sheet materials generate much less burr as compared to others. For example, Mat 3 shows 30% reduction in burr as compared to Mat A, even though, the tool wear exists when Mat 3 is blanked.

Tool wear can be estimated in simple ways with the help of FE simulations through raising the radius of the punch and die corner. The tool wear has a

significant impact on the part edge quality. The tool wear results in forming and lengthening burr as depicted in Fig. 2.16 [Husson et al, 2008]. It is obvious from the diagram that the tool wear impact is more obvious when the blanking clearances are higher (Fig.2.16).

Blanking clearance of 15μm
Punch and die corner radii of 10μm

Blanking clearance of 15μm
Punch and die corner radii of 75μm

Blanking clearance of 60μm
Punch and die corner radii of 10μm

Blanking clearance of 60μm
Punch and die corner radii of 75μm
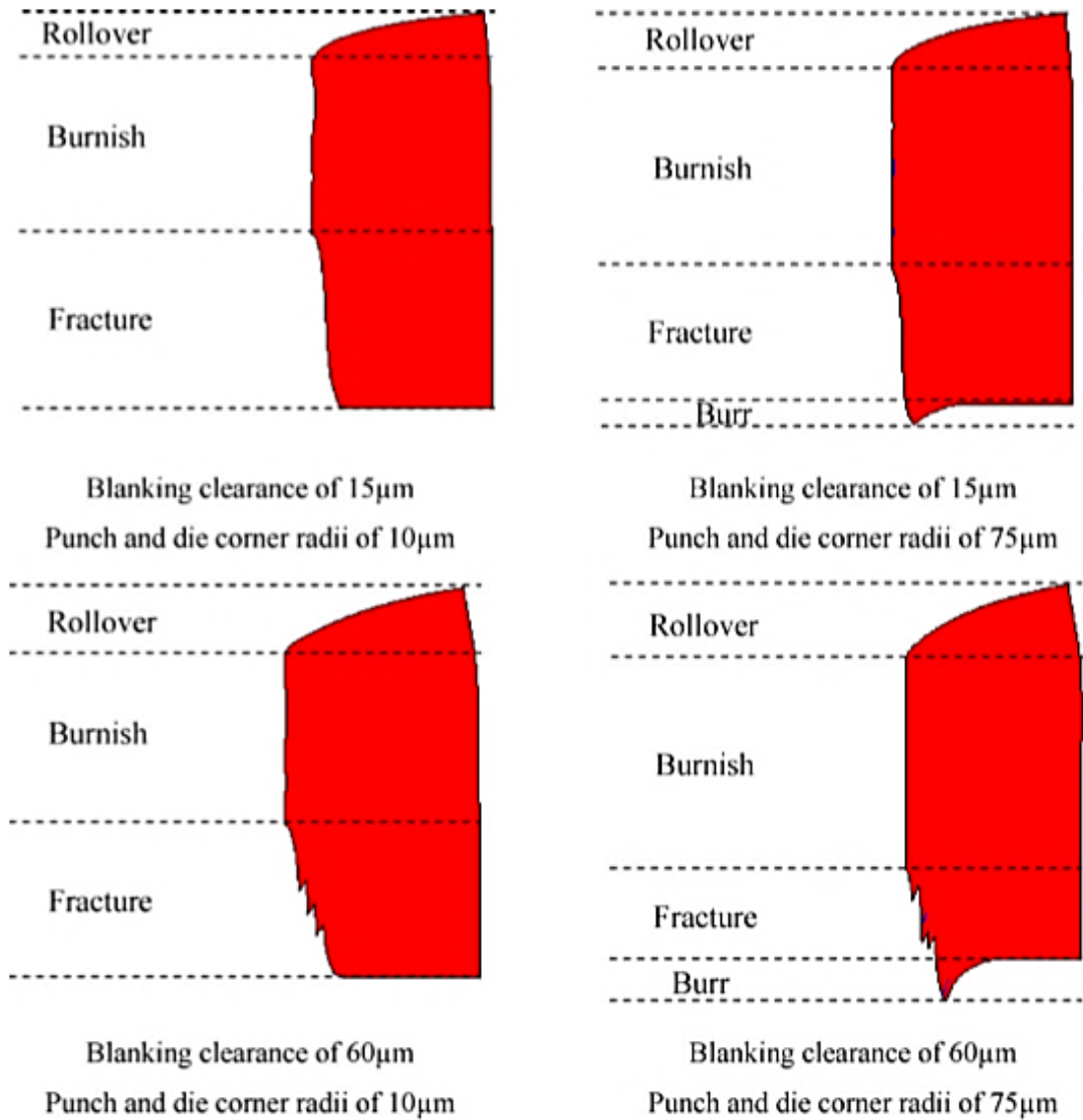
Figure 2.16: Effect of tool wear and blanking clearance on part edge quality as predicted by simulations on a 0.58 mm thick Cu alloy [Husson et al, 2008]

Flanging

There are several factors that affect the flangability of a hole including (i) the sheet material (ii) punch die clearance used in blanking (iii) quality of the sheared hole (iv) shape of the punch used in flanging (v) position of the burr during flanging. A few researchers have researched the influence of blanked edge quality on Hole Expansion Ratio (HER), which resulted in better understanding of this phenomenon; however, more research is needed in this area because it is not very clear how to characterize a blanked edge for flangability. Karelove et al. (2007) studied the influence of cutting methods on the hole flangability of DP800 and CP800 steels. Fig. 2.17 shows that wire cutting causes only minor deviations from the desired hole geometry. The sharp edges created by wire cutting can have a detrimental effect because they are the possible stress concentrators during the hole expansion process. This phenomenon can be explained in another way. Despite the fact that the wire cutting process is highly accurate, the HER increase was not significantly higher than the earlier measure for drilled holes. This study shows strong influence of the hole-edge, and the hole surface quality on the hole flangability of the material.
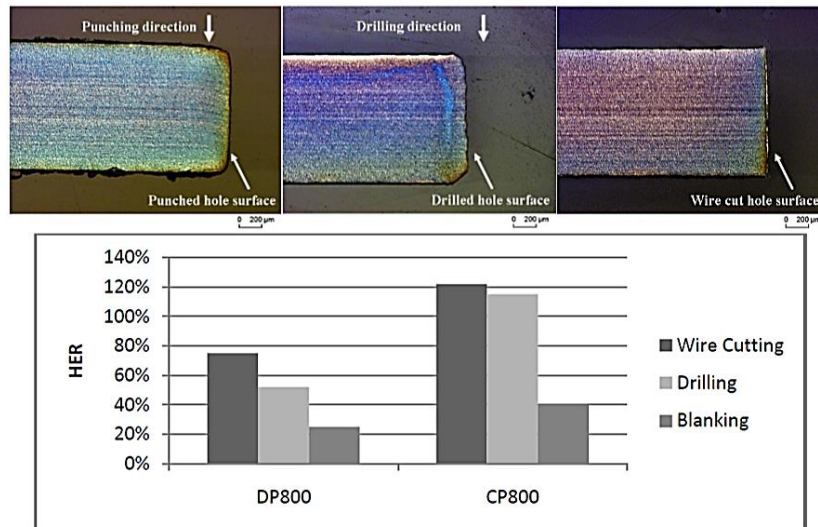
Figure 2.17: Micrographs of cross-sectional area in punched (top) (a), drilled (b) and wire cut (c) hole of DP800; (bottom) Influence of the hole edge condition on HER

Mori et al, (2010) conducted similar studies, in which, secondary smoothing operation was carried out to improve the hole flangability. DP980 grade material was used in the mentioned study. The smoothing operation was conducted with a punch that had a 30° lesser conical angle than the angle on the flanging punch (60°). The smoothing load was changed to see its effect on HER. Fig.2.18 shows the blanked edge after smoothing with different loads where the fractured zone is smoothed. The difference in smoothing load causes a difference in the edge quality before flanging. This in turn makes a difference in the flangability, which is shown in Fig.2.19. These experimental studies have shown that the quality of blanked edge is a significant factor for hole-flangability of a material.
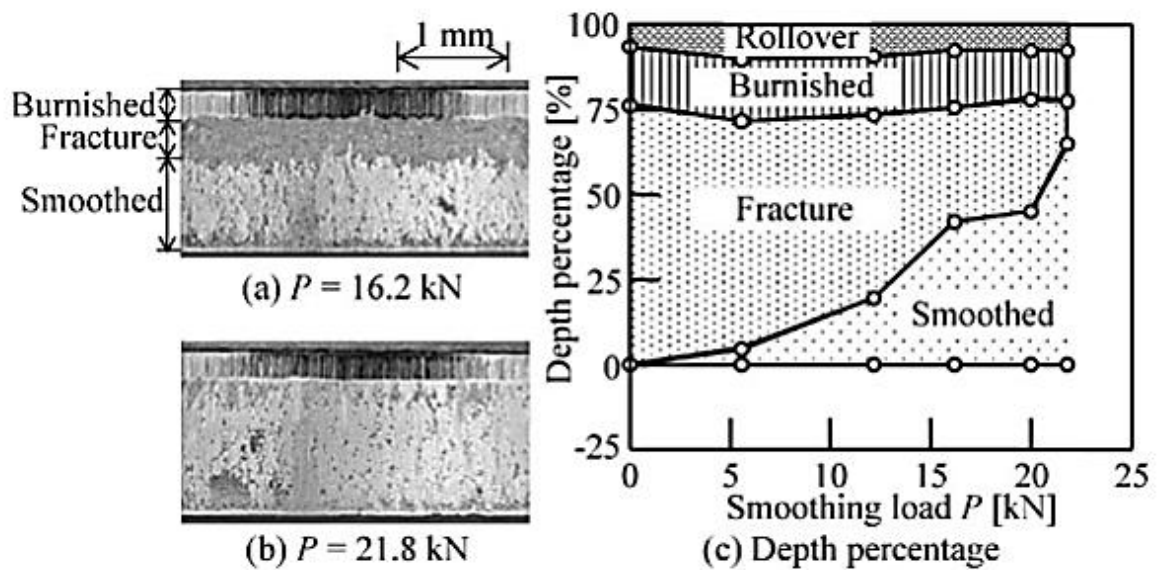
Figure 2.18: Smoothed surface, relations between rollover depth percentage, fractured, smoothed, and burnished surfaces: (a) P=16.2kN; (b) P=21.8kN; (c) %depth [Mori, 2010]
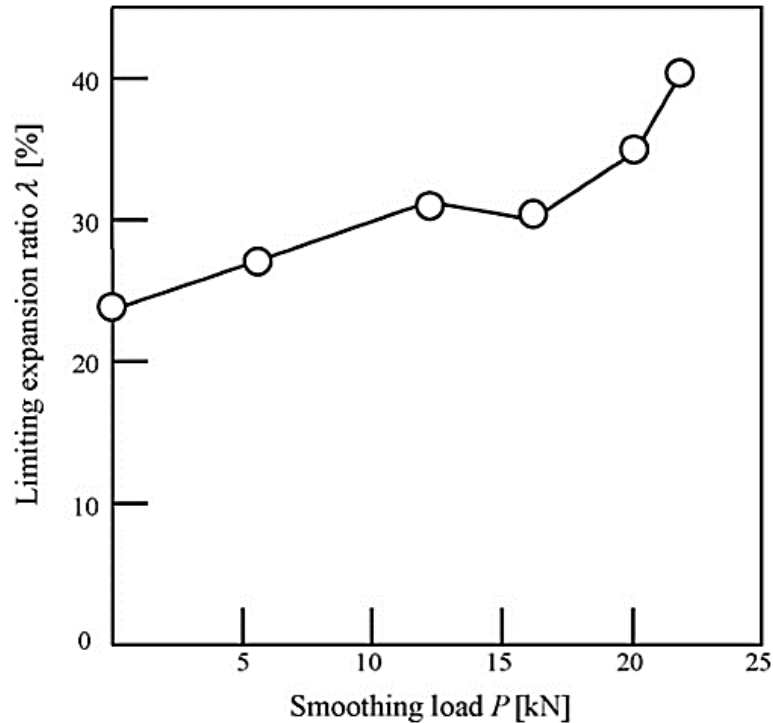
Figure. 2.19: Relation between smoothing load and limiting expansion ratio (LER) [Mori, 2010]

2.7 Polycrystalline diamond compact (PDC)

Polycrystalline diamond compact (PDC) cutters are very popular in the industries, which require earth and stone drilling such as oil and gas exploration industry. Fig.2.20 shows PDC cutters. They have very high abrasion resistance, which gives PDC cutters a technological edge over other drilling devices because they not only provide efficiency but also provide a low-cost option. They consist of a polycrystalline diamond bonded layer with tungsten carbide substrate, which is a good combination to carry out hard-to-perform drilling operations. The bonding between the two mentioned substances i.e. diamond and tungsten carbide becomes possible at high temperature and pressure sintering procedure. A polycrystalline diamond layer is formed while carrying out this process, which creates sintered material having a tough diamond-to-diamond bond. [Valentine Kanyanta 2014]

PDC cutters might develop a fatigue fracture if they are exposed to repeated high-impact load. This fracture stress reduces when the loading cycles increase. These cracks intermittently develop and grow every time when a successive impact is applied. These cutters consist of a polycrystalline diamond layer, which has a tough grained microstructure, which allows higher impact resistance in comparison with the finely grained variety.

Fig.2.20 illustrates the force trace, which was recorded using a force transducer. Higher and better wear resistance of tough substances gives them edge over alloys and ceramics, and it promotes their usage for cutting and grinding applications in several industries; however, unforeseen breakage and chipping generally result in primary failure, which limits their use in many applications. For several materials, there is a trade-off between toughness and wear resistance, which is a major impediment while developing super hard tools for several industries. In fact, it is desirable for long time but very difficult and challenging in practice both for manufacturing scientists and engineers, as they want to improve toughness to reduce chances of fracture without compromising wear resistance.

Figure 2.20: Polycrystalline diamond compact (PDC) cutter

Syndril secured in the cutter holder (13.4 mm diameter cutters)
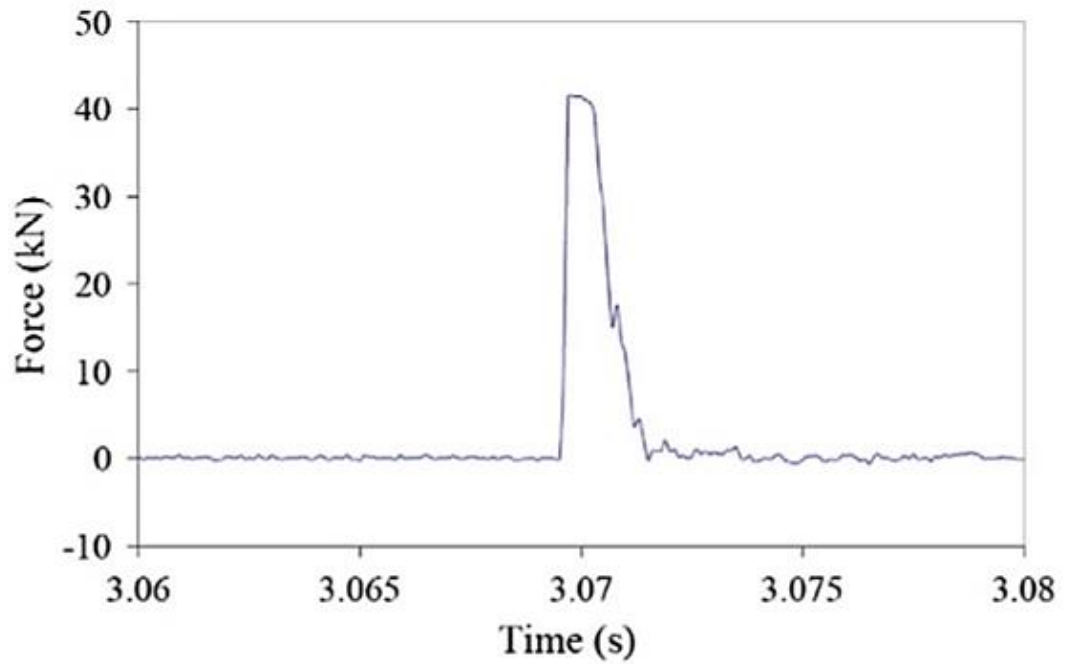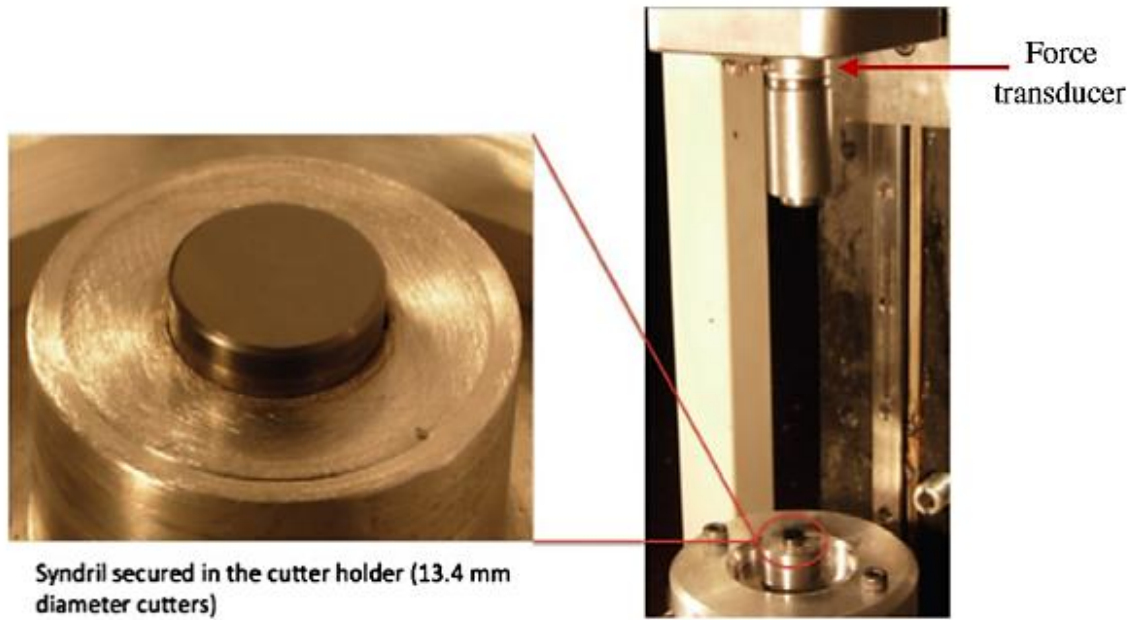
Figure 2.21: (a) The effect of applied cyclical impact force (force transducer recording) and (b) Force pulse blow-up. [Valentine Kanyanta 2014]

2.8 Ductile Fracture

2.8.1 Definition and Features of Ductile Fractures

Ductile fractures differ from brittle fractures. A ductile fracture is a failure process that the material sustains in plastic deformation before it separates into pieces, and this happens because of an imposed stress at a temperature lower than its melting temperature [Callister, 2007]. Fig.2.22 illustrates the tensile stress-strain curves with/without a significant plastic strains loaded to cause a fracture both for ductile and brittle materials [Callister, 2007]. Ductile fracture surfaces have special features that present necking regions with rough and irregular surfaces as compared to the brittle ones, which are schematically shown in Fig.2.23 [Callister, 2007].
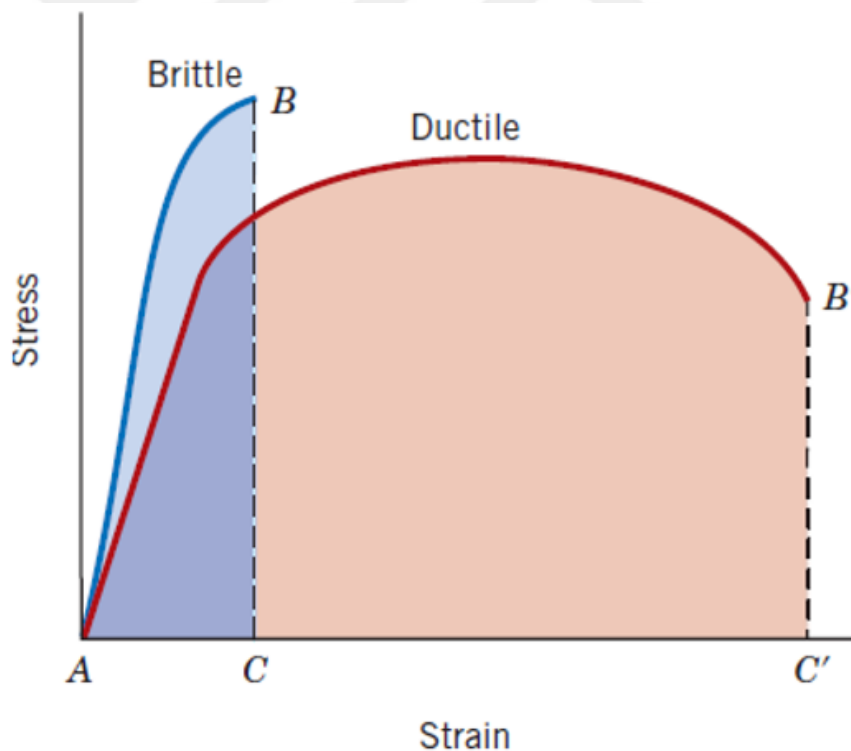
Figure 2.22: Schematic diagram of tensile stress-strain for both brittle as well as ductile materials causing fractures [Callister, 2007]
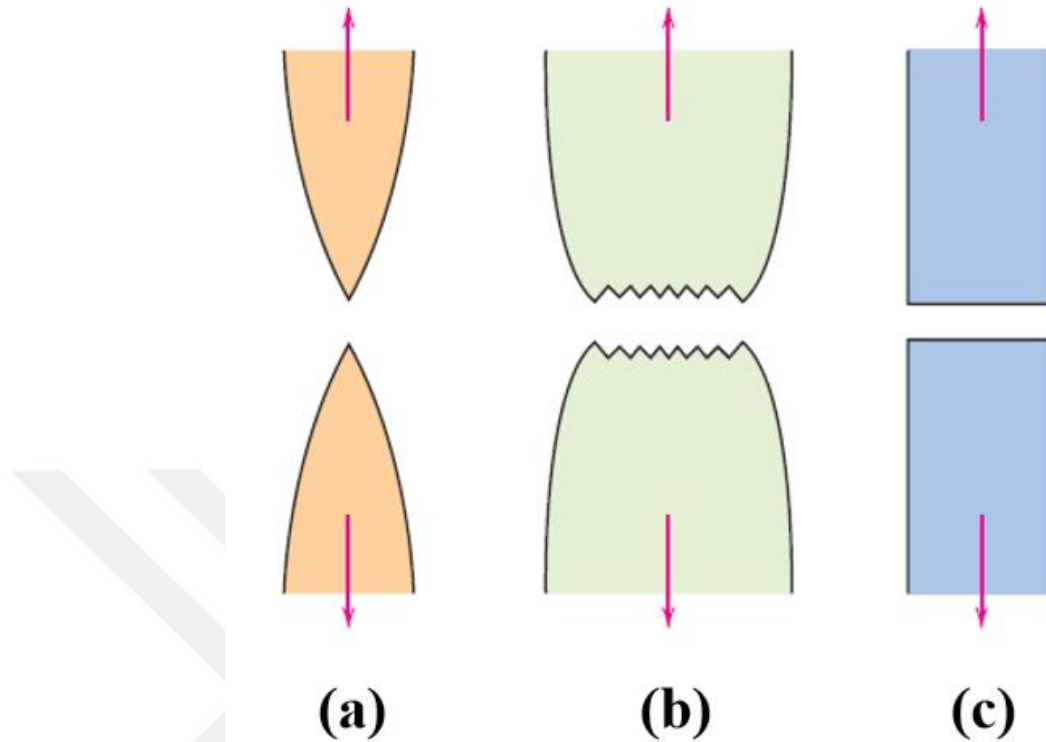
Figure 2.23: (a) Very ductile fracture that causes a specimen to bend over/turn the neck down. (b) Moderate ductile fracture that causes partial necking. (c) Brittle fracture with no plastic deformations. [Callister, 2007]

The researchers observed three principal stages, through which, a ductile fracture emerges: The first is nucleation, which is followed by fracture growth, and finally, coalescence of voids takes place. It is shown in Fig.2.24. Initially, micro voids nucleate at specific point/s when the interface stress elevates to cause a rupture [Argon, 1975]. Secondly, the voids grow until the matrix attains a specific plastic limit because of plastic strain and hydro-static stress [Thomason, 1998]. Thirdly, the inter-voids cause plastic failure across the sheet with strain localization between the voids. Then, it begins to internally neck down between the adjacent voids [Cottrell, 2012]. These voids further coalesce and the inter-void matrix cracks with a "knife-edge" fracture on the surface [Thomason, 1998].
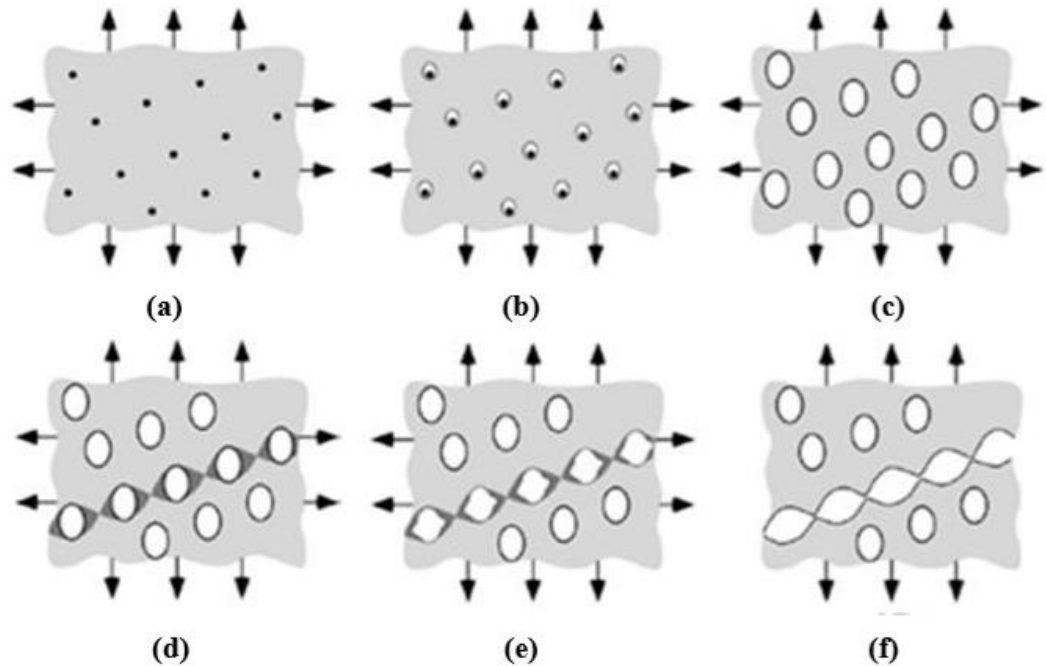
Figure 2.24: Nucleation, growth, and coalescence of voids in ductile metals: (a) inclusions, (b) void nucleation, (c) void growth, (d) strain localization, (e) necking among voids, (f) void coalescence/fracture. [Anderson, 2005]

A "cup and cone" shape was a typical ductile fracture feature obtained under uni-axial tensile tests. Fig.2.25 depicts the "cup and cone" fracture process. After necking, some small micro-voids first emerge in the internal parts of a material, which are illustrated in the Fig.2.25(b) [Callister, 2007]. The micro-voids then enlarge and coalesce to form a crack as shown in Fig.2.25(c), and the long axis of this elliptical crack is perpendicular to the direction of stress [Callister, 2007]. Finally, the crack rapidly propagates through the outer ring of the specimen, and shear deformation bands are formed at 45-degree angle from the tensile stress axis, which is shown in Fig.2.25(d) [Anderson, 2005]. The internal and central parts of the fracture seem fibrous and irregular as shown in Fig.2.25 (e) and Fig.2.25 (a) [Anderson, 2005]. It is called as "cup and cone" fracture as it is similar to a cup and the adjacent one has a conical shape, which is shown in Fig.2.26 (a).
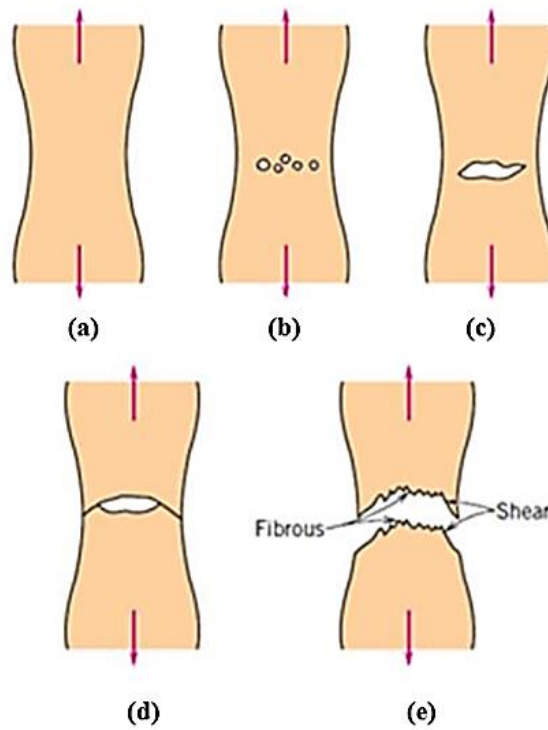
Figure 2.25: Formation of "cup and cone" fracture in stages (a) Emergence of necking, (b) Formation of a small cavity, (c) Cavities' coalescence that results in crack formation, (d) Propagation of crack, (e) Last shear fracture that takes place at 45º from tensile direction. [Ralls, 1976]

Figure 2.26: (a) "Cup and cone" fracture formation observed in aluminum. (b) A brittle fracture found in not-so-tough steel.

Ductile fracture plays an important role in an effective finite element simulation of machining. Its importance was studied and reported by Bil et al. [2004] and Liu and Guo [2000]. The criteria for fracture initiation and the evolution of fracture are necessary requirements in the finite element modelling. Two key factors on the ductile fracture behaviors include loading conditions and the material itself. In addition, a ductile form of fracture is generally affected by factors including stress/es, temperature variations, and the rate, at which, strain is exerted. These factors will be discussed later.

2.8.2 The Impact of Strain Rate and Temperature on Ductile Fracture

During metal cutting, metal deformation takes place at high strains, top strain rates, and maximum temperature; therefore, Johnson and Cook (1985) studied the impact of strain rate and temperature on ductile fractures. Three types of experimental stress-strain curves have been illustrated in Fig.2.27 using Split Hopkinson tension bar test at high temperatures [Johnson, 1985]. This test is dynamic, which focuses on the effect of an imposed stress wave on the specimens, and the device structure (shown in Fig.2.28).
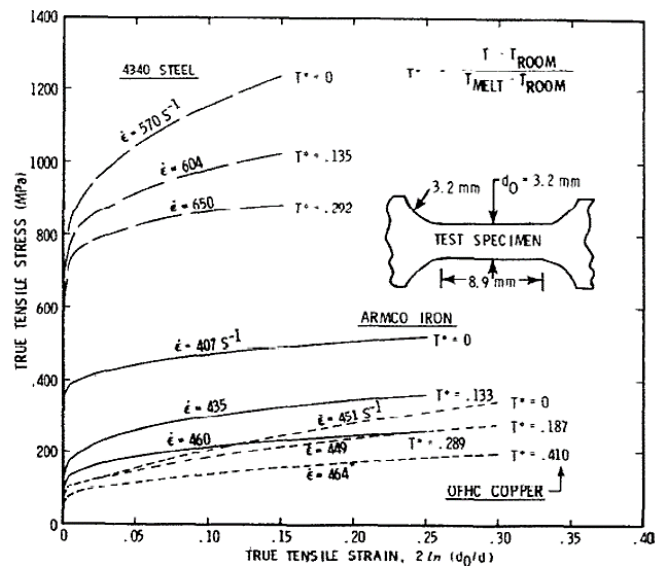
Figure 2.27: Torsion Test of average shear strain at the fracture. [Johnson, 1985]

38
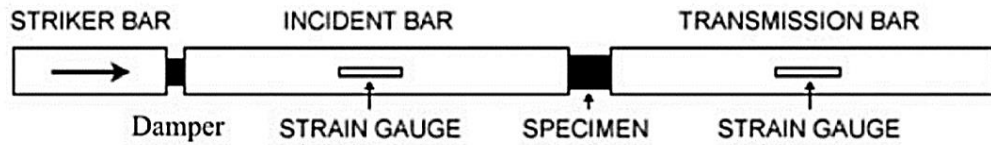
Figure 2.28: Split Hopkinson device. [Autenrieth, 2009]

Fig.2.29 shows the analysis of the fracture strain with respect to temperature and strain. The figure shows fitted straight lines, which were calculated by the "least squares" method to cover the average temperature for each test from the beginning to where the fracture occurs [Johnson, 1985]. Hence, it is shown that the ductility of material increases with higher temperatures. The strain rate impact is given in Figure 2.8 Here, T*= 0 and T* represents dimensionless temperature. In this case, the strain-fracture ratio from high strain rates to low strain rates is more than 1. In other words, a higher stain rate will increase the strain-fracture ratio of a material.
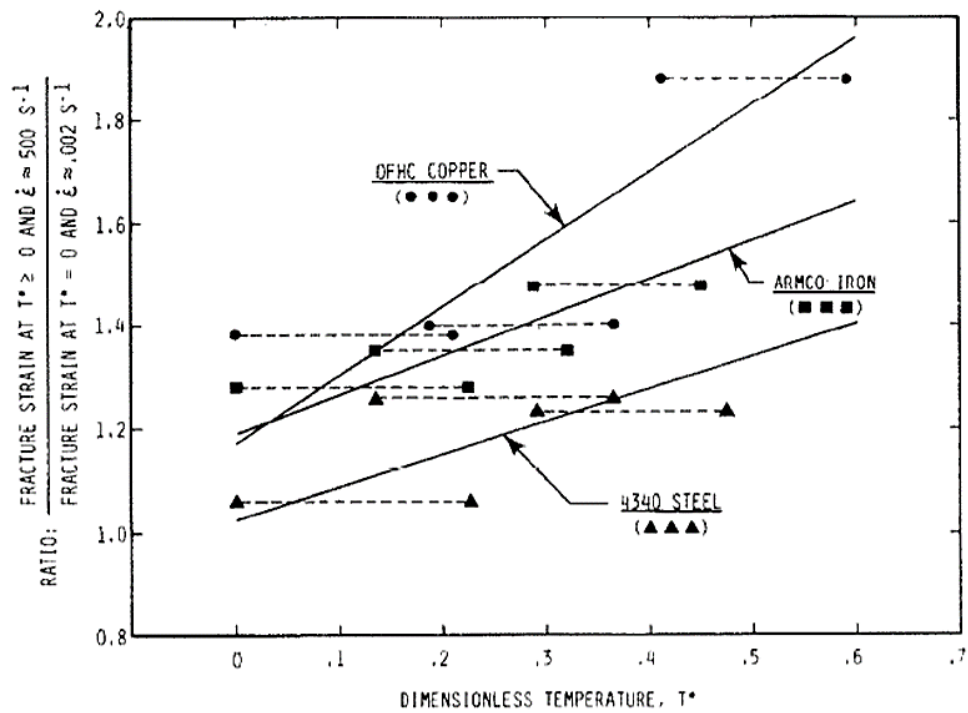
Figure 2.29: Impact of temperature and strain rate. [Johnson, 1985]

Strain rate and temperature have definitive impact on ductile fractures, but it is not the same for different materials. In other words, the influence of these two factors on ductility strongly depends on the material itself. Fig.2.30 shows totally different relationships between the strain-rate or from temperature to strain to fracture for Weldox 460 E steel as compared to the results presented by Johnson and Cook [1985]. It is shown in Fig.2.30 that the strain-fracture ratio reduces when strain rate increases. Moreover, the temperature sensitivity of the fracture strain is not monotonous; so it is neglected. The effect of temperature on strain-fracture relation begins from 300°C and it is significant at higher temperatures [Borvik, 2001].

(a)

(b)
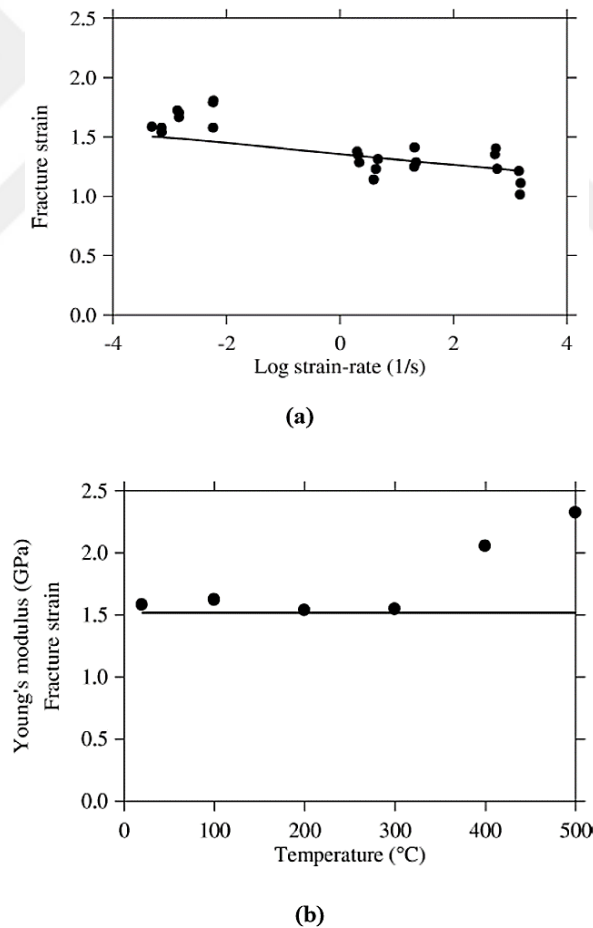
Figure 2.30: A comparison between model results (straight lines) and experimental data (dotted lines) for Weldox 460-E steel: (a) Fracture strain vs. log strain rate, (b) Fracture strain vs. temperature. [Borvik, 2001]

2.9 Ductile fracture models

2.9.1 Plasticity model (JC)

The Johnson Cook fracture model has been applied that includes the impact of stress triaxiality, strain rate, and temperature. It is shown in Equation 2.1 [Johnson, 1985].

$$\bar{\varepsilon}_f = [D_1 + D_2 \, exp(D_3\eta)][1 + D_4 ln\dot{\varepsilon}^*][1 + D_5 T^*] \qquad 2.1$$

Here variables including D1 to D5 can be termed as parameters of the material, σ* is the ratio of the average of the first set of brackets of the formula, which monotonously represents the stress triaxiality impact, it follows Hancock [1976], and it can be traced back to the concept of the void growth explained by McClintock [1968], Rice and Tracy [1969]. This model is based on damage-accumulated criteria assumed in a linear way as shown in Equation 2.2 [Johnson, 1985].

$$D = \sum \frac{\Delta\varepsilon}{\varepsilon f} \qquad 2.2$$

Here $\Delta\varepsilon$ represents equivalent plastic strain increment while ε_f represents equivalent strain required for a fracture. The fracturing process takes place at D=1.

This fracture model is quite popular because it offers formulation simplicity, easy calibration and considers useful material parameters discussed by Johnson and Holmquist [1989]. Cook and Johnson [1985] only determined the positive stress triaxiality range based on some tensile and shear tests, and no small or negative value of stress triaxiality has been found. For steel, Johnson and Cook [1985] even neglected the data of torsion testing in the fitting curve. Perhaps, one function is not able to express two different fracture mechanisms over the range of stress triaxiality from negative to positive including shear de-cohesion and void growth. It is proved that ductility of aluminum is not a monotonic function of stress

triaxiality [Wierzbicki, 2005]. For effectively applying the Johnson-Cook fracture model, the researchers extended this model in different ways. Liu et al. [2014] proved that Johnson-Cook fracture model can be used as a damage initiation model, and it is coupled with damage evolution in metal cutting simulations. Moreover, the damage evolution combines the impact of two different fracture modes. Bao and Wierzbicki [2004b] extended the Johnson-Cook fracture model in their fracture locus to make the high stress triaxiality of a component similar to Johnson-Cook fracture model but the other parts were expressed in different ways.

EXPERIMENTAL WORK AND MATERIALS

3.1 Workpiece materials

The work-piece material, which has used for investigation, was Steel alloy 36-A. Its chemical composition is given in Table 3.1. The materials were hot rolled and annealed to assure the tensile strength of 758 MPa. The annealing process was carried out within the temperature range 843–871°C for two hours followed by cooling down to room temperature in the next two hours. After the annealing process, the tensile strength was reduced to approximately 550 MPa. Aluminum alloy 5052 was also used while evaluating the performance of the novel tool introduced in the thesis. Its chemical composition is given in Table 3.2.

Table 3.1: Chemical Composition of Steel 36A.

Materials	C	Si	Mn	Ni	Cu	Cr
Steel 36 A	0.41~0.51	0.17~0.37	0.50~0.80	≤0.30	≤0.25	≤0.25

Table 3.2: Chemical Composition of Aluminum 5052

Materials	Mg	Cr	Fe	Si	Mn	Zn
Aluminum 5052	2.2-2.8	0.15-0.35	0.40	0.25	0.10	0.10

Figure 3.1: Workpiece Materials

3.2 Blanking Die

The blanking die material, which was used for investigation, was 1.2379 steel. Its chemical composition is given in Table 3.3. This component is composed of three main parts (shown in Fig.3.2), which are:

1- Punch Holder

This part is labeled as "A" in Fig. 3.2. It is used to adjust punch movement for assuring no deflection from the die block.

2-Die Block

The die block (Fig. 3.2-part B) is the female part of a complete blanking die, which is used to manufacture the piece parts according to the required specifications.

3- Punch

A punch is a male member of a complete die, which mates or acts in conjunction with the female die to produce the desired effect on the work-piece material. A die can be a simple tool, which is composed of a punch, a die block, and a stripper but it can be used for extremely complex mechanisms and operations (Fig.3.2 Part C).

Table 3.3: Chemical Composition of 1.2379 steel (wt.%).

Element	C	Mn	Si	Cr	Mo	Ni
Content%	1.512	0.221	0.673	10.63	0.683	0.282
Element	Co	P	S	V	W	Fe
Content%	0.219	0.0311	0.0321	0.81	0.258	84.61
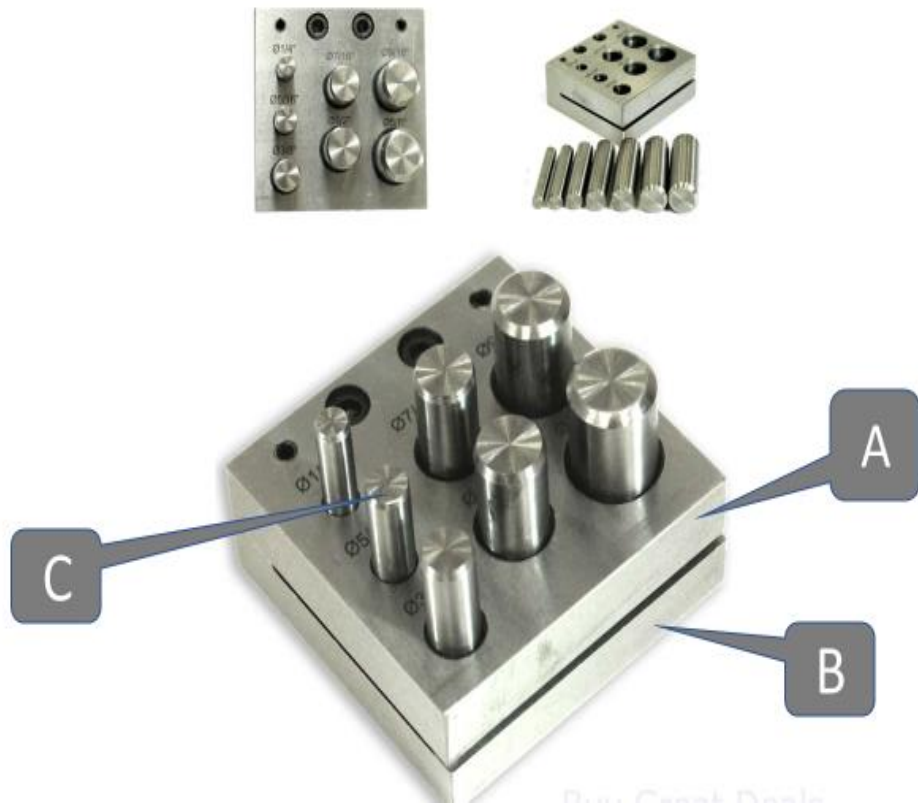
Figure 3.2: The blanking die used in the study

3.3 Punch test

The punch tests were performed at room temperature as well as some elevated temperatures (25, 100, 160 and 285˚C). For this purpose, an Instron SFL2702 Environmental Chamber was used with the MTS Series 810 hydraulic testing machine. The load cell system of the MTS testing machine was chosen at 250KN. All the tests were performed with the same crosshead velocity of 1.67 mm/sec to assure quasi-static conditions.

Figure 3.3: Punch test

3.4 Impact of various parameters on blanked-edge quality and punch-load/stress

In the following experiments, the effects of blanking clearance, punch tip geometry, corner radius, heat, PVD coating, friction, and PDC (Polycrystalline Diamond Compact) punch on the sheared edge quality have been investigated.

3.4.1 Punch-die clearance

The clearance between the punch and the die (i.e. the blanking clearance) is a major process parameter for the blanking process. It is a well-established fact in the literature that blanking clearance has a significant effect on blanking force and shear-edge quality.

In this experiment, we have chosen three values for clearance to study its effect on cutting force and edge quality. The punch diameter should be reduced to obtain different clearance values at a distance of 5mm, which is possible by applying the turning process after heat treatment on the punch head. It is shown in Fig.3.4.

Clerance 1 = 0.04 mm , Clerance 2 = 0.1 mm , Clerance 3 = 0.3 mm
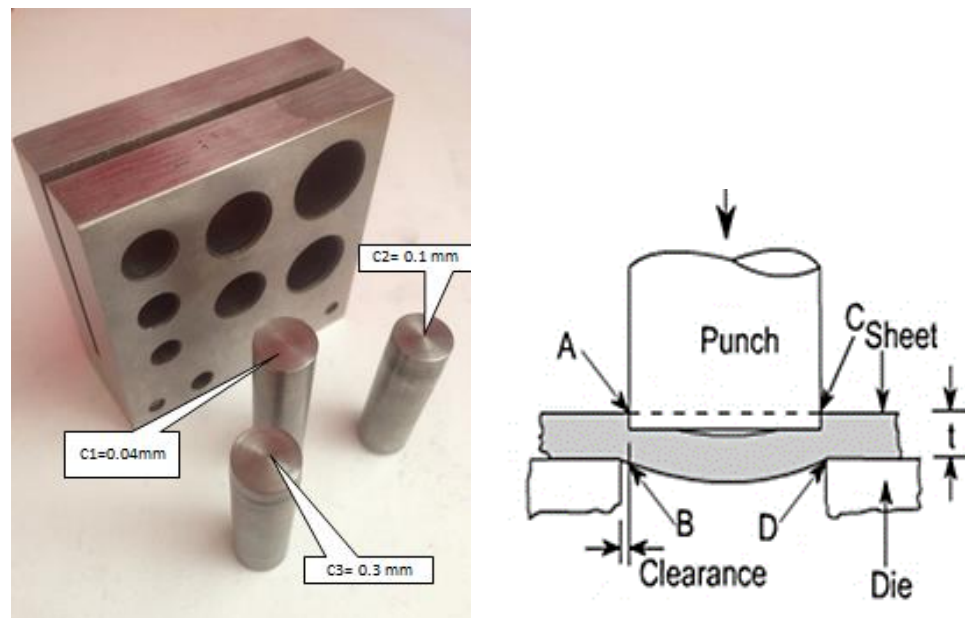
Figure 3.4: Punch-die clearance

3.4.2 Punch tip geometry

Depending on the strength and thickness of the blanked material, it is possible to estimate the expected punch load during the blanking process. If the punch cannot sustain high loads or in case of existence of snap-through forces, punch load must be reduced. The load on the punch can be reduced by altering the punch-tip geometry by having either a shear angle or by a conical punch.

A new design has been developed as a part of this study, which can be termed as flat-face center point as shown in Fig. 3.5. This design provided us with tensile areas before cutting, which contributed to reducing the elasticity of the workpiece surface.

Figure 3.5: Punch-tip geometry

To determine the effect of the tool head on the cutting force and to assure the quality of the edges, the following six tools were considered.

1	Flat face punch		4	Flat-face center-point punch	
2	Shear punch		5	Concave shear punch	
3	Concave punch		6	Y shear punch	

3.4.3 Punch corner radius

The punch corner radius can be considered as a simulation of tool wear, which is shown in Fig. 3.6. This part affects the change in the punch corner radius when a cutting force was applied, and the quality of the edges was studied. In this context, three different corner radii were selected, which are given below:

$$R_p = 0.01 \ mm$$

$$R_p = 0.1 \ mm$$

$$R_p = 0.2 \ mm$$
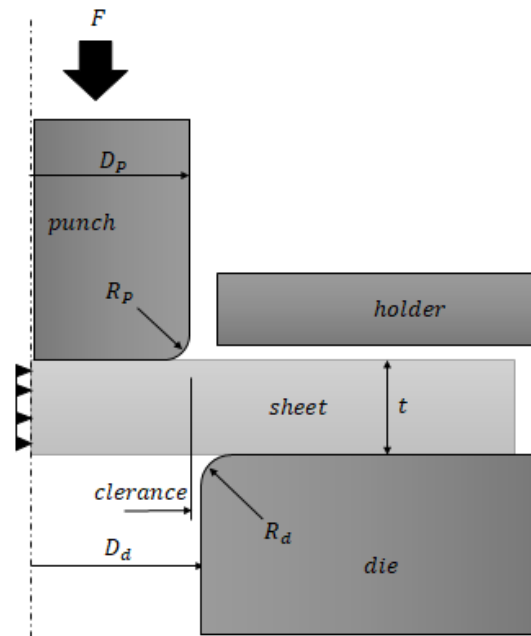
Figure 3.6: Item of blanking process (left) and its schematic depicting corner radius (right)

3.4.4 Effect of temperature on the blanking process

In the academic circles of applied engineering, there is a great interest in knowing further about the heat because it has diverse effects on the blanking process. The heating of the sheet metal and tool parts, which is done during the blanking process, may directly affect the material behavior; therefore, it may affect the work-piece quality and the tool life. In addition, the temperature is an essential selection criterion for choosing the right lubricant and tool coating. Thus, there is a great deal of interest in knowing the role of blanking temperature.

In this segment, the effects of different temperatures on the strength and the quality of the edges of a workpiece were investigated. The samples were heated using a furnace (shown in Fig. 3.7) to raise their temperatures before initiating the blanking process. In fact, they were overheated by around $10°C$ to assure the following sample temperatures of the five selected samples:

$$T_1 = 25°C \quad T_2 = 100°C \quad T_3 = 160°C \quad T_4 = 270°C \quad T_5 = 500°C$$
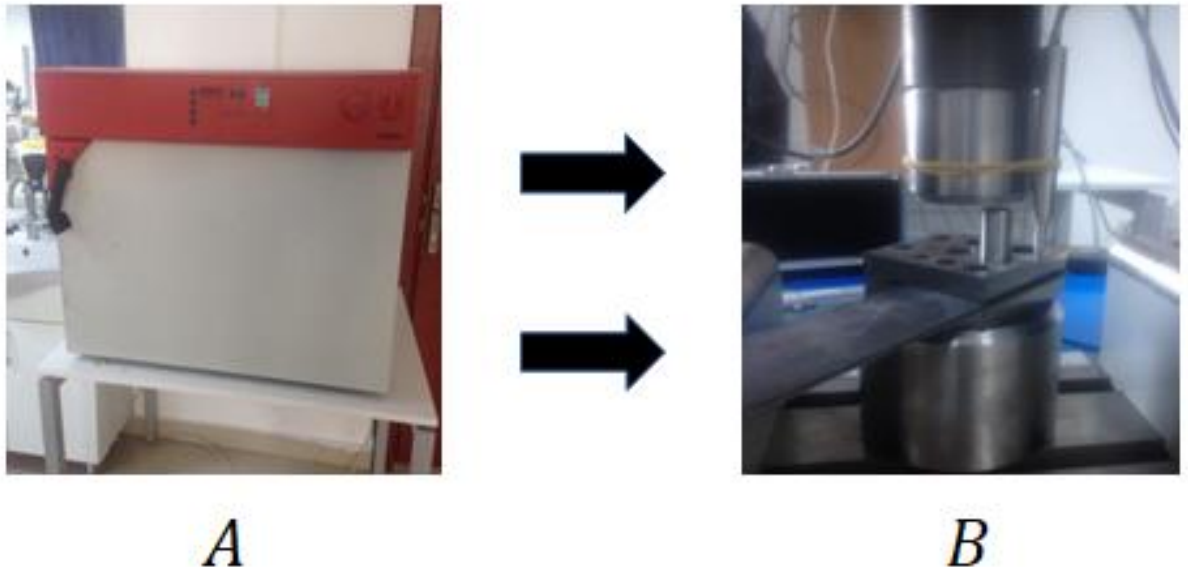
Figure 3.7: (A) Heating the samples, (B) Blanking process

3.4.5 PVD coating on punch

In these experiments, 1.2379 cold-work tool-steel was used as a punch material. As a workpiece material, 2-mm-thick and 40-mm-wide hot-rolled low-carbon 36-A steel was used. The chemical compositions (wt.%) of the steel punch is as follows: 1.55 C, 0.30 Mn, 0.25 Si, 12.0 Cr, 0.70 Mo, and 1.0 V. The punches were hardened and then tempered to get a core hardness of 60HRC. The microstructure of the punch consists of primary and secondary carbides of Cr, Mo, and V, which exist in the fine-tempered martensitic matrix, as shown in Fig. 3.8.
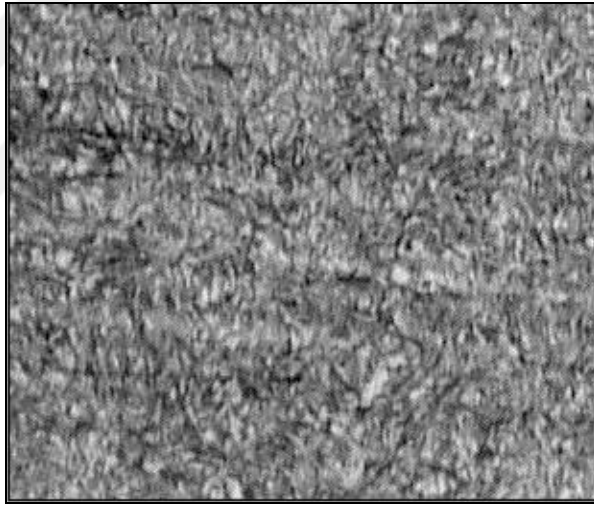
Figure 3.8: The microstructure of the punch

After applying the heat treatment, the punches were ground to reach a surface roughness (Ra) $\pm$ 0.2 μm, as shown in Fig.3.9. The experimental study was performed for the coated and uncoated states of 1.2379 tool steel. The TiSiN, AlCrN, AlTiN, TiN, and CrN coatings was carried out at Ionbond, IHI Group, Istanbul by using a HaUzer Rapid-Coating-System (HCS) deposition machine, which is shown in Fig. 3.11. In Fig. 3.10, we have shown the coating with a thickness of ca. 4 μm and a hardness of 3200 HV 0.05.

Figure 3.9: Surtronic 3+device to measure the surface roughness
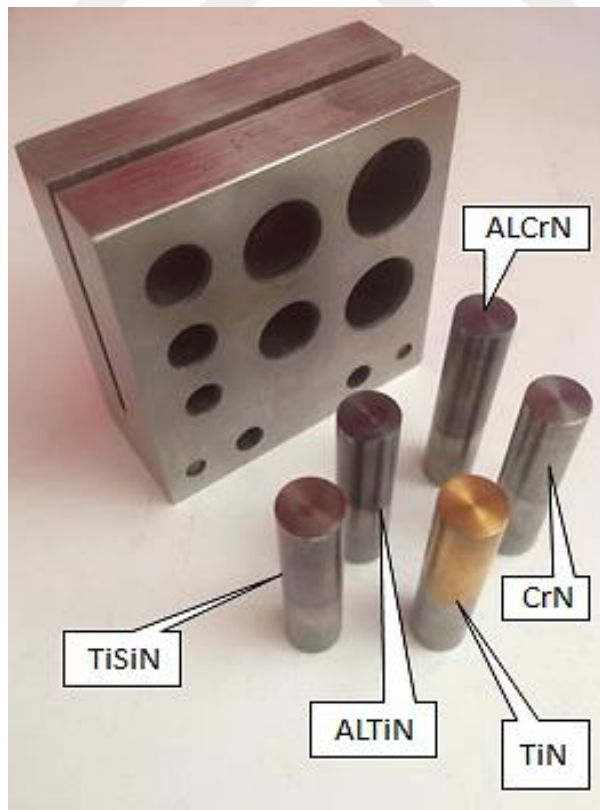
Figure 3.10: TiSiN, AlCrN, AlTiN, TiN, and CrN coatings

Figure 3.11: Hauzer Rapid-Coating-System (HCS) deposition machine

3.4.6 Effects of friction

The effects of friction on part edge quality, punch load and punch stresses were also studied. The coefficient of friction remained in the range of about 0.1-0.6. Since there is a difference between the coefficient of friction for different types of coatings, its effect on the quality of edges, cutting force and wear resistance were studied. The following table summarizes the friction properties of the different punches used in the experiments.

Table 3.4: The friction coefficient of all the punches.

Punches	Types of coating	lubrication	Coefficient of friction
Punch 1	TiSiN	No	0.4
Punch 2	AlCrN	No	0.55
Punch 3	AlTiN	No	0.6
Punch 4	TiN	No	0.5
Punch 5	CrN	No	0.55
Punch 6	No coating	With oil	0.6
Punch 7	PDC	No	0.65

3.4.7 PDC (Polycrystalline Diamond Compact) Punch

In this study, PDC punch was tested for wear resistance, which is shown in Fig. 3.12. We tested this punch to compare it with the coating technology in terms of its resistance to wear; so, this part was imported from China. In fact, there are many advantages that make PDC suitable in the blanking process such as:

1) High wear resistance

2) High impact resistance

3) High thermal stability

4) High density (low porosity)
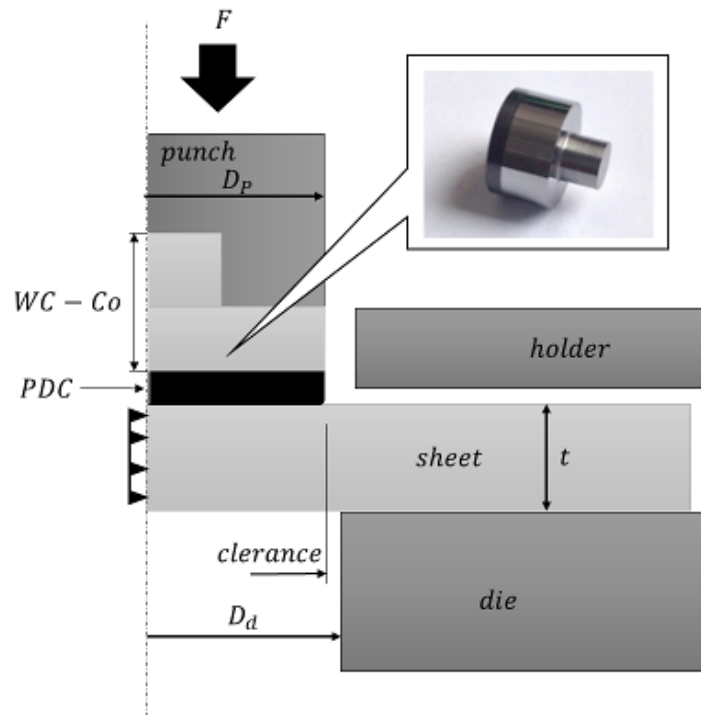
Figure 3.12: PDC (Polycrystalline Diamond Compact) Punch

3.5 Wear test of punches

Seven different punches with different specifications were tested to determine their wear behaviors such as the wear that occurs on the edges when a sample undergoes large number of cutting processes. In order to test, a manual set-up was manufactured, which has been illustrated in Fig. 3.13. After inserting the die in the experimental apparatus, it was noticed that torque was noticed at the lever when the cutting operation was completed, and later, the punch head returned to its original position with the help of a spring. To investigate the amount of wear on the edge of the punch, the cutting operation was performed 1,000 times per punch. Table 3.5 shows the coating, lubrication, and the number of times every punch has been used.

Table 3.5 Test specifications for different punches

the punches	types of coating	lubrication	Number of cycles
Punch 1	TiSiN	No	1000
Punch 2	AlCrN	No	1000
Punch 3	AlTiN	No	1000
Punch 4	TiN	No	1000
Punch 5	CrN	No	1000
Punch 6	No coating	With oil	1000
Punch 7	PDC	NO	1200
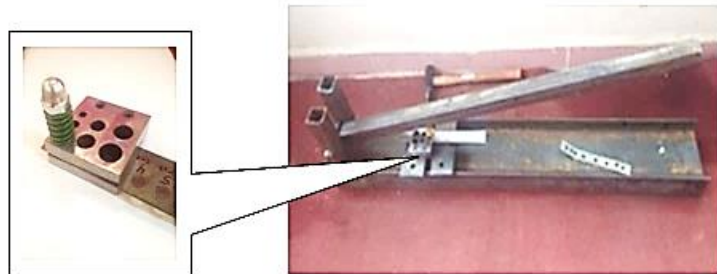
Figure 3.13: Manual Punching

56

3.6 Analysis of Wear by Scanning Electron Microscopy (SEM)

Scanning Electron Microscopy (SEM) is very effective for microanalysis and failure analysis of solid inorganic materials. Electron microscopy is performed at high magnifications. It generates high-resolution images and precisely measures very small features and objects. This technique has been used in our experiments to notice and report even the minutest change in the samples after the experimental process. This examination was conducted at the Institute of Material Sciences and Nanotechnology (UNAM), Bilkent University.

Figure 3.14: Scanning Electron Microscopy (SEM)

NUMERICAL
MODELLING

In this Section, the details about the developed numerical is given. Firstly, the theory of the Finite Element Method (FEM) including the details of the time integration schemes used in the analysis is briefly explained. Secondly, the material model used, Johnson-Cook, is introduced. Lastly, the details about the FEM of the cutting process is given.

4.1 Introduction to Finite Element Modeling (FEM)

Generally, the engineering analyses pertaining to mechanical processes or technology are conducted using differential equations, which help finding out fundamental physical rules including energy conservation, equilibrium, mass conservation, Newton's laws, principles of thermodynamics, and Maxwell's equations. It is noticed that when these principles are applied, solving equations is sometimes not possible specifically in case of non-linear models, which are solved using partial differential equations. Some basic issues pertaining to everyday geometrical problems, for instance, rectangle of a circle having basic boundary conditions, can be solved.

FEM is a discretization process applied in structural mechanics, and it includes sub-division of a mathematical model in disjointed components (which do not overlap), they are used in basic geometry, and they are termed as finite elements. Every element responds to a finite degree of freedom with an unknown function/s or nodal points.

Then the behavior of a mathematical model is approximated using a discrete model, which can be obtained through assembling several elements. This concept of disconnection assembly is a natural concept that takes place when many artificially constructed and natural systems are examined. For instance, a structure such as a bridge, airplane, or engine may be a combination of simple components. Contrary to FEM, finite elements don't overlap.

4.2 Finite-element model

FEM helps resolving complicated engineering problems in those situations, when the orthodox analytical process either fails or have limitations. This method is generally used for discretizing arbitrary domains with simple elements, using which, it is easy to solve differential equations (Fig 4.1). For every element, this model assumes a convenient approximation and the equilibrium conditions. If these conditions are met, the values of the unknown constants and variables including displacement, strain and stress can be found (Rao, 1999).
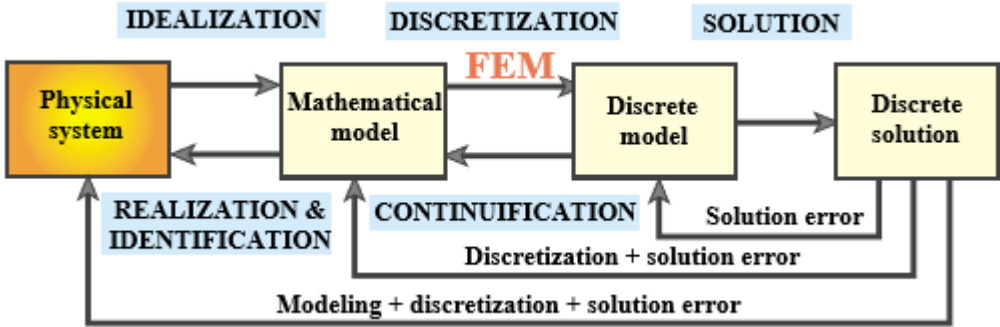
Figure 4.1: Physical simulation steps (Felippa, 2007)

We can list the FEM model in steps given below (Huebner *et al.*, 2001):

- **Discretizing continuum**

The continuum needs to be converted/segmented into elements.

- **Choosing interpolation functions**

Every element is assigned its node, so, the polynomials represent interpolation function that represents the field variable variation of an element. In this case, we have given a displacement field that has been expressed with the help of a shape function $N(x)$:

$$u(x) = N(x)d^e,\qquad 4.1$$

Here, d^e shows the element's nodal displacement, $N(x)$ represents the distribution of nodal displacement.

- **Finding properties of the elements**

The properties of the elements are determined through the matrix equations. Here FEM shows dependent variables like elastic strain D^* as well as stress σ:

$$D^* = u' = Bd^e,$$ 4.2

$$\sigma = C:D^*,$$ 4.3

In this case, u' is a displacement gradient and C represents elasticity while B stands for strain matrix.

- **Using element properties for solving the system equations**

When the matrix equations combination takes place, they show the overall system's behavior based on the following equilibrium equation:

$$\sigma' + \rho b = 0,$$ 4.4

In this case, ρ represents density while body forces are debited as b. Equation 4.4 has been expressed in its strong form, and it can be converted into a weaker form with the help of test function $\delta u(x)$, which is introduced for satisfying kinematic constraint. This virtual work principle is as follows:

$$-\delta W = \int_{\Omega} \sigma \delta D^* d\Omega - \int_{\Omega} \rho b \delta u d\Omega - \int_{\Gamma} g \delta u d\Gamma,$$ 4.5

In this case, both b as well as g are surface loads and body components, Ω is continuum domain and Γ shows traction boundary conditions. If we put equations 4.1 and 4.2 in equation 4.5, we obtain the following boundary-value problem:

$$\sum_{i=1}^{n_{el}} \delta d^{i^T} \left\{ \int_{\Omega} B^T \sigma d\Omega - \int_{\Omega} N^T \rho b d\Omega - \int_{\Gamma} N^T g d\Gamma \right\} = 0.$$ 4.6

In this case, the assembly operator creates an equation system for every element.

- **Imposing boundary conditions**

The system of equations is changed according to the boundary conditions in the elements/nodes.

- **Solve the system equations**

The solution of simultaneous equations is found for obtaining unknown nodal variables. In case of Equation 4.6, the first term represents internal nodal forces, which have taken place because of induced stresses, as shown in Equation 4.7, and the rest of it is right according to external nodal forces (Equation 4.8).

$$f_{int} = \int_{\Omega} B^T \sigma d\Omega = k^e d^e,$$
4.7

$$f_{ext} = \int_{\Omega} N^T \rho b d\Omega + \int_{\Gamma} N^T g d\Gamma.$$
4.8

The equations 4.7 and 4.8 attain a situation of equilibrium in the middle of external and internal nodal forces. We can solve them with the help of an iterative scheme that shows a solution in terms of a displacement field. Equation 4.7 k^e represents the elemental stiffness e, which is a displacement function in case of non-linear systems: $k^e = k^e(d^e)$

- **Computing of other variables**

Some significant fields such as strains or stresses are computed using displacement field Equations 4.2 & 4.3.

4.2.1   Iterative Solution Technique

These techniques are applied for FE analyses as they make it possible to find the unknown variables and constants in a non-linear system. This non-linearity exists because the stiffness matrix is either displacement-dependent and/or force-dependent. This non-linear behavior is linked with solid mechanics, and it takes place because of geometric, structural or contact non-linearity.

Major displacements and rotations might result in geometric non-linearity in the presence of even a little strain. It shows that structural deformation is significant,

so, the finite-deformation theory applies in this case instead of small-strain theory. Non-linearity is also obvious when small displacements exceed any dimension of a deformed structure, for example, a thin-sheet metal (Bathe, 1996).

Material non-linearity might also occur because of a non-linear stress-strain relation, in which, material behavior depends on the existing deformed state or previous deformation. Material non-linearity might not just exist in a non-elastic region because it is found in elastic regions as well. This happens in case of hyper-plastic substances such as rubber. Moreover, interaction between deformable and other bodies also causes non-linearity. The process of deformation is a major cause behind non-linearity.

Non-linear equations are solved through many techniques including the direct iteration process, Euler's method, and modified, quasi and simple Newton-Raphson processes. The Newton-Raphson process has been applied for solving non-linear equations in the current thesis. It has been selected as it offers a quicker convergence rate than all the other options (Systemes, 2010).

The Newton-Raphson process is repetitive in nature and works by finding root of an equation. The non-linear equation $f_{ext} = k^e d^e$ has been expressed in equations 4.7 and 4.8. For finding the solution to this equation, we need to define the residual function: $r(d) = f - k(d)d$. In this case, the objective is minimizing the residual displacement value d, which has to be re-calculated until accurate value is found.

The expression $r(d^{i-1}) = f - k(d^{i-1})d^{i-1}$ shows the process, through which, the residual value is computed iteration after iteration. The Taylor series is used for the expansion of residual on i^{th} iteration while the increment Δd^i is given below:

$$r(d^i) = r(d^{i-1} + \Delta d^i) = r(d^{i-1}) + \left[\frac{\partial r(d)}{\partial d}\right]_{d^{i-1}} \Delta d^i + \text{high} - \text{order terms}. \quad 4.9$$

When iteration creates residual force $r(d^i)$, it becomes zero. If we neglect high order terms as they contribute very little, it results in the equation given below that computes increment in displacement:

$$\Delta d^i = \frac{-r\left(d^{i-1}\right)}{\left[\frac{\partial r(d)}{\partial d}\right]_{d^{i-1}}},$$ 4.10

In this equation, the right-side denominator is *Jacobian matrix*. The solution approximation is calculated as soon as the iteration lasts using the formula given below:

$$d^i = d^{i-1} + \Delta d^i.$$ 4.11

The iteration carries on until a specific tolerance level is attained.

The Newton-Raphson process takes more time the Jacobian matrix has to be created and solved after each iteration. In the alternative process modified Newton-Raphson method, the Jacobian matrix is occasionally recalculated. In case of Newton-Raphson method, the Jacobian approximation is calculated, which is generally used to solve non-linear problems (Systems, 2010). There is a major shortcoming, and that is their instability and accuracy for many non-linear cases, but still, they need shorter solution time.

4.2.2 Convergence Control

The criteria for convergence are finalized during the calculations, which concludes iterations after achieving the required accuracy level. The computation should be accurate and spend appropriate computational time. If we go for pinpoint accuracy, excessive computation time will be spent on attaining exactness/high accuracy, but that kind of accuracy isn't actually needed. When the tolerance levels are excessively loose, equilibrium error will be higher, and the solution will be incorrect, so there is a trade-off between accuracy and computation time and effort. In case of commercial FE software's, the criteria for convergence are generally reliant on relative and/or absolute residual forces' value, $\frac{(r(\Delta d^i))^T r(\Delta d^i)}{(r(d^i))^T r(d^i)} < \text{TOL}$, and displacement values, $\frac{(\Delta d^i)^T \Delta d^i}{(d^i)^T d^i} < \text{TOL}$. In this case, equilibrium is attained after satisfying both the equilibrium checks for each iteration. In the FE simulations 5×10^{-3} is used as the TOL value.

4.2.3 Methods to Perform Time Integration

When the effort is made to calculate the unknowns including stress, displacement, and strain, the integration of rate equations should be done according to time. When the constitutive rate equations show non-linearity, integration is possible in increments while stress/other variables are updated in each increment. There are two categories of computational algorithms: Explicit and implicit.

In case of explicit algorithms, the data obtained at time t helps finding out unknowns on time interval $t + \Delta t$. These explicit processes include Euler as well as Runge Kutta methods (Huang, 1991). During explicit FEM analyses, the matrix stiffness is updated after every increment, after which, a new load is applied. This method has a drawback that it works in small time intervals for accurate solution that takes long time for computation, and if the process is left incomplete, the solution becomes incorrect. The explicit methods are time taking, and the time needed for a solution is comparable to the time needs for a wave that propagates through the analyzed structure (Bathe, 1996). This critical time Δt_{cr} is calculated using the stiffness and mass as follows:

$$\Delta t \leq \Delta t_{cr} = \frac{T_{Nmin}}{\pi} = \frac{2}{W_{Nmax}} \leq \frac{2}{W_{Emax}}, \qquad 4.12$$

Here Δt_{cr} represents step size of the critical time, T_{Nmin} represents least time period of the finite-element mesh, W_{Nmax} represents the system's top natural frequency, and W_{Emax} represents the individual elements' top natural frequency (Bathe, 1996).

In case of implicit algorithms, the data/information on time intervals t and $t + \Delta t$ helps calculating the unknowns pertaining time: $t + \Delta t$. For instance, Euler method is an example of a totally implicit process. In case of choosing an implicit process, Newton-Raphson iterations are needed after every increment that helps attaining equilibrium in the forces of the internal structure in the presence of externally applied loads having specific tolerance (mentioned in Section 4.2.2). In case of explicit analysis, equilibrium is not enforced that makes implicit analysis more correct. By choosing implicit analysis, it is easier to handle issues including

snap thru, cyclic loading, and snap back when sophisticated control processes like displacement and arc length control are applied. In case the Jacobian stiffness matrix is used for implicit analysis, it should be updated as well as reconstructed every time after iteration, so its computation is expensive.

4.3 Explicit analysis

While planning/conducting analysis, the problem should be numerically solved. In case of dynamic analysis, this explicit time integration becomes useful while solving problems pertaining to high-speed deformations in short time as it helps calculating a lot of incremental points at lower computation cost. It is preferable for contact definition cases. The size of the element as well as time needed for running explicit analysis has a direct link with each other.

In this type of analysis, the velocity and the displacement are known at the start of every increment, which means no need for inverting global mass and stiffness matrix after every increment, and it reduces computation work. In this case, the time increments should be smaller as compared to the critical time increment, which makes the process conditionally stable while the increments are small for preserving the resulting stability. When there are smaller incremental, incremental results do not deviate much from the exact solution. In this case, the accuracy is higher if calculations are done for new increment, so, there is no requirement to control accuracy.

This method's stability is linked with time, during which, a stress wave moves through the element. In case of smaller element, or a high-speed wave, the time increment should be limited. Normally, the increment is smaller as compared to the time needed for a stress wave to move across an element, covering node-to-node distance. In this way, this method is effective for analysis because its analyzing time is just a little more than the stability limit. A few quasi-static

methods, which have proper mass scaling, decrease the speed of wave that results in increasing the critical time increment for analyzing.

The explicit process suits high-speed/dynamic incidents as well as slow/quasi-static analyses. For high-speed events, small increments require lengthy calculations, which are needed to understand large deformation in short time. In case of quasi-static analyses, generally deformation is slower that causes a dynamic response. This dynamic impact is negligible. The contact treatment is simplified that makes it suitable for quasi-static/dynamic analysis between the surfaces. The time requirements for analysis depends on the model size as well as the overall simulation time with a condition that the mesh size will remain unchanged. Increasing any two factors increases the calculation time.

The explicit process is generally considered better before applying the implicit method as it can convert a mass matrix into a diagonal matrix, which is also considered as a lumped mass. It reduces calculations, which are required for time increments up to 4000 times in case of a 3D FE analysis. This means that the data storage requirement for every incremental calculation is quite lower if the explicit method is chosen.

Explicit analyses method includes using central difference for calculating next increment. In that way, the satisfactory conditions for equilibrium equations apply at the start of every increment t_i. The calculation of acceleration on t_i helps finding displacement at t_{i+1} and velocity at $t_{i+1/2}$. These calculations are less expensive, and they are conducted with the help of "lumped" element matrices. The displacement u^N_{i+1} and velocity $\dot{u}^N_{i+1/2}$ can be computed using the following expression:

$$u^N_{i+1/2} = u^N_{i-1/2} + \frac{\Delta t_{i+1} + \Delta t_i}{2} \ddot{u}_i^N \qquad 4.13$$

$$u^N_{i+1} = u^N_i + \Delta t_{i+\dot{u}^N_{i+\frac{1}{2}}} \qquad 4.14$$

In the above-mentioned expressions, u^N represents the degree of freedom while i represents the increments. The procedural efficiency lies in using lumped stiffness in the form of diagonal matrices, which is easy to compute in the start of every increment as shown by Equation 4.15. Since these matrices can be easily inverted, so, the vector multiplication needs just a single process for every degree of freedom. In this case, the acceleration is computed as follows:

$$\ddot{u}_i^N = ([M]^{NJ})^{-1} \left(\{R^{ext}\}_i^J - \{R^{int}\}_i^J \right) \tag{4.15}$$

Here, $[M]^{NJ}$ represents mass matrix $\{R^{ext}\}_{i,}^J$ represents applied load vector while $\{R^{int}\}_i^J$ shows internal force vector. The elements contribute to this internal force vector in a way that the global stiffness matrix isn't required.

4.3.1 Stability

The mentioned process' stability depends on the top system frequency. Equation 4.16a exhibits the system's limit with/without damping.

$$\Delta t \leq \frac{2}{\omega_{max}} \left(\sqrt{1 + \xi_{max}^2} - \xi_{max} \right) \tag{4.16a}$$

$$\Delta t \leq \frac{2}{\omega_{max}} \tag{4.16b}$$

In the expression given above, ω_{max} represents highest natural frequency, while ξ_{max} is the concerned dampening ratio.

While operating ABAQUS, small damping is introduced in the shape of bulk viscosity for controlling high frequency oscillations, which might take place when the analysis is conducted. This impact also applies like a linear impact; however, in case of solid continuum elements, it applies as a quadratic impact while the

effect, which is utilized for compression state prevents high velocity from collapsing, and so, the volume immediately reduces to zero.

4.3.2 Estimating the size of stable time increment

It is donated by Δt, and generally, it is smaller as compared to the critical time increment size (Δt_c):

$$\Delta t \leq \Delta t_c = \frac{l^e_{min}}{c_d}$$ 4.17

Here, l^e_{min} has the least value and impact on the model while c_d represents the speed of sound for element. c_d that is given in Equation 4.18. We only get the estimate of the highest stable time increment. Normally, using shorter time increment is better to conduct the analysis. In case of 2D models, ABAQUS applies reduction factor having value range $\frac{1}{\sqrt{2}}$ and 1. In case of 3D models, the value lies in the range $\frac{1}{\sqrt{3}}$ and 1. The stress wave moves with a certain speed within a material, which depends on Young's Modulus E and density ρ.

$$c_d = \sqrt{\frac{E}{\rho}}$$ 4.18

In the expression given above, it is obvious that the critical time increment increases when the softer material is used (low Young's Modulus value) or the density is higher. It results in manipulating the time required for running explicit analysis with the help of software.

4.3.3 Time reduction

The requirement for time to perform the explicit analysis depends on the simulation time, size and number of elements. When the mesh size is given, the simulation time period becomes a decisive and final factor. For decreasing the

time needs for analysis, a few methods are used. Speeding up a simulation is possible but if the simulation speed is increased a lot, it results in undesired kinetic impact observable in the form of high inertia, which might change the result of a simulation, while some parameters change because of it. It is not recommended to increase the simulation speed in case of existence of rate dependent parameters because in that case the result will change without letting the user notice it.

It is also possible to save time through mass scaling and raising the material density ρ, which decreases the simulation time period rather than wave propagation time, which raises the Δtcr value, and it speeds up the simulation. Changing density does not change rate dependent parameters; however, it causes inertia and consequently increases simulation.

Generally, a model consists of a mixture of large and elements, but it has smaller elements as well, which move slower, and besides, the size of small elements determines the increment length. When the small elements are significant in numbers, the mixed time integration process is used. While using ABAQUS, this process gives different lengths of time increment according to the element size. Larger elements have fewer time increments as compared to the smaller ones. The application of the central-difference integration rule has been illustrated in Section 4.3.2 with different time lengths.

4.3.4 Energy monitoring

For conducting explicit dynamic analysis, monitoring a model's energy is important. In this case, the overall energy of a model needs to be a constant while there should be small artificial energies as compared to real energies, for example kinetic and strain energies. In order to conduct quasi-static analysis, the kinetic energy should be a specific fraction of the strain energy. In case of contact/constraints, the energy dissipated through constraint/contact should be monitored. In all the cases, they are close to zero.

4.4 Fracture of ductile metals

The fractures of ductile metals are caused by two major processes:

1. Ductile fracture that takes place when voids nucleate, grow, and coalesce.

2. Shear fracture that takes place because of localization of the shear band.

In soft metals, necking occurs due to extensive plastic deformation. After necking, voids or crack nucleation start in the solid and grow. Then, coalescence of micro voids occurs that leads to separation. Fig. 4.2 illustrates the elongation and crack formation because of stretched voids by connecting the voids. [Billal, M.K., et al 2015]
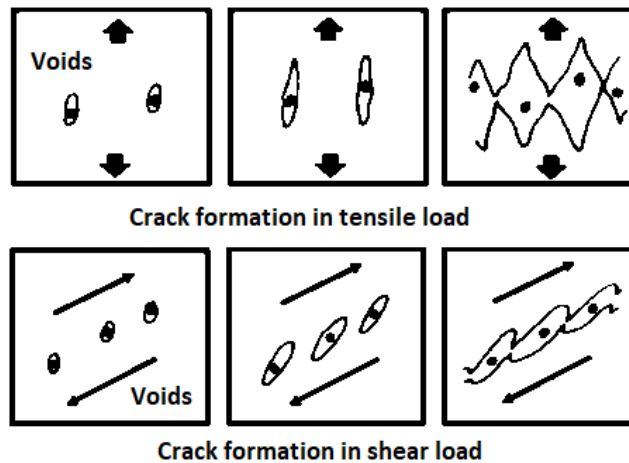
Figure 4.2**:** Crack Formation Under Tensile/Shear Loading [Billal, M.K., et al 2015].

4.4.1 Ductile damage criterion

This criterion predicts the damage as a result of nucleation, and void growth and coalescence. According to this model, the plastic strains at the onset of damage can be expressed below:

$$\bar{\varepsilon}_D^{pl}(\eta, \dot{\bar{\varepsilon}}^{pl}) \qquad\qquad 4.19$$

Here, $\bar{\varepsilon}_D^{pl}$ indicates stress triaxiality, strain rate. $\eta = -p/q$ shows stress triaxiality, p represents pressure stress, q shows Von Mises equivalent stress, and $\dot{\bar{\varepsilon}}^{pl}$ represents equivalent plastic strain rate [Hibbitt, Karlsson, and Sorensen 2016].

The damage initiation criterion meets after satisfying the condition given below [Hibbitt, Karlsson, and Sorensen 2016]:

$$\omega_D = \int \frac{d\ \bar{\varepsilon}^{pl}}{\varepsilon_D^{pl}(\eta,\dot{\bar{\varepsilon}}^{pl})} = 1 \qquad 4.20$$

On every increment, ω_D increases, which can be computed using the following equation [Hibbitt, Karlsson, and Sorensen 2016]:

$$\Delta\omega_D = \frac{\Delta\ \bar{\varepsilon}^{pl}}{\varepsilon_D^{pl}(\eta,\dot{\bar{\varepsilon}}^{pl})} \geq 0 \qquad 4.21$$

4.4.2   Shear damage criterion

This criterion predicts the damage that takes place because of shear band localization. It assumes equivalent plastic strain, which is as follows:

$$\bar{\varepsilon}_S^{pl}(\theta_S, \dot{\bar{\varepsilon}}^{pl}) \qquad 4.22$$

Here $\bar{\varepsilon}_S^{pl}$ is shear stress ratio and strain rate function [Hibbitt, Karlsson, and Sorensen 2016].

$[\theta_S = (q + k_S.\ p)/\tau_{max}]$ shows the ratio of the shear stress, q represents Von Mises stress, k_S is a material parameter (typically $k_S = 0.3$ (aluminum)) [101], p represents pressure stress and τ_{max} is the highest shear stress [Hibbitt, H., B. Karlsson, and P. Sorensen 2016].

The damage initiation criterion is met in case the condition given below is met [Hibbitt, H., B. Karlsson, and P. Sorensen 2016].

$$\omega_S = \int \frac{d\,\bar{\varepsilon}^{pl}}{\bar{\varepsilon}_S^{pl}(\theta_S, \dot{\bar{\varepsilon}}^{pl})} = 1 \qquad 4.23$$

Here, ω_S is a state variable, which affects plastic deformation in proportion to the equivalent plastic strain. After every increment during the increase in ω_S is calculated using the formula given below [Hibbitt, H., B. Karlsson, and P. Sorensen 2016]:

$$\Delta\omega_S = \frac{\Delta\,\bar{\varepsilon}^{pl}}{\bar{\varepsilon}_S^{pl}(\theta_S, \dot{\bar{\varepsilon}}^{pl})} \geq 0 \qquad 4.24$$

4.4.3 Damage evolution

The damage takes place in two forms: elastic degeneration and yielding-stress softening. The stress-strain curve reaction to the damage is shown in Figure 4.3, in which, E represents Young's Modulus, and on the onset of damage, σ_{y0} and $\bar{\varepsilon}_0^{pl}$ represent yield stress and equivalent plastic strain respectively. $\bar{\varepsilon}_f^{pl}$ represents equivalent plastic strain on failure ($D = 1$). The substances lose their capacities to carry load when D becomes equal to 1. This element is then taken out of the mesh when the sectional points lose their load carrying capacities. These reactions of the undamaged real curve are shown through a dashed curve. The damage evolution is demonstrated in two forms of softened yielding stress and degenerate elasticity $((1\text{-}D).\ E)$. The variable D, which represents the damage, and creates a unified impact on all the active mechanisms and computes based on the individual damage variables for each mechanism.

$$\sigma = \frac{F}{A} \ \ \& \ \ \bar{\sigma} = \frac{F}{A - AD}$$

$$\bar{\sigma} = \frac{F}{A(1 - \frac{A_D}{A})} \ , \ where \ \ D = \frac{A_D}{D}$$

$$\sigma = (1 - D)\bar{\sigma} \qquad 4.25$$

Here, D is the long-range comprehensive damage variable, σ is recognized as the true stress, $\bar{\sigma}$ is the effective or undamaged stress, A is an authentic exterior and outward area and A_D means defects in the exterior area.
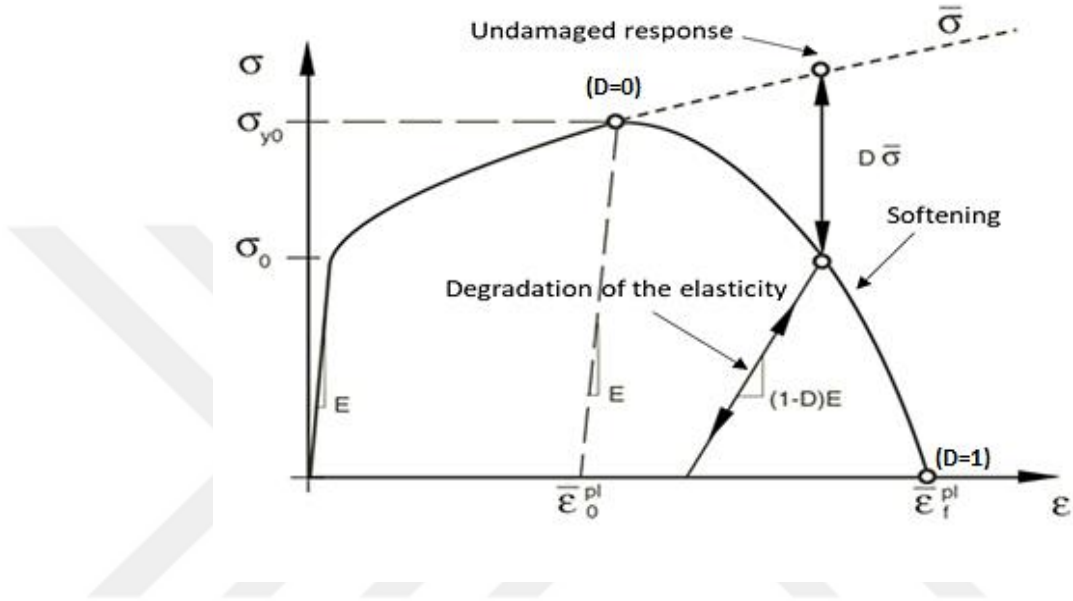
Figure 4.3: Stress-strain curve showing progressive damage degradation [Hibbitt, Karlsson, and Sorensen 2016].

It is, however, noticed that the damage initiation criterion begins at point $D = 0$, and the damage evolution builds up from this point just before the element deletion that occurs at point $D = 1$, where the elements are taken out of the calculations when the stiffness completely ends.

When the damage initiation criterion is achieved, $\dot{u}^{pl}$ (plastic displacement) is identified and recognized with the evolution equation:

$$\dot{u}^{pl} = L_e \dot{\bar{\varepsilon}}^{pl} \qquad\qquad 4.\,26$$

Where, L_e is the element's characteristic length and $\bar{\varepsilon}^{pl}$ is effective plastic strain.

The emergence of damage variable along with plastic displacement is possible to

express in exponential, tabular, and linear forms. The linear damage evolution form with plastic displacement is expressed below:

$$\dot{d} = \frac{L_e.\dot{\bar{\varepsilon}}^{pl}}{\dot{\bar{u}}_f^{pl}} = \frac{\dot{\bar{u}}^{pl}}{\dot{\bar{u}}_f^{pl}} \qquad \text{4.27}$$

If $\dot{\bar{u}}^{pl} = \bar{u}_f^{pl}$, the material stiffness will be completely degraded.

4.4.4 Plasticity model (JC)

The last model was derived keeping in view the physical priorities but now, we will consider a phenomenological model presented by Johnson and Cook (1985). It is very simple and has many available parameters pertaining to large number of materials. This model is mostly applied for simulating dynamic processes such as machining or impact. This model is subjected to strain rates, strains and heating impact. For this model, the von Mises stress is as follows:

$$\sigma = [A + B\varepsilon^n][1 + Cln\dot{\varepsilon}^*][1 - T^{*m}] \qquad \text{4.28}$$

$$T^* = (T - T_r)/(T_m - T_r)$$

The first bracket of Equation 4 - 28 shows dependence on strain while the second one shows instantaneous strain-rate sensitivity, and the third one shows temperature dependence pertaining to stress T_r, the reference temperature. T_m represents the material's melting temperature. In this context, there exists five material constants *n, m, A, B*, and *C*.

4.4.5 Damage model

This model is based on Johnson and Cook (1985) rupture criterion, there the cumulative plastic strain, is expressed as follows [Johnson, 1985]:

$$\bar{\varepsilon}_f = [D_1 + D_2\ exp(D_3\eta)][1 + D_4 ln\dot{\varepsilon}^*][1 + D_5 T^*] \qquad \text{4.29}$$

Here, $\bar{\varepsilon}_f$ represents equivalent strain to fracture, and $\eta = \sigma_m / \bar{\sigma}$ shows stress triaxiality, and σm shows average of 3 normal stresses. Here, $\bar{\sigma}$ represents Von Mises stress. On the other hand, the dimensionless strain rate $\dot{\varepsilon}*$ and homologous temperature $T*$ are same as the ones used by Johnson Cook constitutive model expressed in Equation 4.29. D_1, D_2, D_3, D_4, and D_5 are material dependent fracture constants, which were acquired by fitting the experimental results.

4.4.6 Calibration of the Johnson-Cook Fracture Model

The most important problem for implementing the Johnson-Cook fracture model into metal cutting simulation or other finite element analysis is to calibrate fracture constants for any proposed material.

Johnson and Cook [1985] calibrated the material constants for three kinds of materials: OFHC copper, Armco iron, and 4340 steel. Firstly, the fracture constants $D_1, D_2, D_3,$ are calibrated based on quasi-static tensile tests with smooth and notched round bars and torsion tests as shown in Fig 4.4, and then adjusted the results to $\dot{\varepsilon}^* = 1.0$ using following obtained D_4. The strains to fracture were calculated by $\bar{\varepsilon}_f = 2 \ln(d_0/d_f)$, where d_0 and d_f df are the diameters of the initial and fractured cross section of the necking surface, which were measured by using a photograph of the specimens. The stress triaxiality used for fitting the curve is the average value of the stress triaxiality along the loading process. This stress triaxiality is obtained based on the stress history data of the point in the center of the necking zone from the numerical simulation of these quasi-static tensile tests. D_4 and D_5 were calibrated based on the ratio of the tensile Hopkinson bar test to quasi-static tensile tests as shown in Fig.4.4. The tensile Hopkinson bar test is a dynamic test with high strain rates and with elevated temperatures. However, the temperature effects were expressed with a low degree of accuracy here by Johnson and Cook [1985].
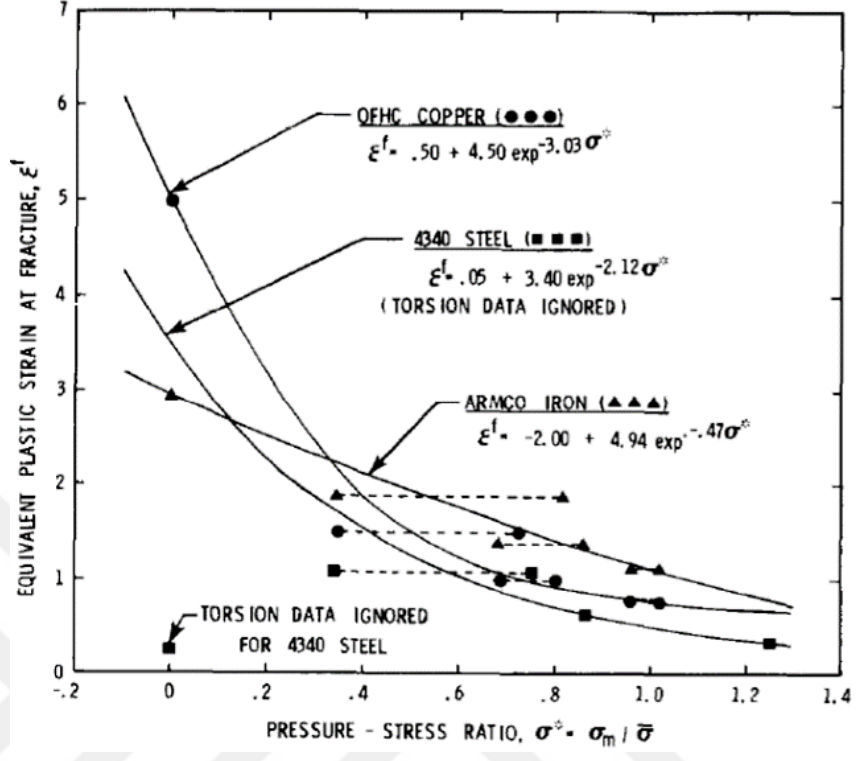
Figure 4.4: Fracture strain vs. Pressure-stress ratio for isothermal quasi-static conditions. [Johnson, 1985]

Borvik et al. [2001] determined the fracture parameters D_1, D_2, D_3 for Weldox 460E steel based on quasi-static tensile tests with smooth and notched round bars without the use of numerical simulations and using the method of least squares to minimize the residual of the fracture strain model, which is expressed in Equation (4.30).

$$\Re(\varepsilon_f) = \sum_{\beta=1}^{N_\beta} \sum_{\delta=1}^{N_\delta} \sum_{\gamma=1}^{N_\gamma} \{\varepsilon_f^{exp}(\sigma_\beta^*, \dot{\varepsilon}_\delta, T_\gamma) - (D_1 + D_2 \exp(D_3\sigma_\delta^*))(1 + \dot{\varepsilon}_\delta^*)^{D_4}(1 + D_5 T_\gamma^*)\}^2 \qquad 4.30$$

where $\sigma_\beta^*, \dot{\varepsilon}_\delta, \dot{\varepsilon}_\delta^*, T_\gamma, T_\gamma^*$ are the discrete value of the stress triaxiality, the strain rate, the dimensionless strain rate, the temperature and the homologous temperature respectively. The material data at $\sigma^* = 0$ is estimated based on Equation (4.31) [Lemaitre, 1992].

$$\varepsilon_f = \varepsilon_{fs}^{exp}\left[\frac{2}{3}(1 + v) + 3(1 - 2v)(\sigma_{max}^*)\right]^{-1} \qquad 4.31$$

where ε_{fs}^{exp} is the true fracture strain measured from a smooth specimen test. However, the extent of the curve with the results of D_1, D_2, D_3 to the range $\sigma^* < 0$ only depended on the hydrostatic tests. D_4. was calibrated based on data from dynamic tensile tests at room temperature and minimized the residual of Equation (4.30). D_5 was calibrated based on data from the quasi-static tensile tests at elevated temperatures with smooth specimens, and $D_5 = 0$ at range from 0ºC to 300ºC as shown in Fig. 2.9 (b). Fig. 2.9 (a), 2.9 (b), and Fig. 4.5 show the comparison between the experimental data and the model results based on the calculated material parameters, respectively.
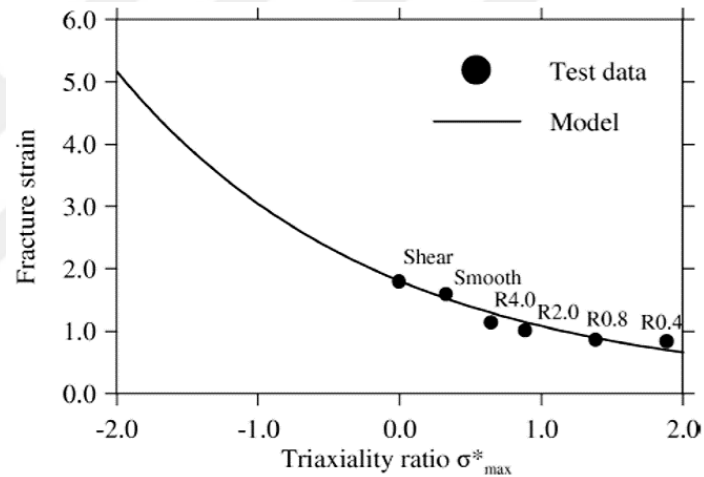
Figure 4.5: Comparison between experimental data to model results for Weldox 460 E steel. [Borvik, 2001]

Wierzbicki et al. [2005] only calibrated the D_1, D_2, D_3 for 2024-T351 aluminum alloy based on the quasi-static round smooth and notched tensile tests as shown in Fig. 4.6. However, the calibrated curve only provides an upper bound curve for material ductility, and the fracture curve of the same material from Johnson and Holmquist [1989] providing a low bound curve for material ductility as shown in Fig.4.6. That means different results were obtained dependent on different experiments. The Johnson-Cook fracture model is only reliable in a certain range of stress triaxiality, and the material parameters are calibrated by using the experiments covering this range of stress triaxiality.
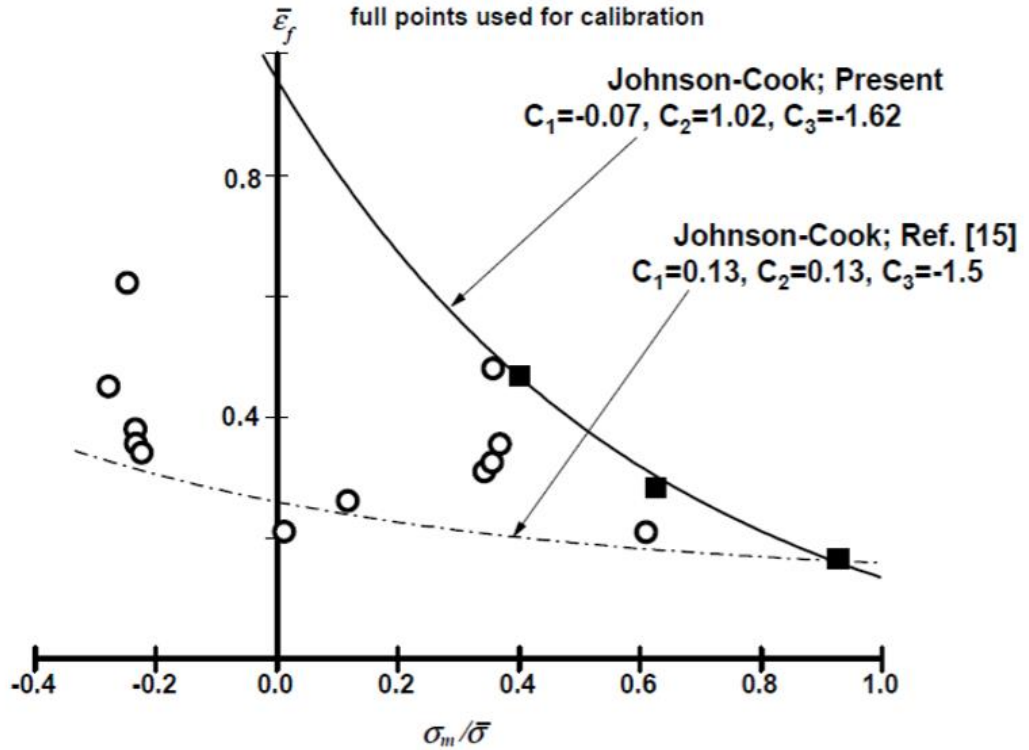
Figure 4.6: Comparison of ductility curves of aluminum. [Wierzbicki, 2005]

All above calibrations are dependent on experimental data, and some combined with the finite element simulation data. However, Vaziri et al. [2010] provided a new calibration for AISI 1045 steel that used the data from ALE based finite element simulation of metal cutting. The best set of material parameters were obtained by a nonlinear least-squares optimization procedure that the objective function is detailed in Equation (4.32) [Vaziri, 2010].

$$LSE = \min_{x} \sum_{i=1}^{4} f_i^2 \qquad\qquad 4.32$$

where x= $[D_1, D_2, D_3, D_4,]$ as a vector, and i expresses the different cutting conditions tests 1, 2, 3 and 4 respectively. The Johnson-Cook fracture model is based on the assumption that the elements fail when the accumulate damage value is $D = D_{cr} = 1.0$, as shown in Equation (4.33).

$$f_i(x) = 1.0 \int_0^{\overline{\varepsilon f,i}} \frac{1}{[D_1 + D_2 \exp(D_3 \sigma_i^*)][1 + D_4 \ln \dot{\varepsilon}_i^*][1 + D_5 T_i^*]} d\overline{\varepsilon_{p,i}} \qquad 4.33$$

where f_i is numerically integrated based on the trapezoidal method. Then the optimized sets of fracture parameters were obtained by using a MAPLE code to the program. The best set of fracture parameters is identified based on an updated Lagrangian simulation of metal cutting by comparing the predicted cutting forces and thrust forces to experimental results.

Majzoobi and Dehgolan [2011] calibrated the material parameters of the Johnson Cook constitutive model and fracture model together. A method combining the experimental, numerical, and optimization technique is used. D_1, D_2, and D_3 were obtained based on a quasi-static tensile test with a notched bar. D_4 was obtained based on a dynamic test with a notched bar by using a high strain rate testing device "Flying wedge". However, no test of temperature effects on the fracture is studied here.

Dzugan et al. [2013] calibrated the fracture parameters based on the fracture locus $\bar{\varepsilon}_{f(\eta,\xi)}$ for the typical steel used in the nuclear power plant industry. They used three kinds of tests including tensile tests with notched round bars, punch tests, and a specially designed test with a specimen with a double curvature. All the tests are quasi static tests at room temperature. Hence, only D_1, D_2, and D_3 were calibrated.

4.5 Finite Element Program

In this thesis the abaqus software is used for finite element analysis (FEA). It has the following parts:

- Abaqus CAE (Complete Abaqus Environment) is used for both analysis and modeling mechanical components and assemblies. It also visualizes FEA result.

 - Abaqus Standard is a common -purpose analyzer with implicit integration process.

 - Abaqus Explicit is used in cases where FEA is needed with explicit integration scheme, which is helpful to deal with non-linear complex and abrupt systems.

 - Abaqus CFD (Computational Fluid Dynamics) software provides capabilities to analyze computational fluid dynamics with pre-processing as well as post-processing options.

. - Abaqus Electromagnetic is software for solving electromagnetic problems.

This software has a graphical interface that allows the user a quick and efficient definition of the geometry of a problem, allocation of material properties, loads, applying boundary conditions, selection of steps required in the analysis, and finally, generation of the finite element mesh. The consistency and adequacy of the model can be assured in various steps; therefore, the model needs special tools such as ABAQUS-CAE for monitoring various aspects of the partitions defined for the model geometry (PART module), mechanical properties of the materials involved (PROPERTY module), grouping these partitions (module ASSEMBLY), the imposition of sequence analysis steps (STEP module), their nature either linear or nonlinear, definition of boundary conditions and loading (LOAD module), generation of finite element mesh (MESH module), and finally obtaining the input file (JOB module) (ABAQUS v.6.16). After generating the pre-processor, the file containing the problem of data entry, which can in turn be further manipulated by the user for situations not adequately addressed by the ABAQUS CAE, can then be executed by the computer simulation finite element method using the modules ABAQUS Standard and ABAQUS Explicit (for metal

punching). The software also has the ABAQUS Viewer post-processor for processing the output files, allowing interpretation of the numerical results, graphical visualization procedures and animation. The various capabilities of ABAQUS allow complex engineering problems involving complicated geometries, nonlinear constitutive relations, occurrences of large deformations, transient loads and interactions between materials, which can be numerically modeled. It should be noted, however, that the process of building a suitable model is not a simple task because that involves a very large number of parameters and options stemming from the range of possible problems that can be modeled with the software (ABAQUS v.6.16).

4.5.1 Data input

The data input file that runs the finite element program ABAQUS STANDARD (or ABAQUS Explicit) is generated by the preprocessor ABAQUS CAE and later modified or completely created by the user using a text editor. It is also observed that the input file can be subdivided into two large groups of information: Data model geometry with a description of the nodes, element types, their connectivity, material properties, boundary conditions and the type of analysis (static or dynamic), loading history data, and information about the sequence of events or imposed loads, which might include specific forces, surfaces, and bodies, which are generated by variations in temperature and pressure.

The ABAQUS program offers a wide variety of finite elements characterized by different numbers and types of degrees of freedom, which are selected by the user depending on the nature of application. It also presents several significant relationships to simulate the mechanical behavior of materials such as elastic-plastic and linear elastic models, which are linked with criteria presented by Mohr-Coulomb and Drucker-Prager etcetera (ABAQUS v.6.16).

4.5.2 Symmetry types

An important aspect of the system behavior is symmetry. When applied, this procedure helps reducing the problem size making it easier to model and analyze by spending less time in general (ABAQUS v.6.16). Symmetry types are:

- Axisymmetric: In this type of geometry, loading, and bonding conditions are all symmetrical with respect to a particular structural axis.

- Mirror symmetry: In this type of geometry, loading and support conditions of the model are symmetrical with respect to one or more axes.

- Cyclic symmetry: It is obvious when there are a finite number of sectors with the same behavioral conditions around an axis of rotation.

- Repetitive symmetry: The template can be designed with only one sector which is repeated in terms of behavior, geometry and loading.

4.5.3 Characterization of the Elements Using ABAQUS

For many applications, formulations or problems, the Finite Element Method uses various types of elements, each with an appropriate solution for each situation being studied or simulated (Marya et al., 2005). A formulation element means a mathematical theory, which defines the behavior of an element. All ABAQUS elements, which belong to the strain/displacement type, are based on the description of Lagrangian or Eulerian behavior. Whether it is Euler's alternative or spatial, the description of the elements is constant in terms of space. The Euler's method is commonly used in fluid mechanic simulations (Marya et al., 2005).

Displacements or other freedom degrees are calculated based on an element node. For other points in an element, the displacement can be measured with the help of nodal displacement interpolation. Normally, the interpolation order depends on and determined through the number of elemental nodes. The elements studied in this research have vertices like an 8-node brick (Fig.4.7), and it applies to the linear interpolation for every direction.
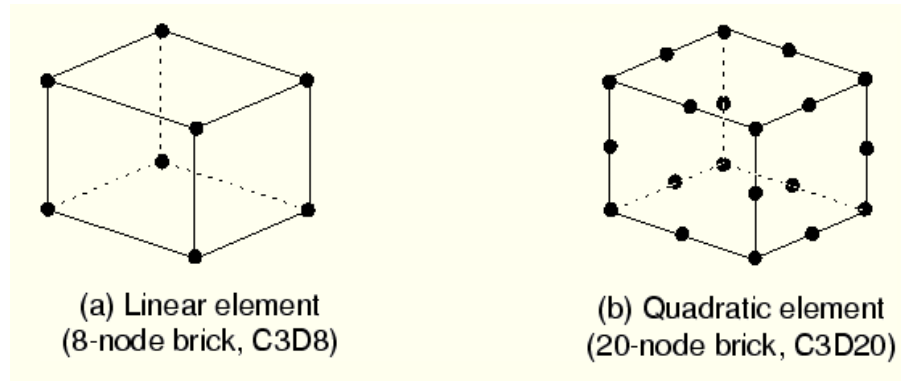
Figure 4.7: BRICK ELEMENTS, LINEAR AND QUADRATIC

4.5.4 Mesh Elements

Mesh, as it is known, is the set of elements and nodes used in the discretization of a geometric model for the calculation with the finite element method (Soderberg, 2006). The process of mesh generation in a model is something of fundamental importance to define the level of accuracy of the results to be obtained. When the number of elements/nodes is high, the result is likely to be more accurate. The mesh should be adjusted optimally to the geometric shape of the studied part of the model; however, its density may locally vary depending on the geometry. This means that in regions with very small details, a higher density of mesh is required. When it comes to rupture, the most likely region that suffers should have a good mesh refinement because accuracy of the stresses obtained in the region must be the best possible. At the same time, these regions usually have complex geometries, which reinforce the need to have a refined mesh. According to Marcondes et al. (2007), the mesh density substantially affects the deformation results. In this study, because of high gradient plastic deformation of the cutting area, a sufficiently dense mesh should be applied. Soderberg (2006) examined the influence of mesh density on the cutting geometry and the rupture "stroke" on a simulation of punching forces. He conducted a study with different mesh refinements. Fig.4.8 illustrates the knitwear used by Soderberg (2006). In their work, it was concluded that the thickness of elements should be sufficient to assess the influence of parameters on the breaking strength.
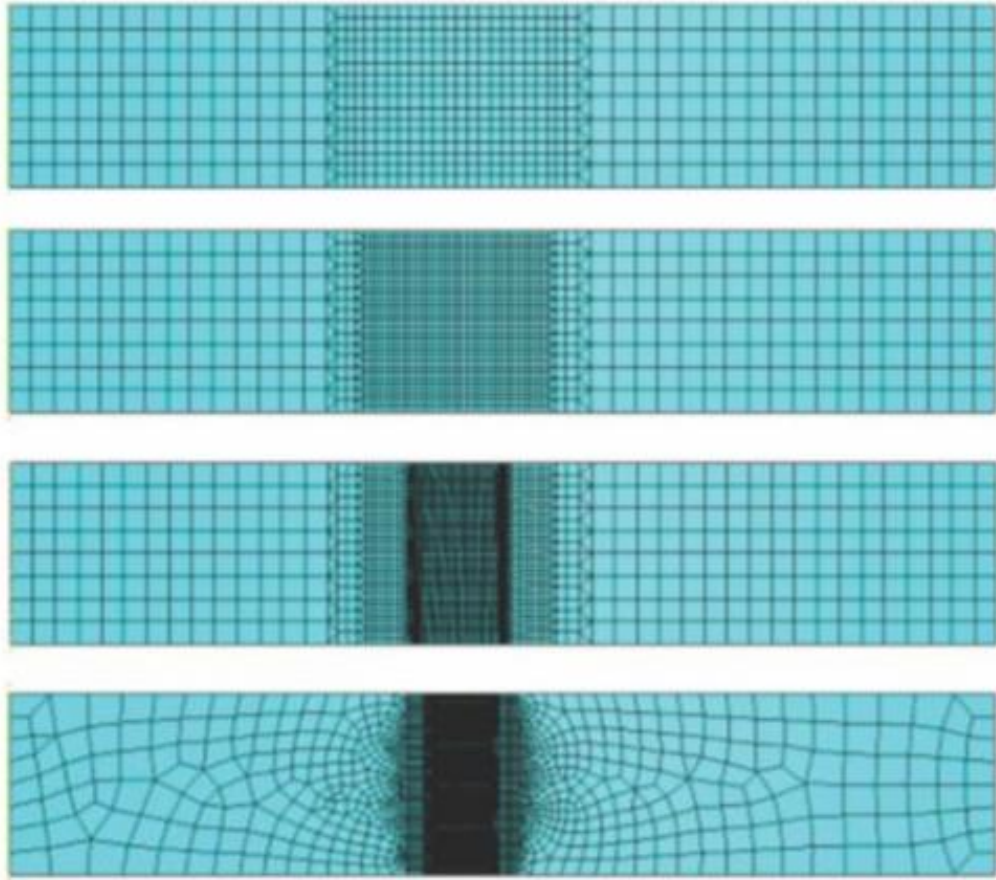
Figure 4.8: MESH REFINEMENT

Element Type

The elements in a structure consist of four-node bi-linear axi-symmetric quadrilateral elements having low integration (CAX4R) as well as three-node asymmetric triangles (CAX3). The triangles help coarsening the mesh to create more computational efficiency. Both elements belong to the family of solid elements, and they belong to the first order, which means that the strain is computed as an average over the element volume instead of the first order Gaussian point. The feature of reduced integration applies to CAX4R element that results in reducing the integration order from the full integration, so, only a single central integration point is used. By using lower integration, the constraints reduce as well, which does not allow "locking" elements, because it results in a stiffer

response. A major drawback of this technique is that for certain modes of deformation; no energy is registered in the element integration point. These modes are usually referred to as "hourglass modes." This problem is addressed in ABAQUS using an "hourglass control algorithm".

4.5.5 Contact between Surfaces

There are some special formulations for finite elements that allow the analysis to include the possibility of contact between the surfaces. This implies a definition of the contact surfaces, a slave and a master, which interact during the simulation creating new boundary conditions for the analysis. While performing analysis, which includes assessment of contact, ABAQUS finds a point closest to the master contact pair surface (see Fig.4.9).
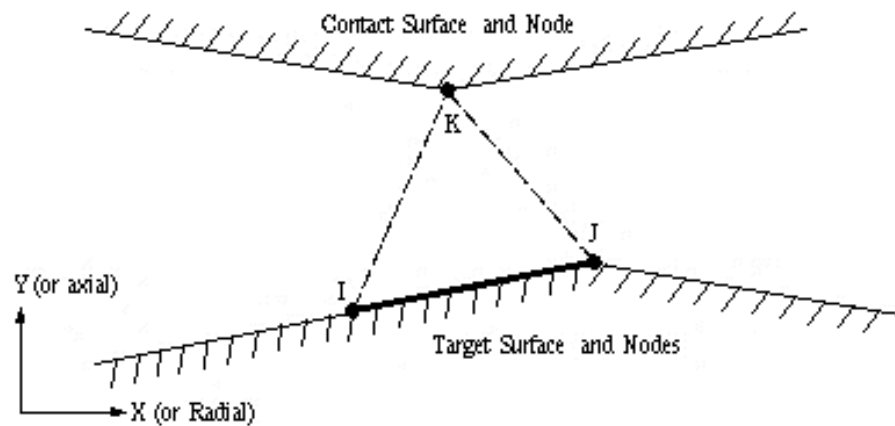
Figure 4.9: Contact between Surfaces

4.5.6 Establishing Contact

ABAQUS provides the conditions for inter-body contact with the help of an algorithm and a master-slave drive. In mechanical problems, we consider the following:

- Every potential contact condition can be defined in terms of a master surface and a slave node.

- Slave nodes do not penetrate in a master surface, but master surface nodes can penetrate in the slave surface.

- Contact direction generally remains normal to a master surface.

4.6 Modelling steps of piercing \ blanking tests

The geometry of the blanking process modelled in this study is presented in Fig.4.10a. The dimensions of the tooling are defined in Table 4.1. The initial sheet thickness t is equal to 2 mm. The sheet is made of a commercial steel alloy, ASTM A 36, a low carbon hot rolled steel.

The material constants for the steel alloy are listed in the next. Numerical simulations have been performed with the commercial FE code ABAQUS/Explicit. The sheet has been meshed with quadratic plane strain elements with reduced integration, denoted as CPE4R in ABAQUS (ABAQUS, 2016). The FE mesh of the sheet and the boundary conditions are presented in Fig. 4.10-4.11. A very dense mesh has been defined in the shearing band with 3685 elements (i.e. the zone between the punch corner radius and the die corner radius) and a coarse mesh has been used for areas not subjected to higher stresses. The tools have been modelled as an analytic rigid surface. The contact between the sheet and the tools has been described by the Coulomb friction model with a friction coefficient of 0.1. The adaptative mesh controls have been activated to allow remeshing. In order to predict the material damage evolution, the damage model coupled with the Johnson and Cook was implemented in ABAQUS/Explicit FE code. During the simulations, the damage initiation and its propagation has been simulated using the element deletion module.

Table 4.1- Tooling dimensions

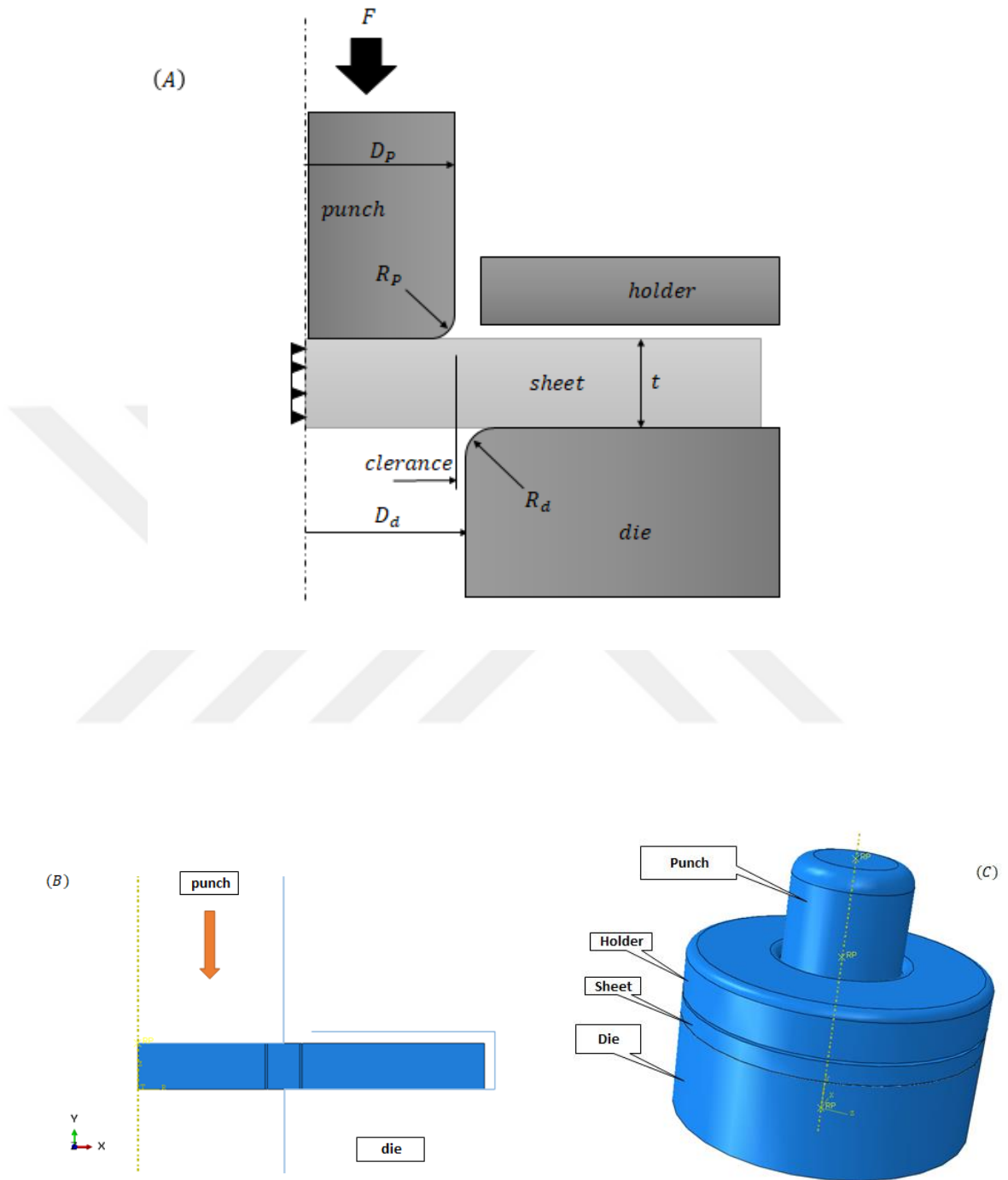| Punch diameter D_p	9.4, 11, 12,6 mm
Die diameter D_d	9.48, 11.08, 12.68 mm
Punch corner radius R_p	0.01,0.1,0.2 mm
Die corner radius R_d	0.01 mm
Thickness of sheet t	2 mm
Punch die clearance	2%,5%,15%
Cutting velocity	1.67 mm/s

Figure 4.10: (A)The geometry of the blanking process (B) 2D model (C) 3D model

Use model 2D in axi-symmetric such as (flat face, Flat face center point, and concave punch), and use 3D model in non axi-symmetric such as (concave shear, Y shear, Shear punch) show as Fig.4.11.
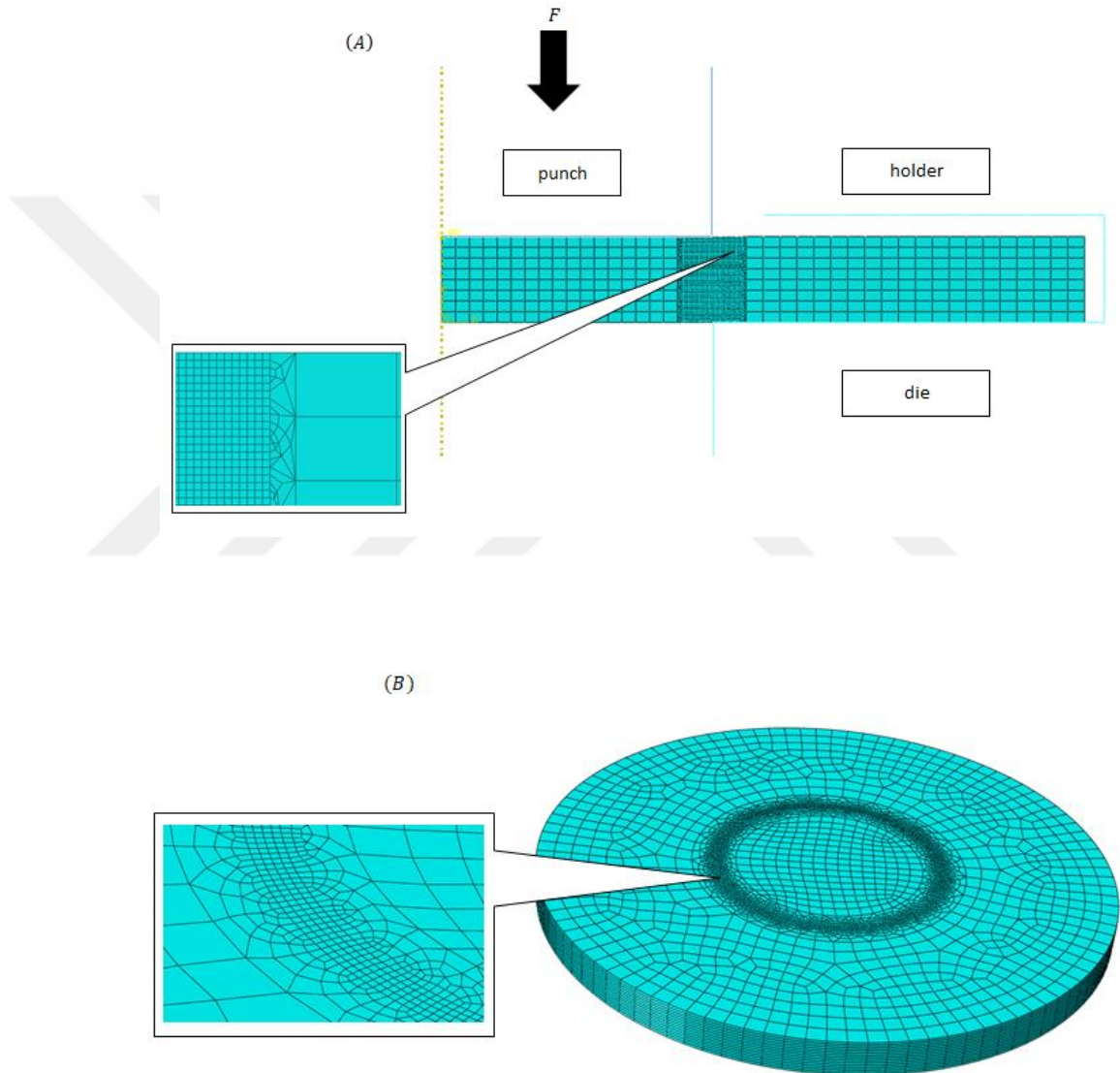

Figure 4.11: The FE mesh of the sheet (A) 2D model, (B) 3D model.

4.6.1 Material parameters

The physical and mechanical properties of the sheet material, Steel 36A, is given in Table 4.2 The constants used in the Johnson-Cook material model and its complementary damage model are given in Tables 4.3 and 4.4, respectively. They were taken from the literature (Johnson and Cook, 1985). Tables 4.5-4.6 presents the material model for AL 5052. This material was used in the next Section in the calibration of the FE model.

Table; 4.2 Physical and mechanical properties of Steel 36A

Density (kg/m^3)	7850
Youngs modulus (Pa)	210000
Poisson Ratio	0.29
Specific Heat Fraction (J/kg . ℃)	486
Inelastic Heat Fraction	0.9
Thermal Conductivity (W/m . ℃)	52
Expansion Coefficient (m/m . ℃)	1.2e-5

Table 4.3: Material constants of the Johnson-Cook constitutive model used in the modelling Steel 36A.

A (MPa)	B (MPa)	n -	m -	Melting Temperature T_{melt} (℃)	Transition Temperature T_{room} (℃)	C -	Epsilon Dot zero $\dot{\varepsilon}_{ref}$ -
286	500	0.228	0.917	1430	25	0.017	1

Table 4.4. Constants of the Johnson-Cook Damage model used in the modelling of Steel 36A.

(D_1)	(D_2)	(D_3)	(D_4)	(D_5)	Melting Temperature T_{melt} (℃)	Transition Temperature T_{room} (℃)	Reference Strain rate
0.403	1.107	0.1	0.00961	0	1430	25	1

Table 4.5: Material constants of the Johnson-Cook constitutive model used in the modelling AL 5052.

A (MPa)	B (MPa)	n -	m -	Melting Temperature T_{melt} (°C)	Transition Temperature T_{room} (°C)	C -	Epsilon Dot zero $\dot{\varepsilon}_{ref}$ -
130	120	0.18	1	1430	25	0.014	1

Table 4.6. fracture constants of the Johnson-Cook Damage model used in the modelling of AL 5052.

(D_1)	(D_2)	(D_3)	(D_4)	(D_5)	Melting Temperature T_{melt} (°C)	Transition Temperature T_{room} (°C)	Reference Strain rate
0.2	0.8	-1.5	-0.01	0	1430	25	1

4.6.2 Boundary Conditions

In the simulations the tool is modelled to move with a speed of 1.67 mm/s (Fig.4.12). Additional information regarding the developed model including the boundary conditions are shown in Table 4.7.
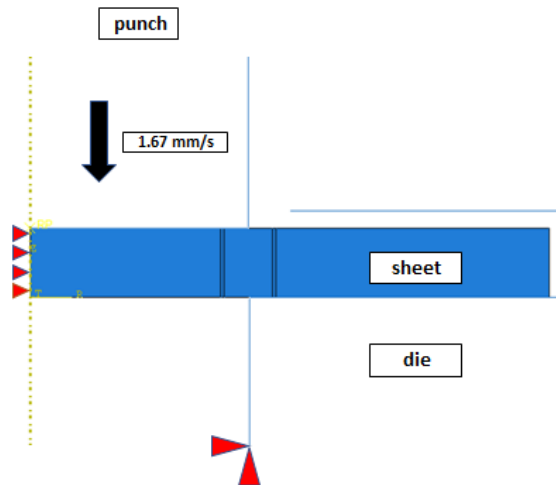
Figure 4.12: The boundary conditions of the blanking proses model.

Table 4.7: Simulation Parameters and Boundary Conditions

Object	Simulation Parameters & Boundary Condition
Punch And Die	- Rigid body - Elastic constant $E = 650$GPa
Sheet material	- Plastic body - Axisymmetric
Holder	-No pressure

4.6.3 FE simulations of blanking

To sum up, blanking is a very high deformation process ending up with the removal of the material, where stresses and strains in the deformation region of the sheet material reach to very high levels. Although simulating this process using FE methods is fairly common, accuracy of the model depends on the input data such as the flow stress curve of the material, thermal properties, damage parameters used to predict crack propagation.

Figure 4.13: FE simulations of blanking

RESULTS AND DISCUSSIONS

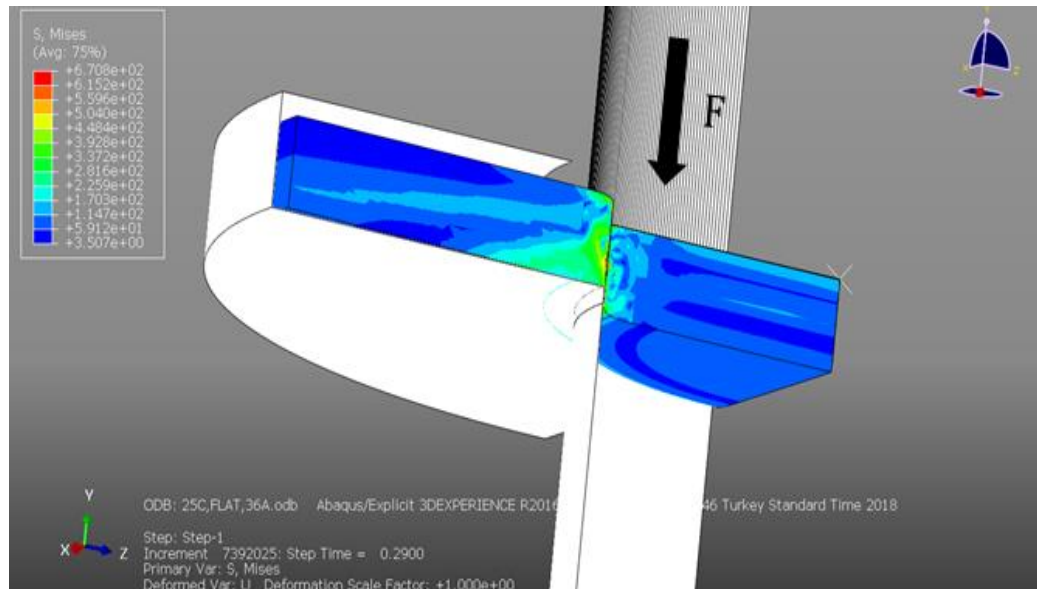In this chapter, the blanking process presented in Fig. 5.1 was investigated from different perspectives. First, the developed model was validated with the experiments. Second, the effects of various parameters including the clearance, corner radius of the punch, temperature and friction on the process in terms of the cutting force and the shear-edge quality were studied both experimentally as well as numerically. Finally, the influence of the tools with different coatings and polycrystalline diamond compact punch was experimentally studied.
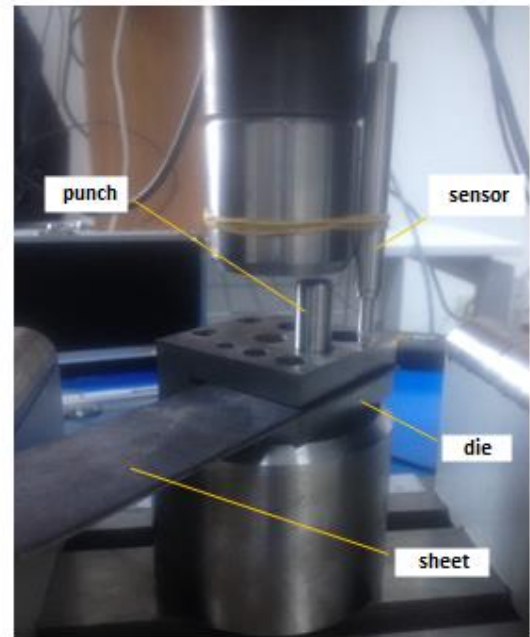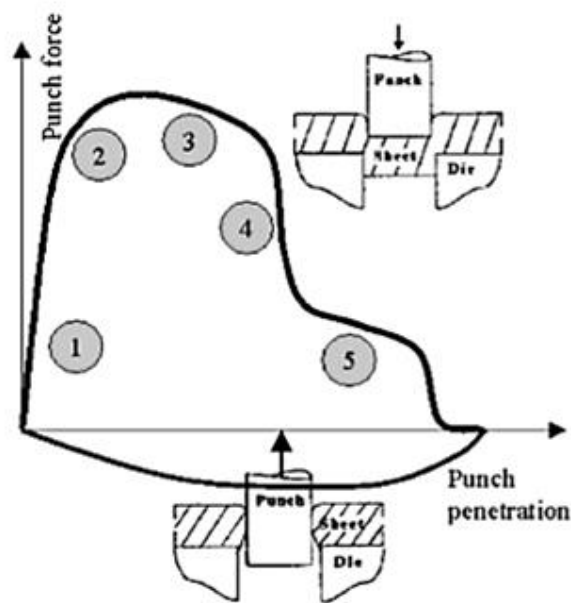

Fig 5.1: Blanking Process

5.1. Validation of the FE Model

The force-displacement curves were obtained when the blanking process was applied using a tool having a single sheared edge, both experimentally and numerically. The comparison of curves is shown in Fig. 5.2. The figure shows that agreement between them has been achieved, which ultimately validated the developed numerical model.
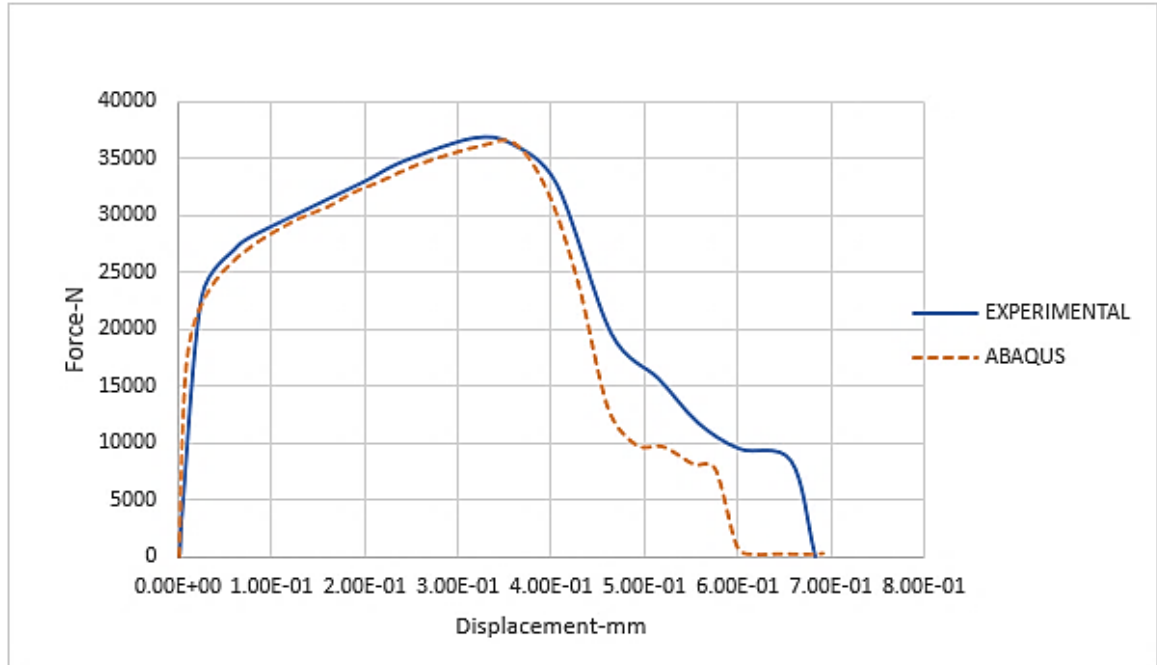
Figure 5.2. Experimental and numerical punch force vs displacement.

The sheared edge of the workpiece material obtained by SEM is investigated in our study. Particularly, we focused on its characteristic features such as rollover depth, burnish depth and fracture depth. Fig. 5.3 presents the experimental and numerical comparison between these parameters. Their matching proved the accuracy of the numerical model.

The predicted burnish depth and the predicted fracture depth values are closer to the experimental values. The rollover depth is slightly overestimated by our simulations as a consequence of the spring back phenomena observed after inactive unloading. Nevertheless, the predicted sheared edge shows clear agreement with the sheared edge, which has been experimentally obtained. To conclude, the predictions of the presented model show fair agreement with the experimental data. The Johnson and Cook damage model is suitable to simulate sheet metal blanking processes (Fig. 5.3).
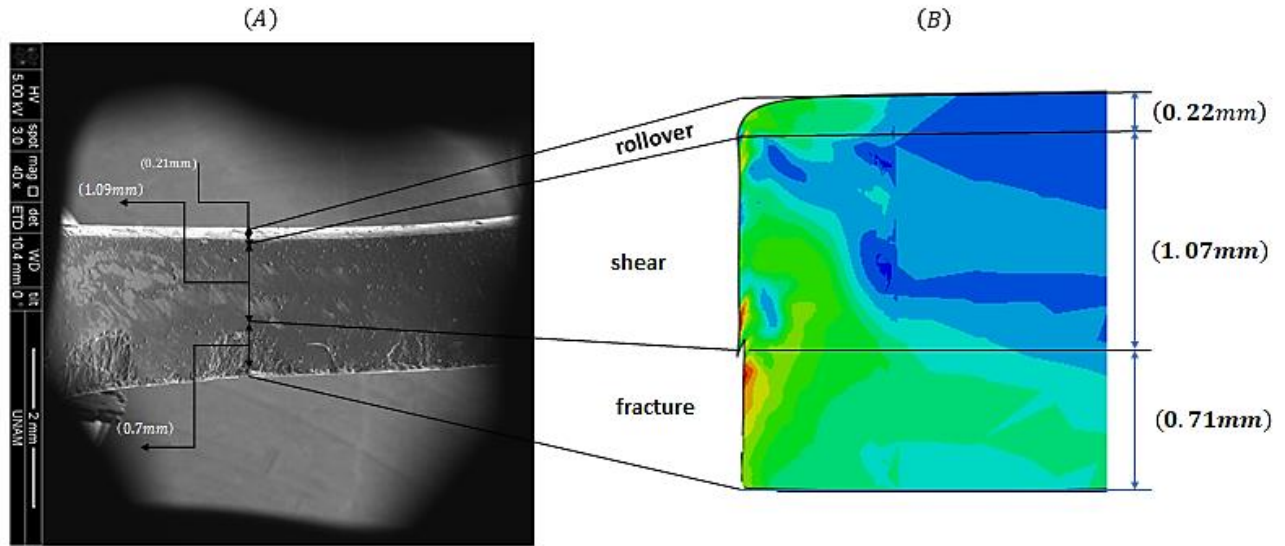
Figure 5.3: Characteristic features of (a) sheared edge achieved by SEM and (b) sheared edge predicted by FE simulations

Fig. 5.4 presents the deformation history of the blanking process. Initially, a primary crack occurs under the punch corner radius, which then propagates in the direction of die corner radius with a slope that is proportional to the blanking clearance. With the increase of punch penetration in the sheet, a second crack occurs over the die corner radius. The delay of occurrence of this second crack increases with increasing blanking clearance. Both the cracks continuously propagate and finally connect to each other leading to sheet separation. The present model was used to conduct a parametric study to evaluate the influence of different parameters on the characteristic features of the sheared edge.

Figure 5.4: Simulated crack initiation and growth during the blanking process.

5.2. Influence of various parameters on blanked edge quality and punch load/stress

In this section, the effects of blanking clearance, punch tip geometry, corner radius, temperature, friction, PVD coating, and PDC (Polycrystalline Diamond Compact) punch on the quality of the sheared edge are 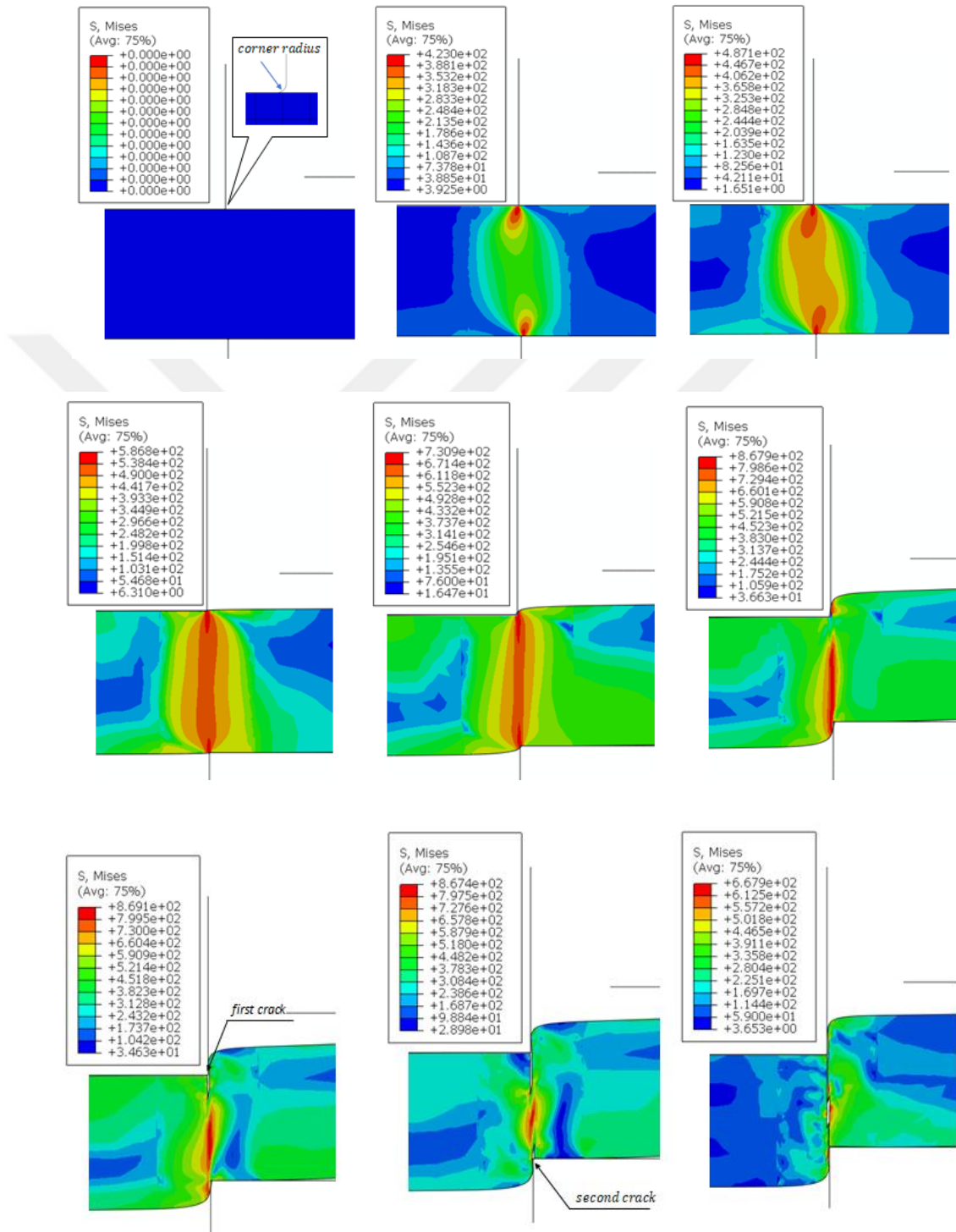presented. The numerical studies of the last two parameters were not conducted, and they are left for future research; therefore, we only discussed their experimental results.

5.2.1. Punch-die clearance

The clearance between the punch and the die, i.e. the blanking clearance is a significant parameter in the blanking process, and it significantly affects the blanking force and the surface quality of the sheared edge. In this study, various FE simulations have been performed for blanking clearance values ranging between 0.2% and 15%. Fig. 5.5 presents the respective force-displacement curves including the experimental results for clearances of 0.2% and 15%. It was found that there is agreement between them. It was observed that this parameter had no significant effect on the maximum force; however, with increased clearance, the cutting process was completed at larger tool displacements, and a small force reduction, which ultimately increased the cutting energy.
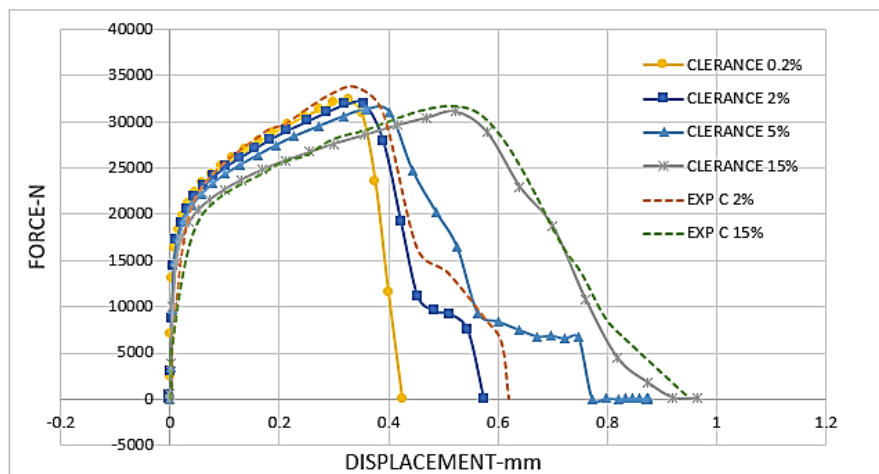

Figure 5.5: Comparison between experimental and simulated force-displacement curves at different clearances

99

The characteristic features of the sheared edge for various clearances have been illustrated in Fig.5.6. It was observed that blanking clearance has a strong impact on the rollover and the fracture depth. In the blanking process, the sheet metal is firstly bent, then, along with increase in the punch penetration, the shearing process occurs. The increase in the clearance allows the material to flow more easily between the punch and the die. As a result, bending increases and the predicted rollover depth increases as well; therefore, crack initiation occurs at larger punch penetration. In this case, the crack initiation is delayed and the predicted fracture depth decreases. The fracture thickness predicted by FE simulations is presented in Fig.5.6. As the blanking clearance increases, the predicted fracture thickness significantly increases.

Table 5.1 shows the dimensions of different shear areas measured after the cutting process, which is completed to compare the values. Negative effect was noticed on the purr zone in case of 15% clearance. When the clearance is smaller than 0.2%, no effect is observed on the quality of the edges but increase in the pressure on the edges of the tool was noticed that results in rapid wear. At 5% clearance, the fracture depth was relatively larger. Overall, 2% clearance is considered as optimum in terms of wear resistance and the edge quality of the cut.
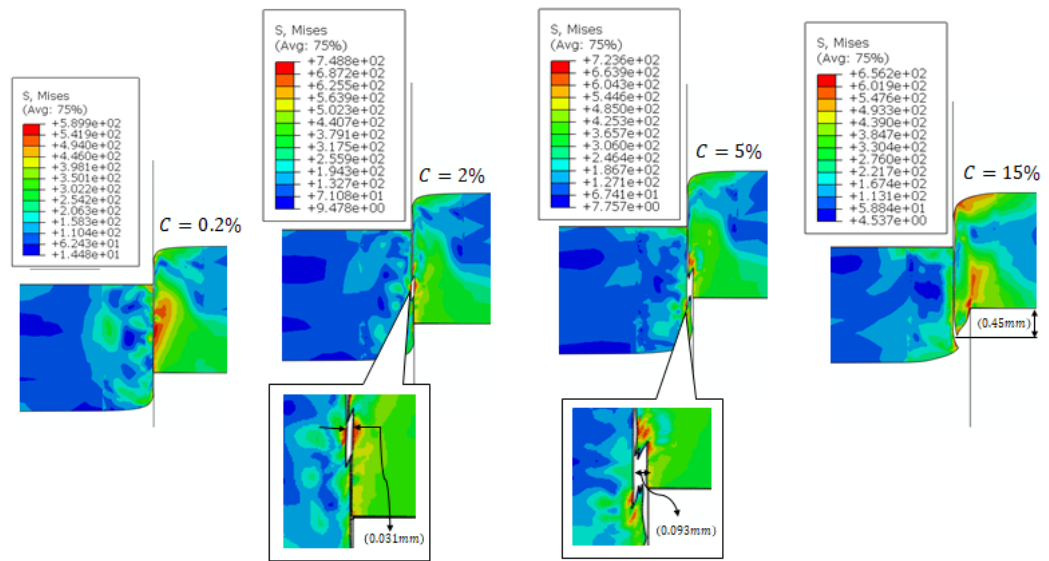

Figure 5.6: Simulation for different clearances.

Table 5.1: Effects of the clearance on the cutting zone

Clearance mm	Force N	Rollover mm	Share zone mm	Fracture zone mm	Purr zone mm
Clearance 0,2%	32331	0.18	1	0.82	0.01
Clearance 2%	31345	0.21	1.1	0.7	0.03
Clearance 5%	31238	0.21	1.32	0.47	0.03
Clearance 15%	31234	0.4	1.6	0	0.45

5.2.2 Punch tip geometry

We know that reducing the required load value reduces the tool wear. For our experiments, we considered different geometries of the tool head, which are shown in Fig. 5.7. These geometries include flat, concave, shear, concave shear and Y shear faces. Fig. 5.8 shows the respective force-displacement curves. It is observed that there is a 40% drop in the cutting force as compared to the traditional flat punch when the concave shear-punch was used. We also noticed 20% reduction in the cutting force when the tool with a single shear was used and even better performance became possible when a double shear was applied. It is observed that the concave shape is difficult to manufacture, and it makes the grinding difficult, and on the other hand, it has no effect on the cutting force. Consequently, changing the head of the tool may be very useful for resisting the wear in terms of reducing the force required for cutting. Depending on the type and strength of the metal to be cut, appropriate punch head can be selected out of the range of different punch heads.
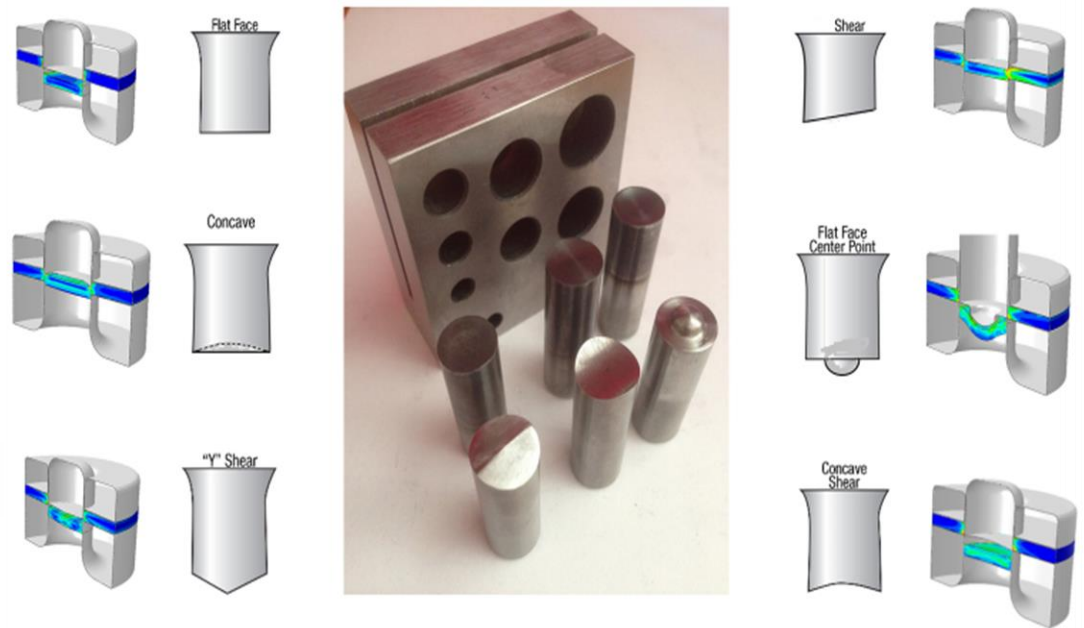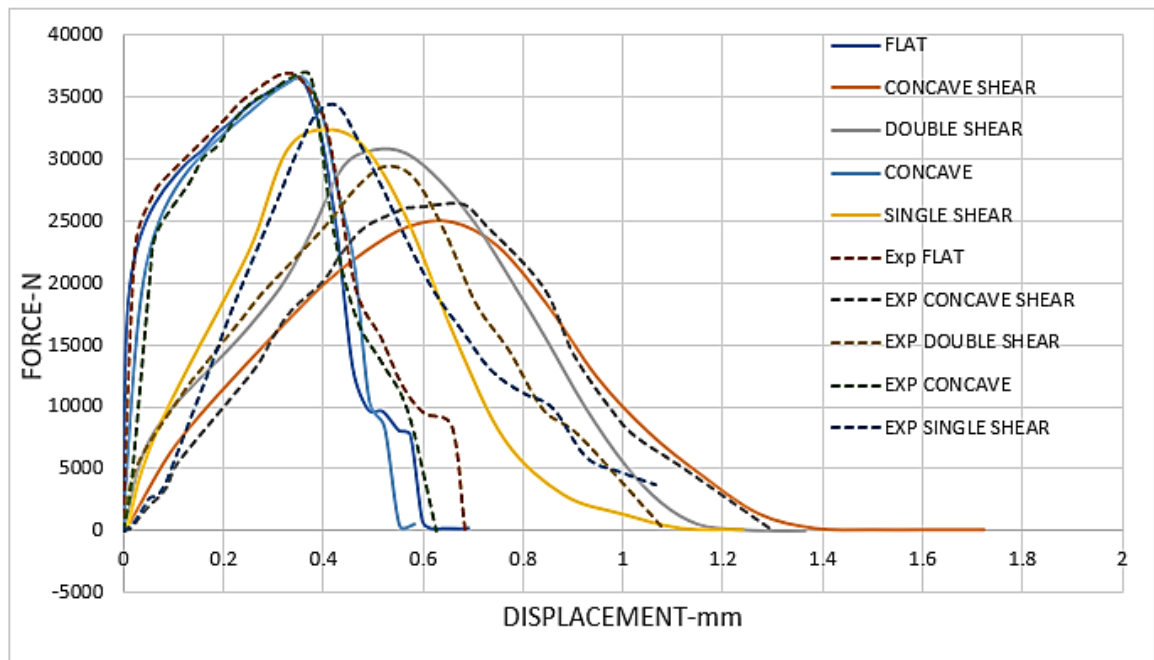
Figure 5.7: Different punch tip geometries.

Figure 5.8: Punch load during blanking using different punch tip geometries.

Additionally, a novel tool design that combines a flat face and a hemispherical part in the center is also considered as an alternative, which is called as flat face center point (see Fig. 5.9). This tool initially creates a deep drawing in the sheet material where a tension zone is produced, and then, the cutting takes place at a later stage (Fig. 5.9, 5.10). The respective force-displacement (F-d) curve of the experiment on the flat punch is shown in Fig. 5.11. The performance of this tool is also checked for different sheet materials such as AL5052. Its F-d curve is presented in Fig. 5.12. The experimental and numerically predicted values showed excellent agreement for both sheet materials. It is obvious that although there is a slight decrease in the maximum load, the energy increased in case of flat-faced tool. It is negatively reflected from the wear resistance despite the fact that the rollover zone increased from 0.18 mm to 0.24 mm (Fig. 5.9) but this increase is acceptable. As mentioned earlier, the change in the shear response results in the tensile operation in the shear zone (see Fig. 5.9)
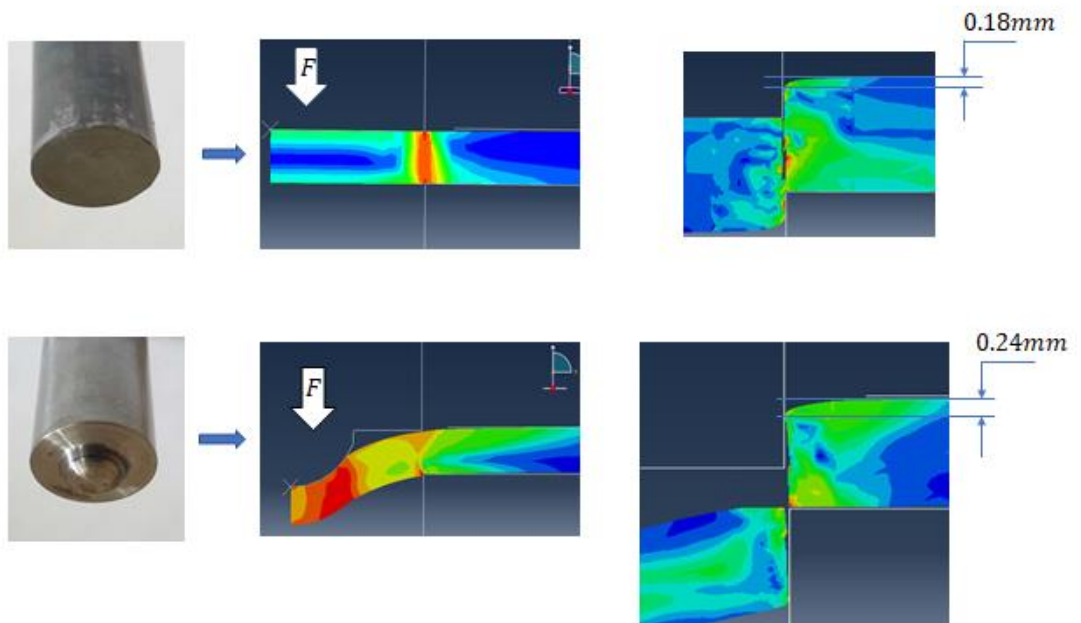

Figure 5.9: Comparison between the shape of the shear - flat and center point punch
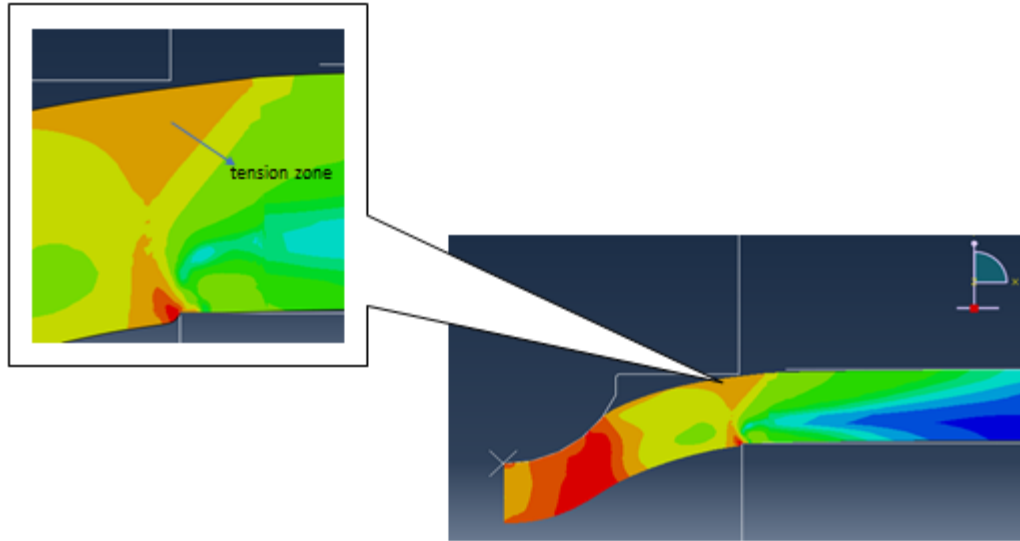
Figure 5.10: Tension zone before cutting
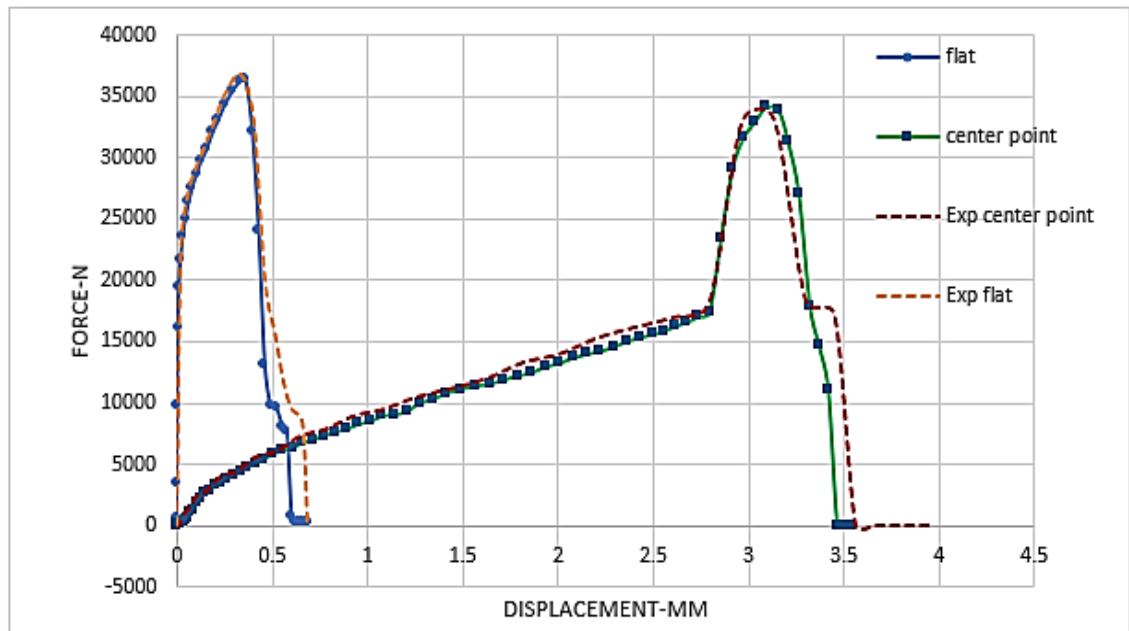
Figure 5.11: Punch load comparison between a flat and a center-point punch used for blanking A36 steel
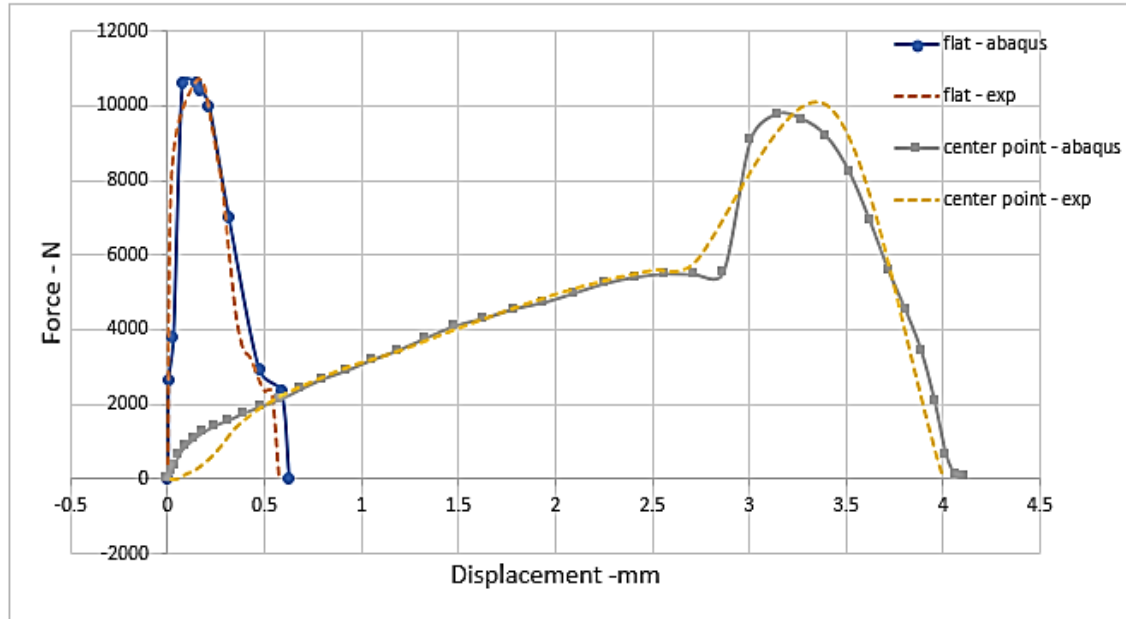
Figure 5.12: Punch load comparison when a flat and a center point punch are used for the blanking AL-5052

5.2.3 Corner radius

In this part, the effects of the corner radius of the punch on the blanking process have been investigated. Three different values of this parameter are considered: 0.01 mm, 0.1 mm and 0.2 mm. The force-displacement curves are presented in Fig.5.13. A reasonable match between the experimentally and numerically obtained curves is established. With increasing punch corner radius, cutting is completed at greater punch penetration while the cutting force remains constant, which in turn leads to boost the cutting energy. Fig.5. 14 shows the respective Von Mises stress distributions in the workpiece material. The lengths of the burr, rollover, shear and fracture surfaces are presented in Table 5.2. Increase in the tool radius leads to higher burr on the edges of the hole.

The effects of the punch corner radius on the quality of the product and shear response were assessed. The angle radius can be considered as a parameter in that leads to wear on the tool head ring, and it happens after producing several

workpieces. A higher punch corner radius improves the tool life because the stress distribution on the edge of the radius with rounded tool is more uniform than the one, which has a sharp angle. Hence it has a better wear endurance.

The edge quality has been compared for three corner radius values of the tool: 0.01 mm, 0.1 mm and 0.2 mm (Table 5.2 and Fig. 5.15). They were found to be interrelated: The higher the tool edge radius is, the higher the burr on the hole-edges will be. It was found that increasing tool-edge radius leads to reducing the tensile area.
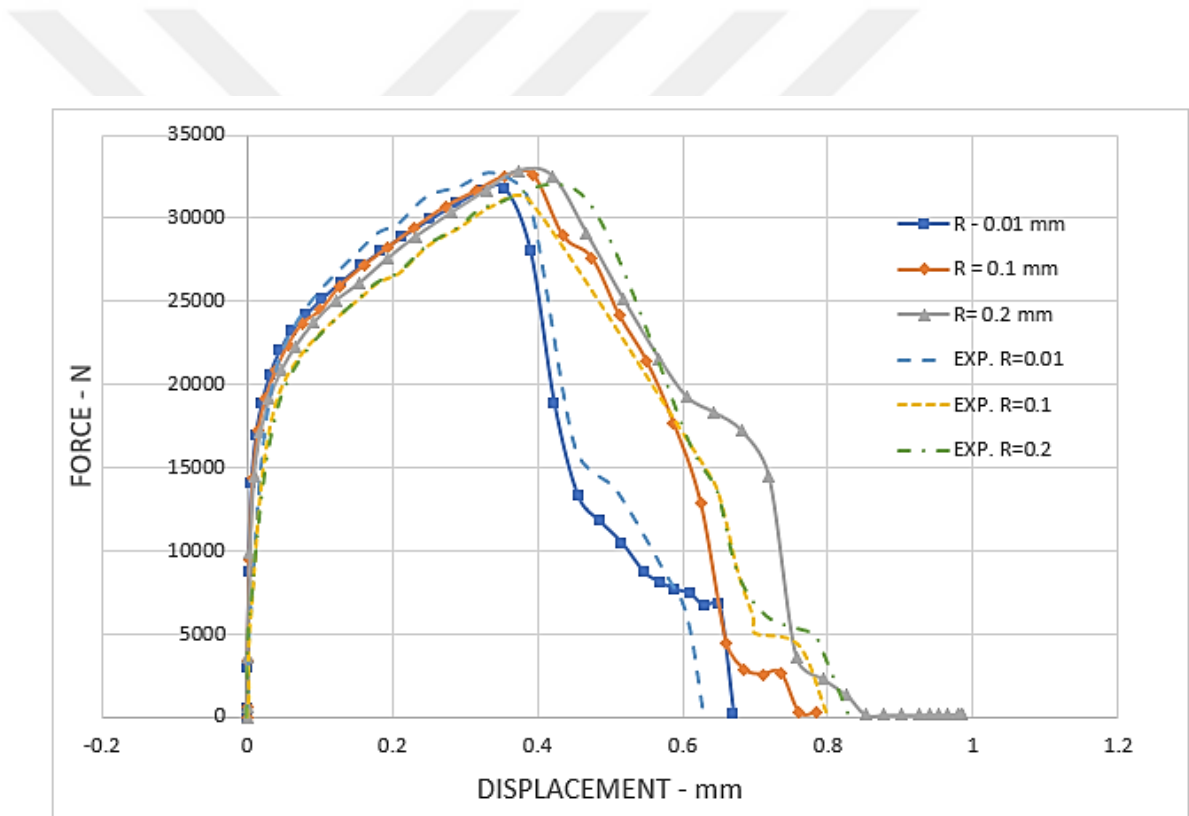
Figure 5.13: The effect of punch corner radius on the cutting force
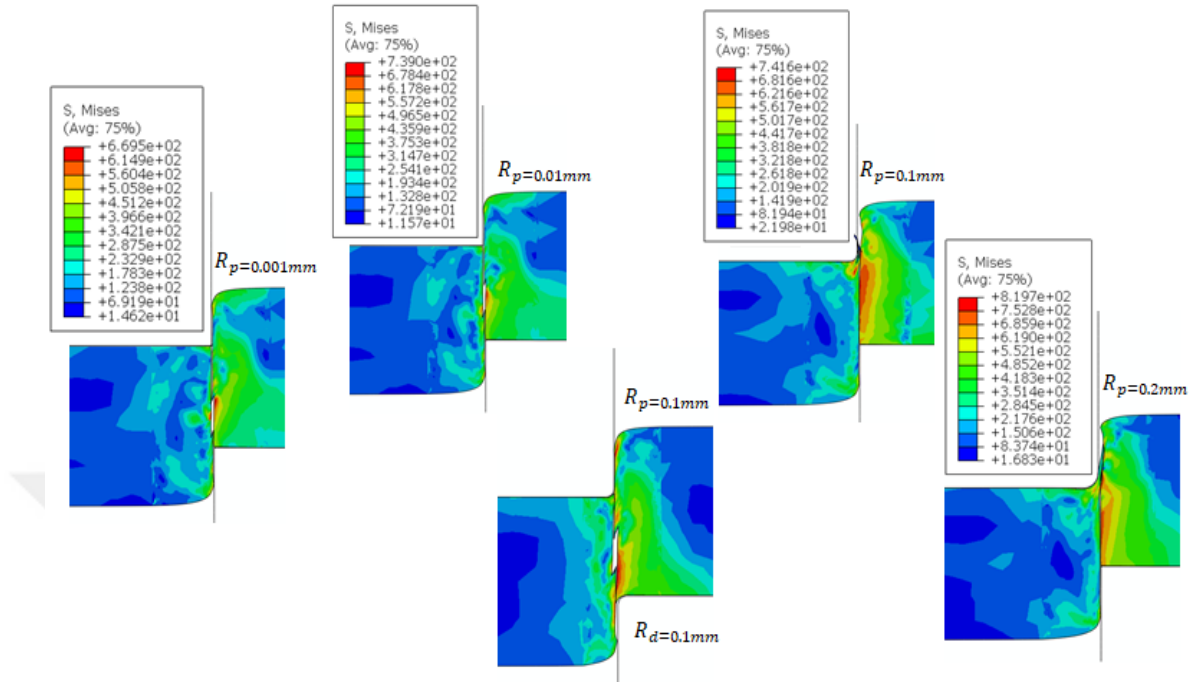
Figure 5.14: The influence of punch corner radius on the part-edge quality

Table 5.2: Changes in the edges due to changing radius values of the punch

Zone	$R_p = 0.001$	$R_p = 0.01$	$R_p = 0.1$	$R_p = 0.2$
Burr	0.1	0.12	0.25	0.6
Rollover	0.22	0.25	0.28	0.29
shear	1.18	1.1	0.5	0.4
fracture	0.6	0.65	0.78	1.31
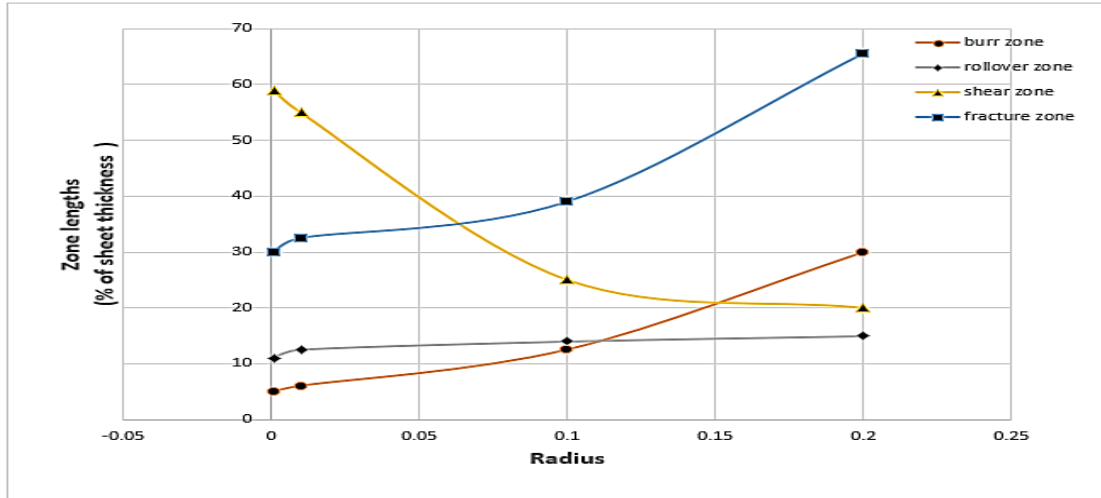
Figure 5.15: Effect of different radii on blanked edge zones

The effect of the corner radius values of the punch on the maximum force are given in Fig. 5.13. It shows the same displacement value but increase in energy.

In the end, we can say that the corner radius enhances the wear resistance, but it isn't useful for maintaining the product quality. For quality products, its value should be between 0.01 and 0.02 mm, in other words, increasing the radius more than 0.02 mm is detrimental to the quality of the edges because it contributes to the appearance of burr, which is large and unacceptable. The radius helps distributing and managing stresses around the edge and reduce the chipping wear.

5.2.4 Temperature effects

In this part, the cutting process has been simulated at 25℃, 100℃, 160℃, 270℃, 500℃ and 700℃, but the experiments were conducted on the first four temperature values. The respective force-displacement curves are presented in Fig. 5.16, which shows reasonable agreement. It is observed that along with temperature rise, the cutting force/energy decreases. For instance, the cutting force was 37kN when the cutting was done at 25℃ while a lower force value of 25kN was obtained at 500℃, which shows inverse relationship. It is an established

108

fact increase in the sample temperature increases ductility and decreases strength. When the cutting force decreased in parallel, the edges of the punch expose to lower pressure values, which increases the tool life. Fig.5.17 shows the Von Mises stress distributions on the work-piece material and figures 5.18-5.20 compared the quality of the sheared edge at 25℃, 270℃ and 500℃. It is numerically determined that resulting stresses decrease when the temperature increases. In addition, the cutting-edge quality substantially improves especially at temperatures between 500℃ and 700℃. These results are consistent with those obtained by SEM results showing improved edge quality with expanded shear zone.

It is worth mentioning that heating the specimens in advance increases the tool life and quality of the product; however, that accrues additional cost in terms of energy consumption and manual work-piece handling at high temperature.
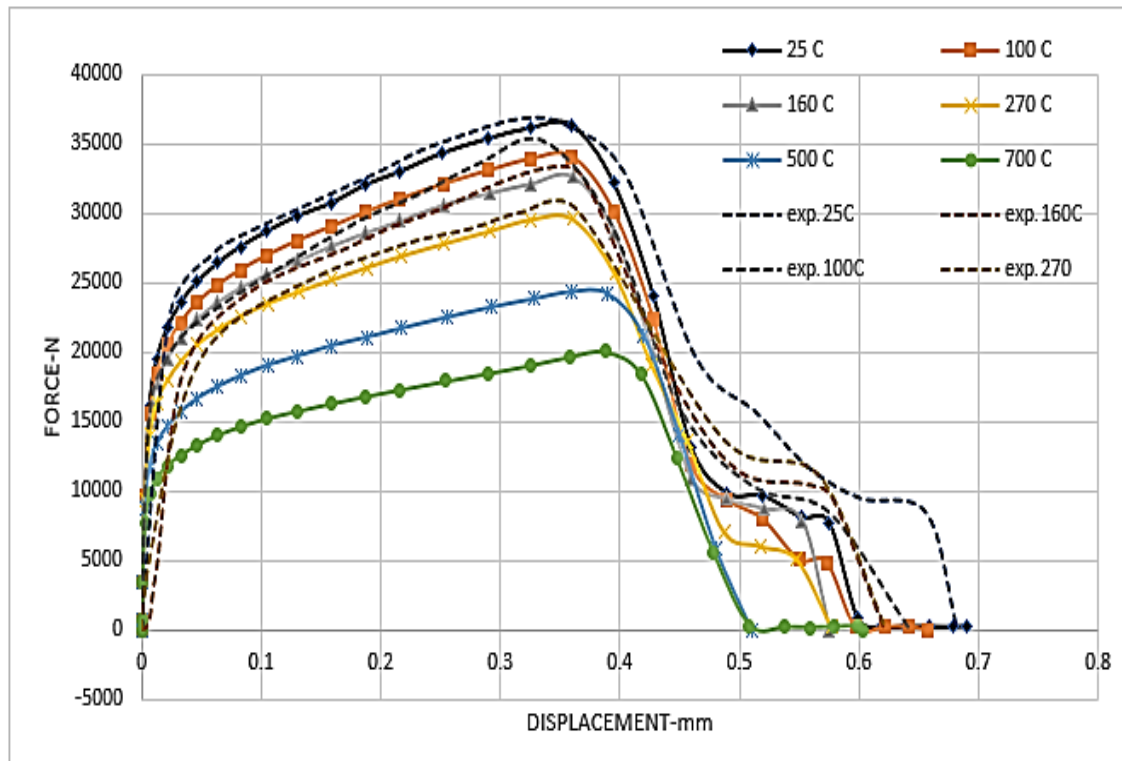
Figure 5.16: Punch load during blanking process at different temperatures.
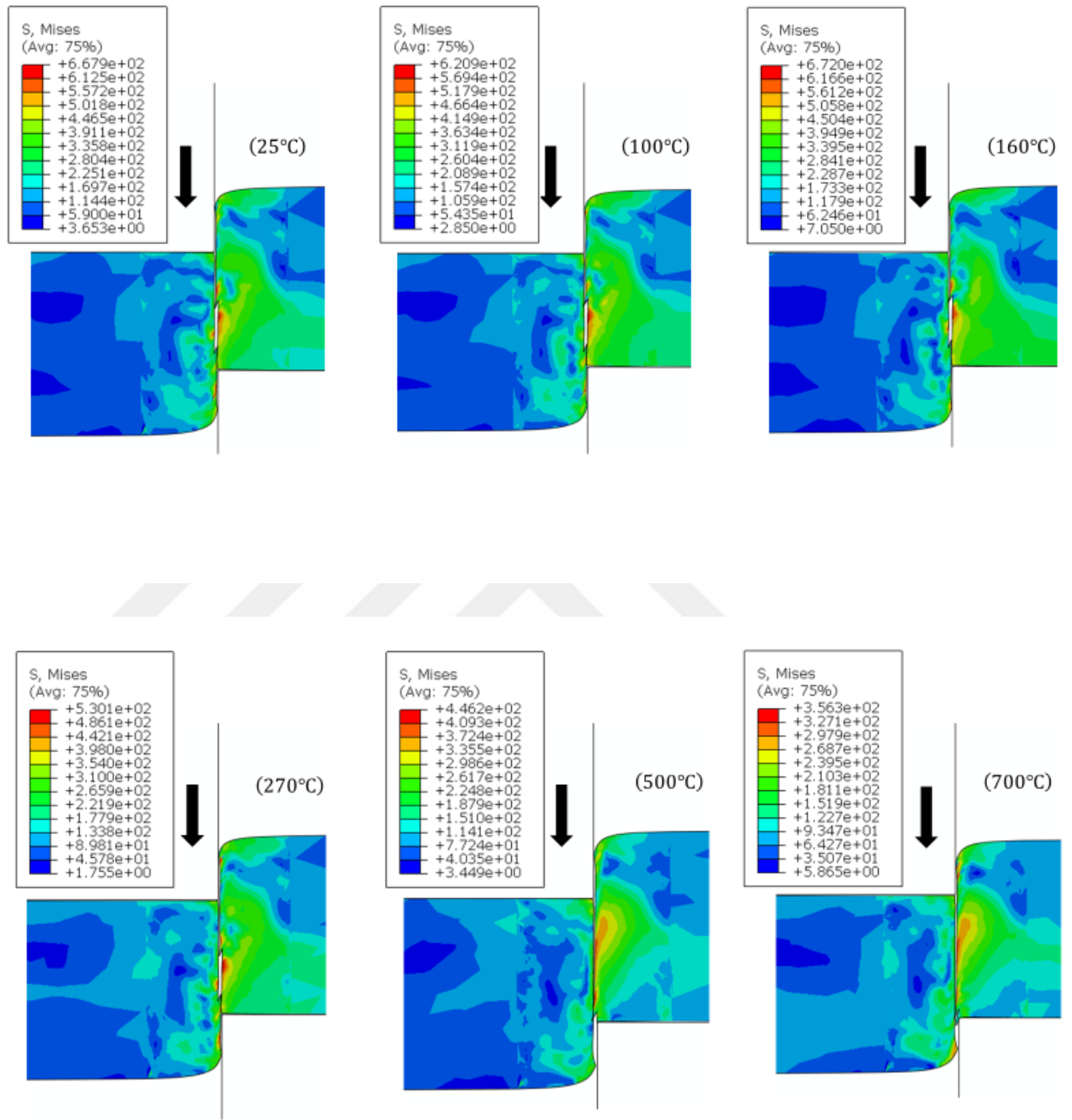
Figure 5.17: Effect of temperature on edges
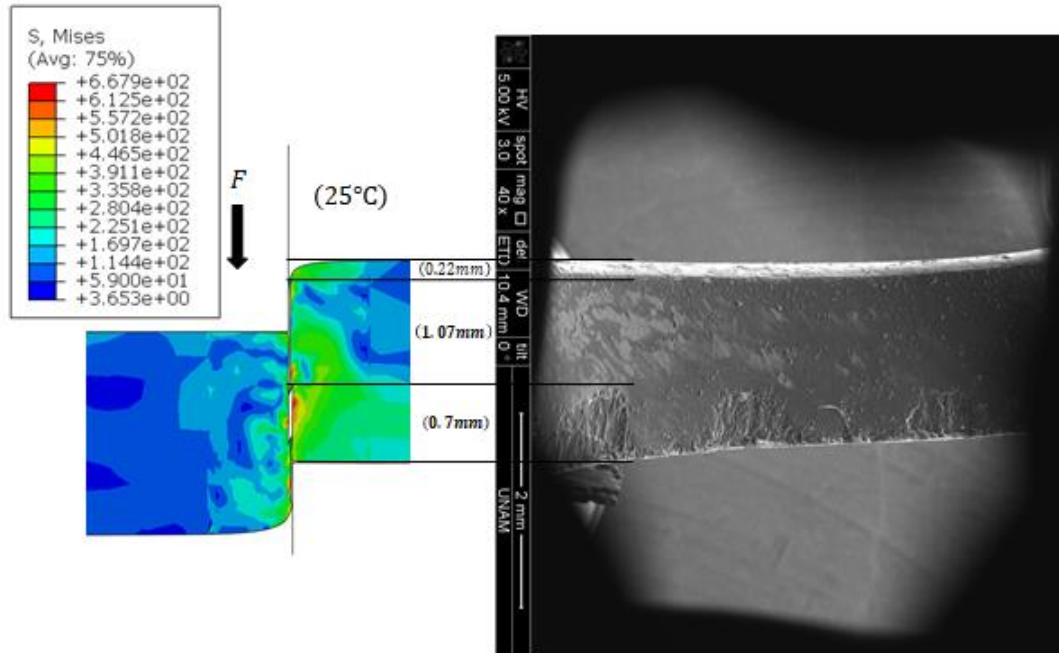
Figure 5.18: Characteristic features of sheared edge while cutting at 25℃ (the process conducted by SEM)
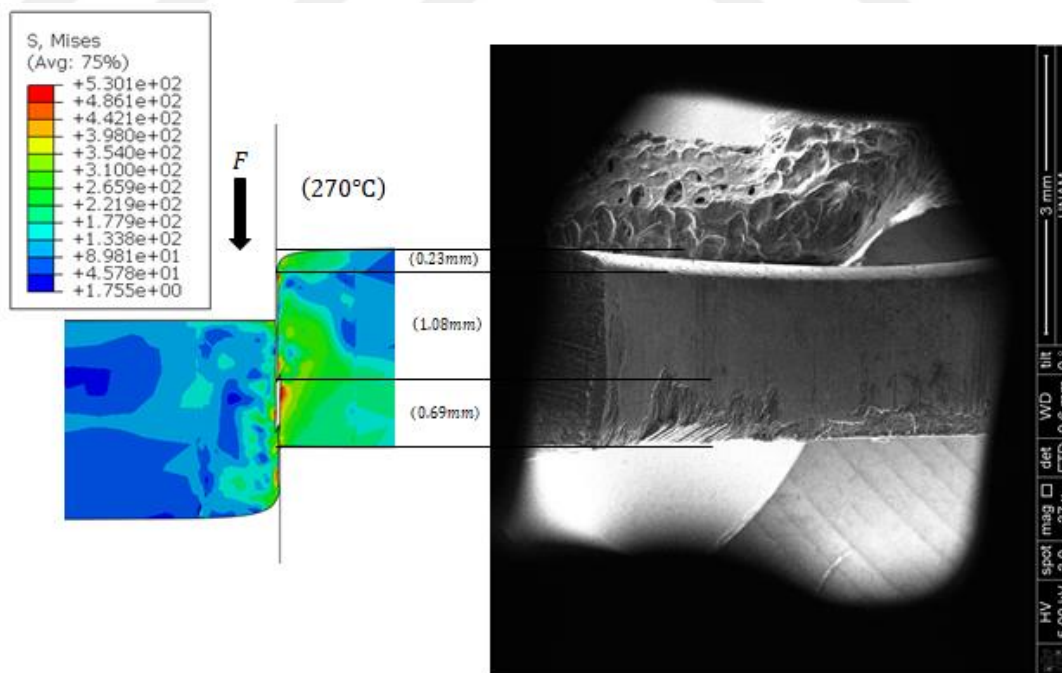
Figure 5.19: Characteristic features of the sheared edge achieved by SEM while cutting at 270℃
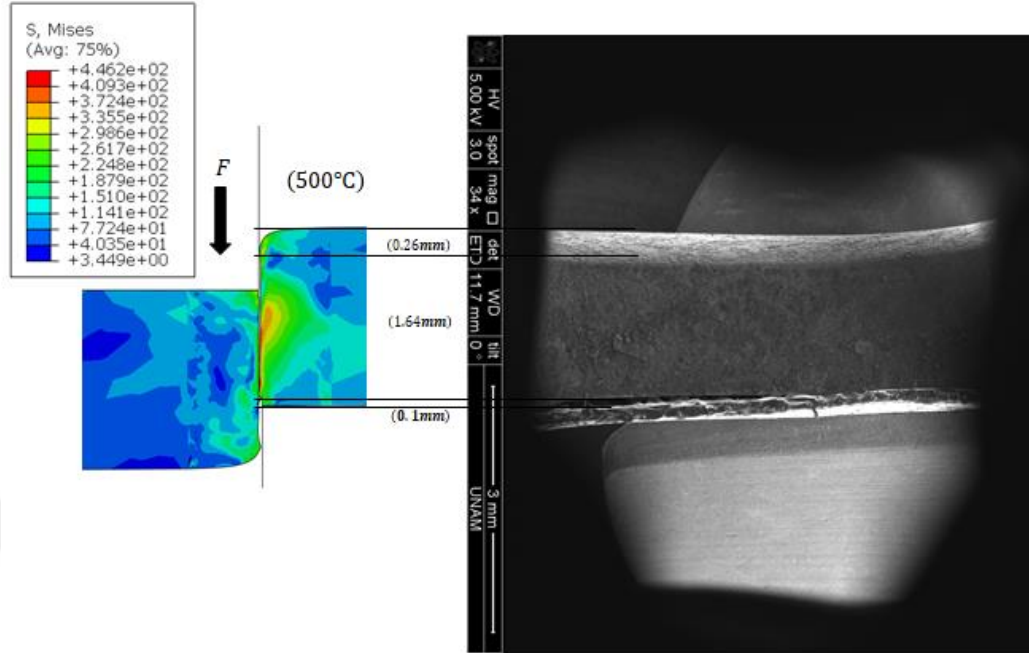
Figure 5.20: Characteristic features of sheared edge achieved by SEM
while cutting at 500℃

Table 5.3: Dimensions of the edges at different temperatures

Zone	25℃	100℃	160℃	270℃	500℃	700℃
Burr	0.08	0.1	0.1	0.11	0.11	0.18
Rollover	0.18	0.2	0.2	0.21	0.26	0.3
shear	1	1.05	1.1	1.1	1.6	1.7
fracture	0.82	0.75	0.7	0.69	0.14	0.1

Fig. 5.21 shows the effect of temperature on the sizes of different areas, when they were measured after the cutting process (summarized in Table 5.3). It is observed that at higher sample temperature, the shear zone significantly increases, and the fracture surface substantially decreases, which proves that the quality of edges is higher. Since the burr and rollover zone increases at more than 600℃ temperature, it results in lower product quality; therefore, approximately 400℃ temperature is considered as optimum.
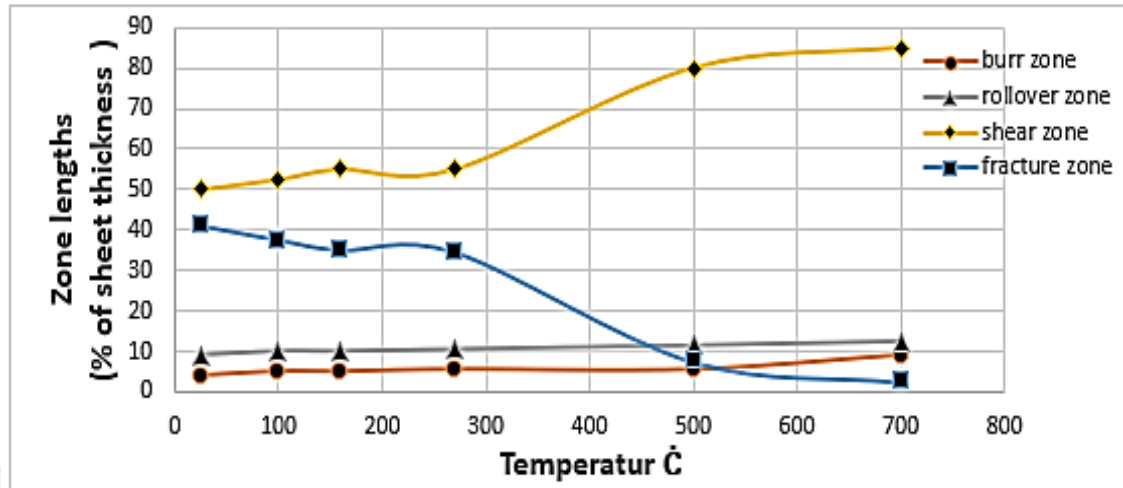
Figure 5.21: Effect of radius on blanked edge zones

5.2.5 PVD Coating of Punches

It is a fact that Physical Vapor Deposition (PVD) hard coating can simultaneously increases the surface hardness (to protect the "cutting" edge) and decreases the frictional forces allowing the punch to withdraw easily, which extends the lifetime of the tool. Optimum tool life is application-specific, and it is possible by selecting the appropriate PVD coating and tool substrate.

It is noticed that significant wear occurs on the side of the punch when it passes and retracts through a metal despite the fact that the punching edge must remain sharp throughout its lifetime. The deflection of the sheet, when it is punched, has a tendency to distort the hole during retraction. This causes the metal surroundings in the hole to scrape against the side of the punch leading to abrasion and wear.

In this part, the impact of coating on the blanking process has been studied. PVD coatings include TiSiN, AlCrN, AlTiN, TiN, and CrN, which are coated by using Balzer's Rapid Coating System (RCS) deposition machine with a thickness of approx. 4µm on the 1.2379 steel cutting tools. It must be kept in mind that the same working conditions should be assured to test different coatings during their tests for clear and realistic understanding of wear resistance. To compare the wear on the tool after different coatings, each tool was used 1000 times for the blanking process using the apparatus mentioned in Section 3. All the tests were carried out

under dry cutting without using any lubrication. A scanning electron microscope (SEM, FEI) was used to observe the microstructures of cross sections and worn out surfaces.

Figure 5.22: Microscopic examination of punches in terms of the wear resistance. (a) TiSiN, (b) AlCrN, (c) AlTiN, (d) TiN, (e) CrN coated punches and (f) uncoated punch.
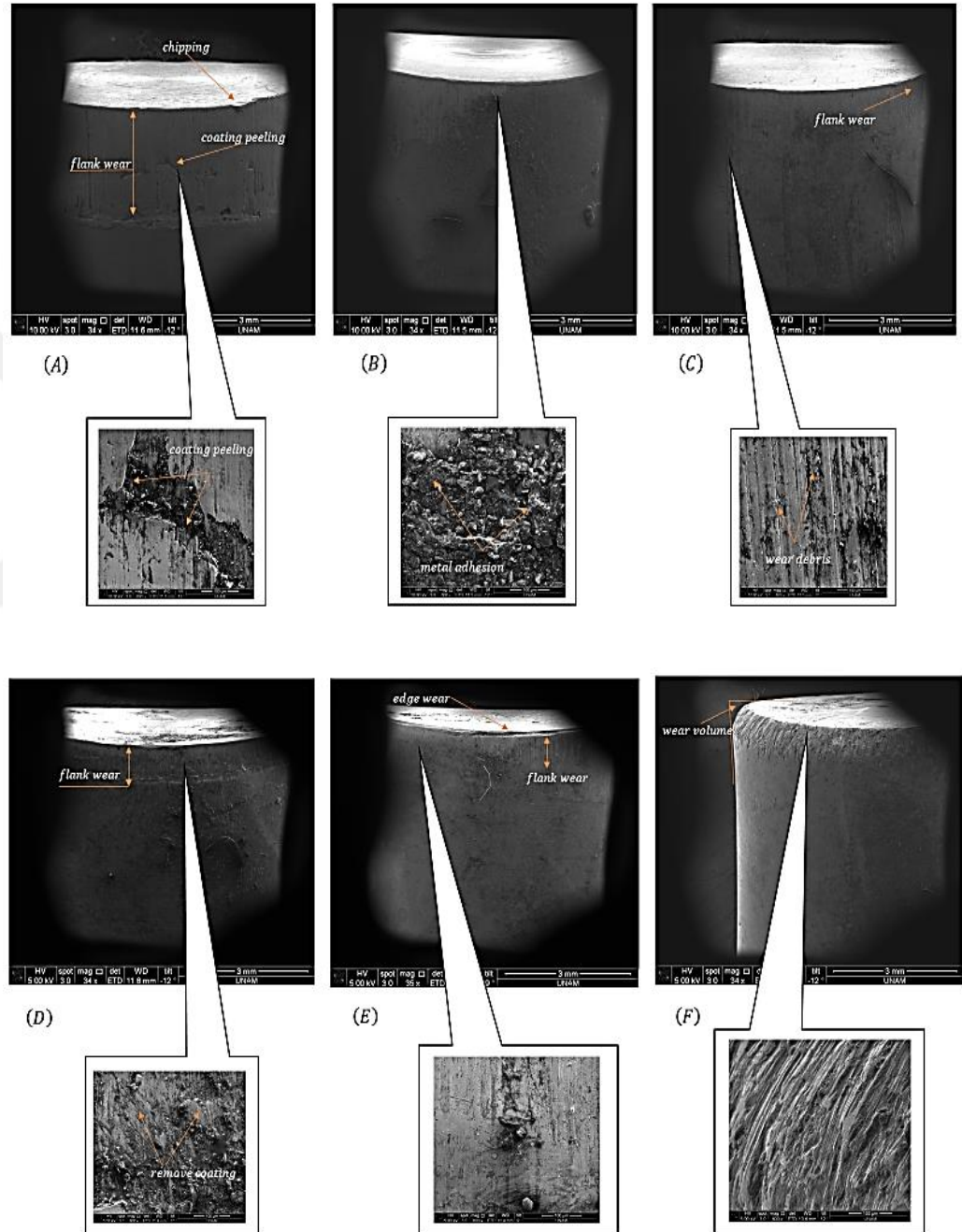
After examining the surfaces of the punches, it is observed that there are different types of wear on the edges with different percentages. In fact, wear evaluation was performed based on the following criteria:

1- Flank Wear
2- Edge wear
3- Face wear
4- Amount of coating removed
5- Amount of coating peeled
6- Metal adhesion

When the TiSiN coating was applied, flank wear, edge wear and peeling in the coating were observed, as shown in Fig 5.22 (a). AlTiN coating was exposed to two types of wear: flank wear and wear debris (see Fig. 5.22 (b)). The coating layer was found damaged in case of TiN coating. For the CrN coating, the damage was substantial, and the ballet was clear on the edges (see Fig.5.22 (e)). It was found that the punch with AlCrN demonstrates the best performance because only a small amount of wear was witnessed on the face of the tool and adhesion of metal exists on its surface.

5.2.6 Impact of friction

The effect of friction has been briefly investigated. The coefficient of friction remained between 0.1 to 0.6 representing the contact between the workpiece and the tool with different coatings. For instance, $\mu = 0.1$, 0.4, 0.5 and 0.55 represent the case with some lubrication, for example, the tools with TiSiN, TiN, CrN coatings. $\mu = 0.6$ represents either AlTiN coating or no coating. Fig.5.23 illustrates the respective force-displacement curves. It is observed that the cutting force does not significantly change for different coatings but when a lubricant is added, a slight decrease in the force value is obtained but lubricated surfaces are not wear-resistant, and besides, lubrication requires extra cost.
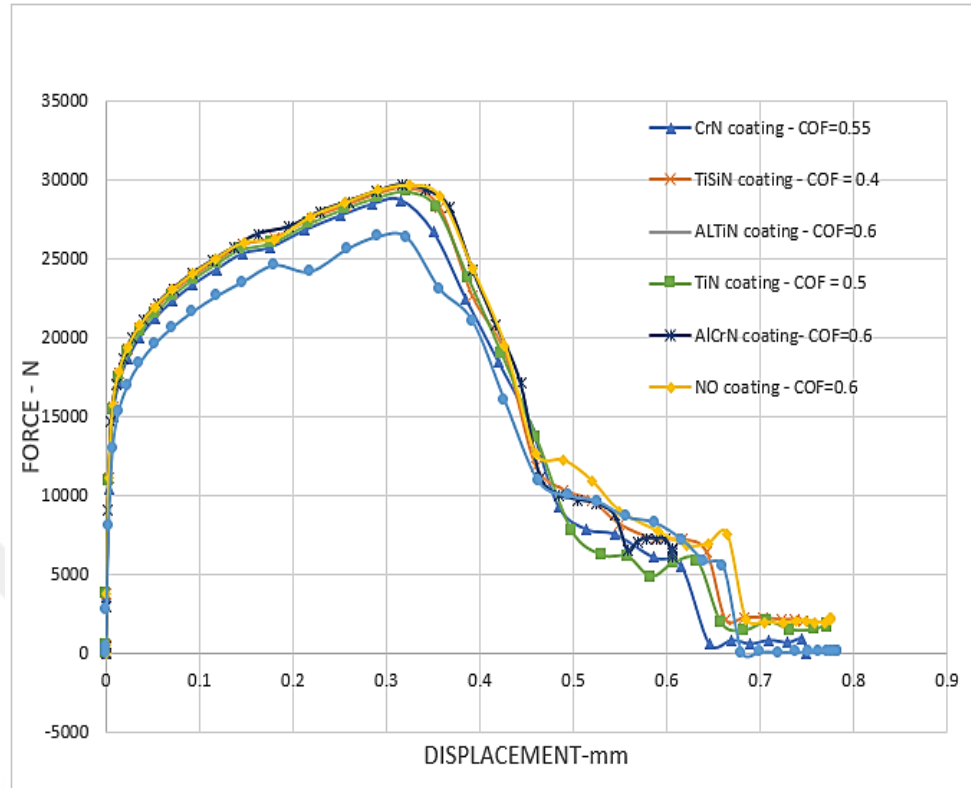
Figure 5.23: Effects of friction on the force

On the other hand, when very low value of friction coefficient such as 0.01 is used, a small increase in the shear edge quality is observed, which is shown in Fig. 5.24. It represents the edge quality for different contact characteristics in terms of the sizes of the rollover, shear and fracture zones. They were obtained from the FE simulations, which are shown in Fig. 5.25. Consequently, the contact condition has no significant effect on the quality of the edges, but it may have an impact on wear resistance, which has been left as a potential topic for a future study.
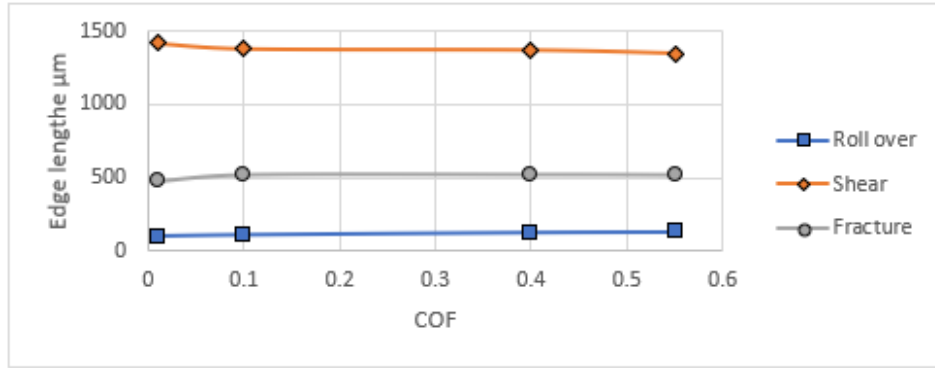
Figure 5.24: The effect of coefficient of friction on part edge quality (obtained using FE analysis)
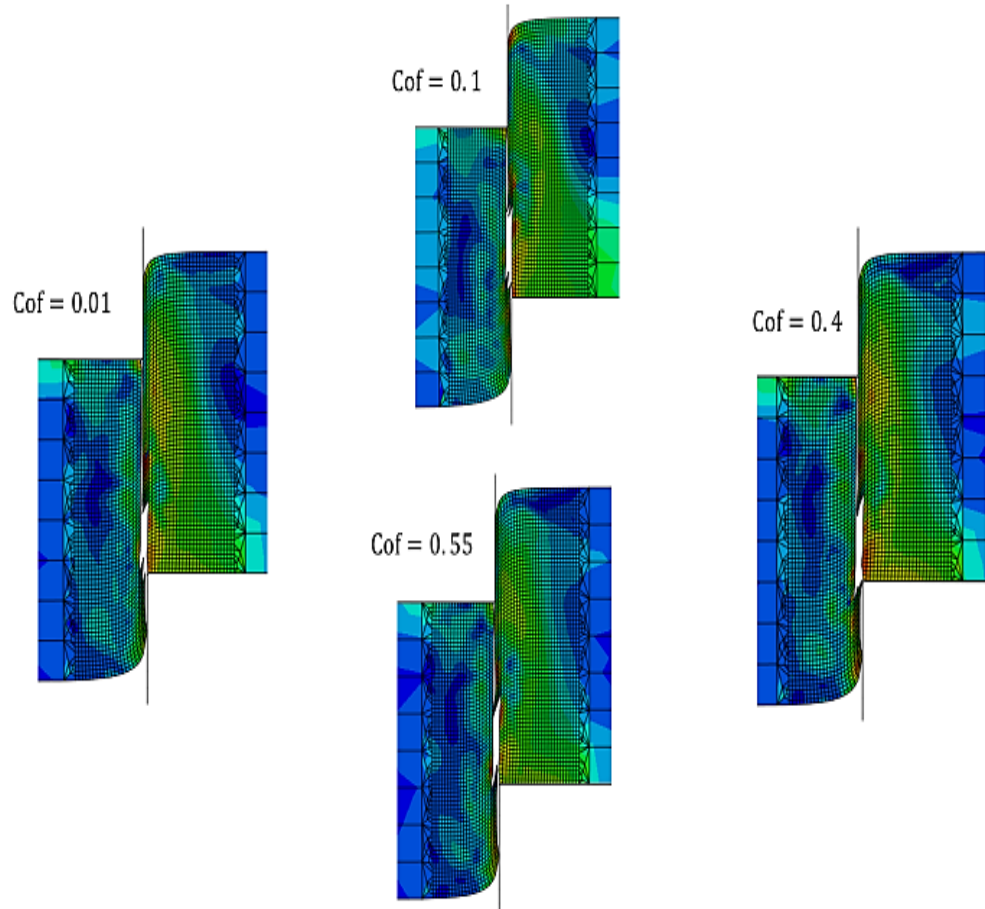
Figure 5.25: Effect of coefficient of friction on the shear edge quality

5.2.7 PDC (Polycrystalline Diamond Compact) punch

Polycrystalline diamond compact (PDC) cutters are widely used in oil and gas drilling operations. Their superior abrasion resistance is the main contributor to their excellent drilling efficiency. These cutters are composed of a layer of polycrystalline diamond bonded in-situ on a tungsten carbide substrate, which is shown in Fig. 5.26. The bonding is applied at a high pressure and high temperature sintering process. The polycrystalline diamond layer is also created during this process to form a sintered material.
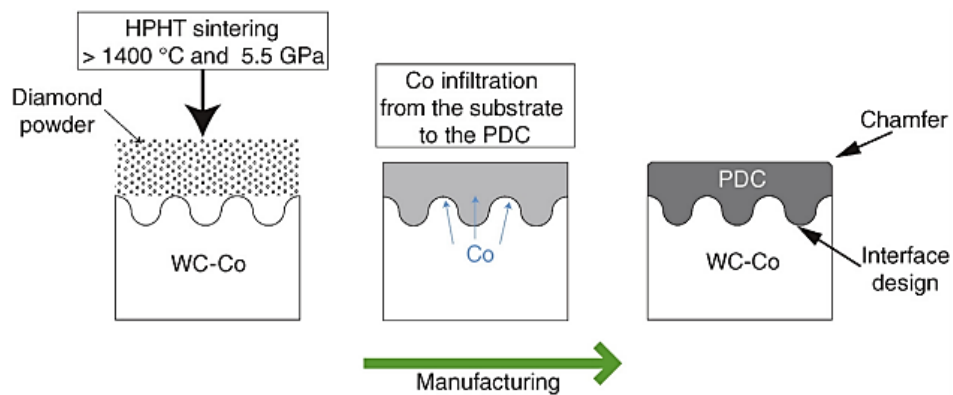
Figure 5.26: Polycrystalline diamond compact (PDC) cutters

The studied cutters have a cylindrical geometrical shape, diameter 13.4 mm and height 10 mm. They are formed by a tungsten carbide–cobalt substrate surmounted by a 2 mm thick PDC component. Manufacturers usually select a specific interface design between the diamond component and the WC–Co component. An optimized interface design is generally more complex than a flat design, and it can efficiently distribute the residual stresses, which emerge between the two materials after manufacturing. For this study, PDC cutters were selected with the same interface design. The conventional cutters were manufactured using a sintered WC–Co substrate. The diamond powder was first put on the substrate and is then sintered at high pressure and high temperature (i.e. HPHT process) over 1400°C and 5.5 GPa. During this step, the diamond grains

formed a dense skeleton and the liquid cobalt infiltrated this microstructure. The amount of cobalt displaced in the PDC part was homogeneous and it is a function of the diamond grain size. This technique is used in this study for the PDC cutter, as shown in Fig. 5.27. The amount of wear was checked on this tool after 1000 cuts with the help of SEM (see Fig. 5.28). In this case, no serious wear was noticed. When its performance was compared with the performance of AlCrN-coated tool, it is demonstrating better performance (see Fig. 5.22), the PDC cutter showed better wear resistance.

An important difference between the use of this technique and any other coating is that even if it develops wear on the tool after high productivity, grinding process on the punch helps extending the tool life. On the contrary, the coated punch gets out of the service after the appearance of the wear on the edges because the grinding process removes the coating; so, it is not feasible.
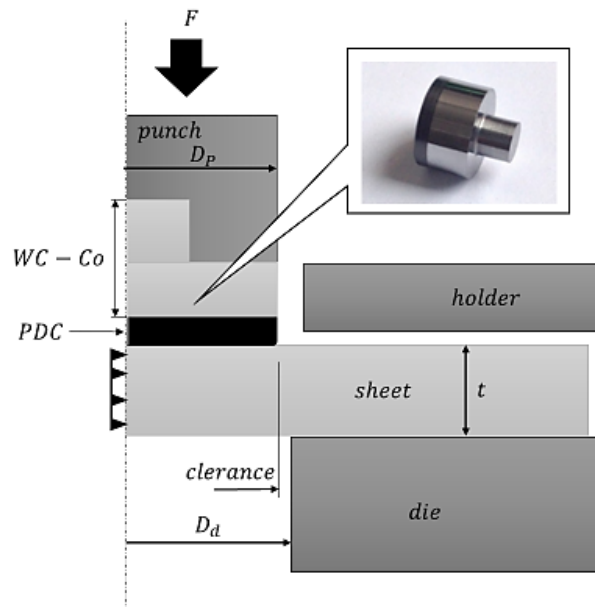
Figure 5.27: Blanking process with PDC punch
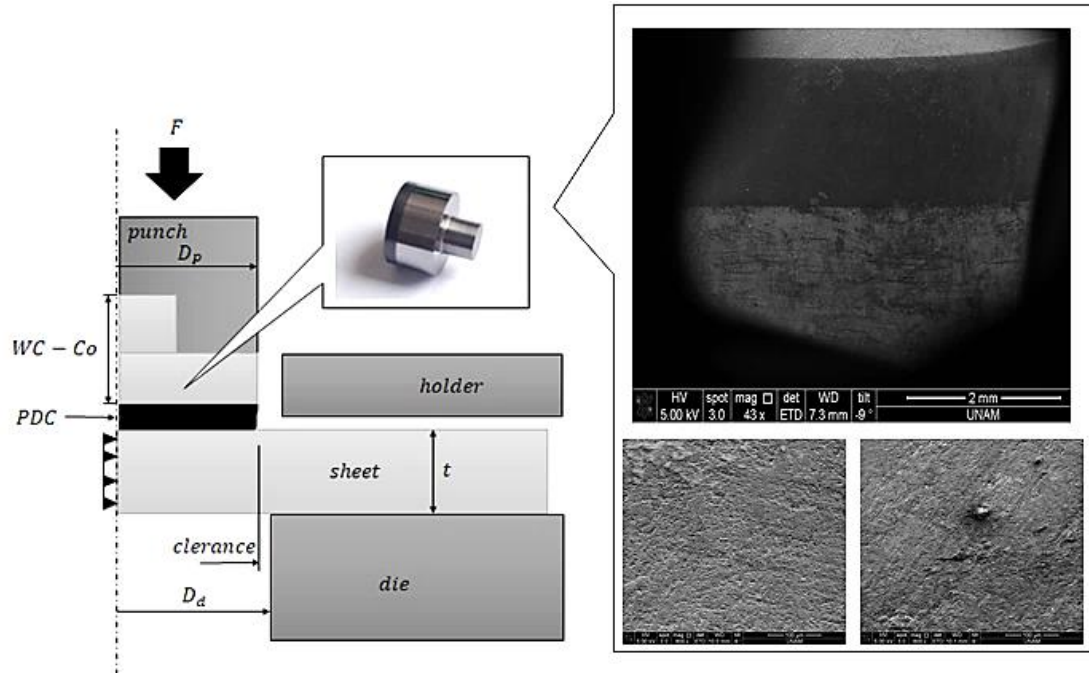
Figure 5.28: SEM micrographs of the top-edge PCD punch

Wear means the progressive loss of material from the surface of a solid body caused by contact. It is the determining factor for predicting the tool´s useful life. It should be minimized in order to maximize tool quality as well as profitability. There are four different wear mechanisms, which determine the wear emergence in active elements of a tool: Adhesion, tribo-chemical reaction, abrasion and surface breakdown. Fig. 5.30 compares the length of flank wear (see Fig. 5.29) on the surface of the tools with different coatings after each one of them was used for cutting 1000 times. The amount of flank wear is highest for uncoated tools and it is minimized with the following coatings: TiSiN, CrN, TiN, AlTiN, AlCrN. It is observed that the flank wear is negligible for a PDC cutter, and hence, it is a good alternative to the blanking process

120
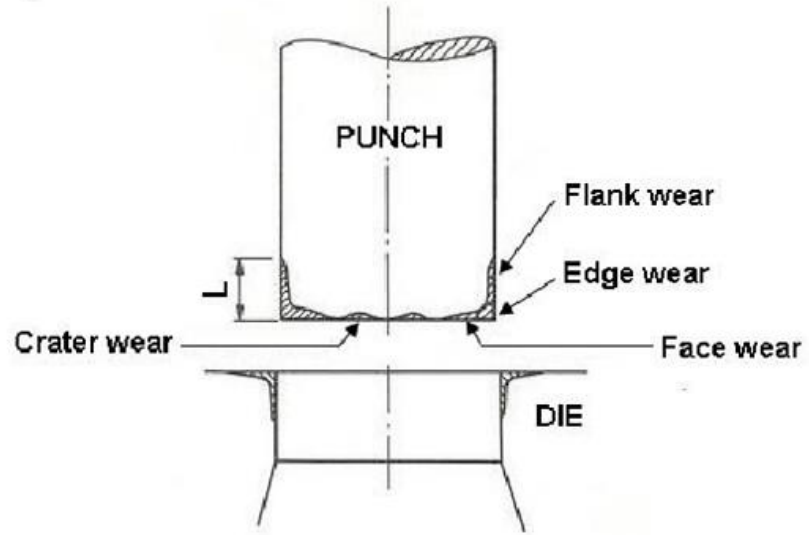
Figure 5.29: Tool wear at blanking process (Shey, 1983)
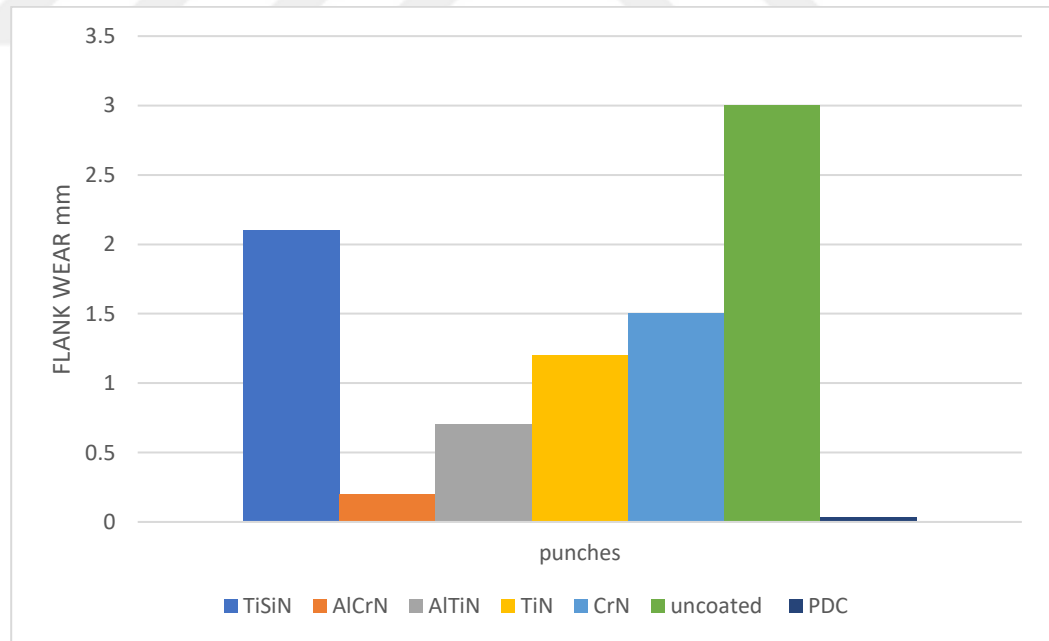
Figure 5.30: Productivity of punches

CONCLUSIONS AND FUTURE WORK

6.1 Conclusion

In this thesis, the blanking process is investigated from various experimental and numerical perspectives. The punch tests were performed at room and elevated temperatures (25, 100, 160 and 270˚C) for 36A steel sheets. The effects of various parameters such as blanking clearance, punch tip geometry including the novel flat face center point punch, corner radius, temperature, type of PVD coating, friction, and Polycrystalline Diamond Compact (PDC) punch on the sheared edge quality and tool wear have been investigated. Scanning Electron Microscopy (SEM) is used for microanalysis of the tool wear and the surface finish of the edges being cut. They are conducted at the Institute of Materials Science and Nanotechnology (UNAM), Bilkent University. 2D and 3D FE models of the blanking process were developed. The Johnson-Cook material model and its complementary damage model were used to represent the sheet material behavior. Moreover, the material constants were taken from the literature. The simulations were performed using commercially available Abaqus/Explicit in a quasi-static manner. A reasonably good agreement between the tests and simulations was obtained.

The following conclusions can be drawn from the experiments and simulations:

- The clearance between punch and the die strongly affects the stress distribution in the sheet material, the amount of resistance the tool exposed to, and the quality of the blanked edge. At less than 5% clearance, a longer shear area and smaller roll-over zone are obtained while 2% clearance is an optimum value.

- The geometry of the tool tip affects the applied load. There were 20% and 40% drops in the cutting force were observed when the single shear and concave shear punches are used respectively. When the novel flat-face center-point punch was used in the process, increase in the energy required and expansion in the rollover zone were observed, which means that it does not provide a promising alternative to the blanking process. A higher punch corner radius improves the tool life due to the fact that the distribution of stresses on the edge of the radius are more

uniform than those of the sharp angle one, which means that it is likely to provide better wear resistance to the tool; however, a higher burr on the edges of the hole was observed. The study also shows that the optimum corner radius of the tool is between 0.01 mm and 0.02 mm.

- With increasing sample temperature, the resulting stresses, the cutting force and the resulting cutting energy decrease. On the other hand, the cutting-edge quality substantially improves when the shear zone significantly increases and the fracture surface decreases; however, it is found that the burr and rollover zone increase at the temperatures above 600°C resulting in a worse product quality. In the nutshell, 400°C may be considered as optimum temperature for the process. On the other hand, the frictional effects remained in significant in the process.

- When the tools were coated with TiSiN, AlCrN, AlTiN, TiN, and CrN, it was observed that AlCrN provides the best wear resistance; however, it was also observed that the wear resistance was minimum when a PDC cutter was used; therefore, it provides a promising alternative to the blanking process.

6.2 Future work

In the future, the blanking process must be extensively investigated in terms of tool wear and surface quality focusing on other important parameters such as punch speed and strain rate effects, and their impact on various tool geometries of the PDC cutter.

REFERENCES

[Anderson, 2005] Anderson, T. L., & Anderson, T. (2005). Fracture mechanics: fundamentals and applications: CRC press. ISBN: 978-1-4200-5821-5.

[Argon, 1975] Argon, A., Im, J., & Safoglu, R. (1975). Cavity formation from inclusions in ductile fracture. Metallurgical Transactions A, 6(4), 825-837.

[Autenrieth, 2009] Autenrieth, H., Schulze, V., Herzig, N., & Meyer, L. W. (2009). Ductile failure model for the description of AISI 1045 behavior under different loading conditions. Mechanics of Time-Dependent Materials, 13(3), 215-231.

[Børvik, 2001] Børvik, T., Hopperstad, O. S., Berstad, T., & Langseth, M. (2001). A computational model of viscoplasticity and ductile damage for impact and penetration. European Journal of Mechanics - A/Solids, 20(5), 685-712.

[Bao, 2004b] Bao, Y., & Wierzbicki, T. (2004b). On fracture locus in the equivalent strain and stress triaxiality space. International Journal of Mechanical Sciences, 46(1), 81-98.

[Bay, 2010] Bay, N., Azushima, A., Groche, P., Ishibashi, I., Merklein, M., Morishita, M., Nakamura, T., Schmid, S., & Yoshida, M. (2010). Environmentally benign tribo-systems for metal forming. CIRP Annals - Manufacturing Technology, 59(2), 760-780.

[Billal, M.K., et al2015]., *Prediction of Component Failure using 'Progressive Damage and Failure Model'and Its Application in Automotive Wheel Design*. 2015, SAE Technical Paper.

[Behrens et al, 2010] Behrens, B.-A., Bouguecha, A., Czora, M., Krimm, R., Matthias, T., & Salfeld, V. Consideration of machine properties in FE analysis of sheet metal forming processes. 2nd INTERNATIONAL CONFERENCE Process Machine Interactions, June 2010, Vancouver.

[Bathe, K.J., 1996], Finite-element procedures, Prentice hall Englewood Cliffs.

[Bell, 2006] Bell, T. Böhler Uddeholm Autosteel Partnership Presentation, 2006.

[Bing & Wallbank, 2008] Bing, G. J. A., & Wallbank, J. (2008). The effect of using a sprung stripper in sheet metal cutting. Journal of Materials Processing Technology, 200(1-3), 176-184.

[Callister, 2007] Callister, W. D., & Rethwisch, D. G. (2007). Materials science and engineering: an introduction (Vol. 7): Wiley New York.

[Cottrell, 2012] Cottrell, A. (2012). Theoretical aspects of fracture. Paper presented at the ICF0, Swampscott-MA (USA) 1959.

[Groche et al, 2007] Groche, P., Großmann, K., Hofmann, T., & Wiemer, H. (2007). Advanced experimental and numerical methods for the analysis of the dynamic forming press behavior. Production Engineering.

[Grünbaum et al, 1996] Influence of high cutting speeds on the quality of blanked parts. Report No. ERC/NSM - S-96-19, Center for Precision Forming, Columbus, OH, USA.

[Huebner, K., Dewhirst, D., Smith, D 2001]., and Byrom, T.,, The finite-element method for engineers.

[Hibbitt, H., B. Karlsson, and P. Sorensen 2016], *Abaqus analysis user's manual V6.16.* Dassault Systèmes Simulia Corp.: Providence, RI, USA.

[Hibbitt, Karlsson, and Sorensen 2016], *ABAQUS: Theory Manual V6.16*.: Hibbitt, Karlsson & Sorensen.

[Huang, Y., 1991], A user-material subroutine incorporating single-crystal-plasticity in the ABAQUS finite-element program: Mech Report, v.

[Hibbitt, Karlsson, and Sorensen 2016], *ABAQUS/Explicit: user's manual V6.16*. Vol. 1.: Hibbitt, Karlsson and Sorenson Incorporated.

[Hernández et al, 2006] Hernández, J. J., Franco, P., Estrems, M., & Faura, F. (2006). Modelling and experimental analysis of the effects of tool wear on form errors in stainless steel blanking. Journal of Materials Processing Technology, 180(1–3), 143-150.

[Husson et al, 2008] Husson, C., Correia, J. P. M., Daridon, L., & Ahzi, S. (2008). Finite elements simulations of thin copper sheets blanking: Study of blanking parameters on sheared edge quality. Journal of Materials Processing Technology, 199(1-3), 74-83.

[Johnson, 1989] Johnson, G., & Holmquist, T. (1989). Test data and computational strength and fracture model constants for 23 materials subjected to large strains, high strain rates, and high temperatures. Los Alamos National Laboratory, Los Alamos, NM, Report No. LA-11463-MS.

[Johnson, 1985] Johnson, G. R., & Cook, W. H. (1985). Fracture characteristics of three metals subjected to various strains, strain rates, temperatures and pressures. Engineering Fracture Mechanics, 21(1), 31-48.

[Jimma et al, 1990] Jimma, T., & Sekine, F. (1990). On high speed precision blanking of IC lead-frames using a progressive die. Journal of Materials Processing Technology, 22(3), 291-305.

[Karelove et al, 2007] Influence of the Edge Conditions on the Hole Expansion Property of Dual-Phase and Complex-Phase Steels by A. Karelova, C. Krempaszky, E. Werner, T. Hebesberger, and A. Pichler.

[Klassen 2011] Klaasen, H., Kübarsepp, J., Tšinjan, A., & Sergejev, F. (2011). Performance of carbide composites in cyclic loading wear conditions. Wear, 271(5–6), 837-841.

[Liu, 2014] Liu, J., Bai, Y., & Xu, C. (2014). Evaluation of ductile fracture models in finite element simulation of metal cutting processes. Journal of Manufacturing Science and Engineering, 136(1), 011010.

[Luo, 1999] Luo, S.Y (1999). Effect of the geometry and the surface treatment of punching tools on the tool life and wear conditions in the piercing of thick steel plate. Journal of Materials Processing Technology, 88(1–3), 122-133.

[Makich et al, 2008] Makich.H., Carpentier.L., Monteil, G., Roizard, X., Chambert, J., Picart, P. (2008). Metrology of the burr amount - correlation with blanking operation parameters (blanked material – wear of the punch). International Journal of Material Forming April 2008, Volume 1, Issue 1 Supplement, pp 1243-1246

[Miles, 2004] Miles, R. (2004). Combating Snapthrough. Metal Forming Magazine, March,2004.

[Mori et al, 2010] Mori, K., Abe, Y., & Suzui, Y. (2010). Improvement of stretch flangeability of ultra-high strength steel sheet by smoothing of sheared edge. Journal of Materials Processing Technology, 210(4), 653-659.

[Felippa, C.A., 2007], Overview of Nonlinear Problems, University of Colorado at Boulder, USA.

[Picas, 2010] Picas, I., Hernández, R., Casellas, D., Valls, I. (2010). Strategies to increase the tool performance in punching operations of UHSS. IDDRG 2010. 325-334

[Podgornik et al 2006] Podgornik, B., S. Hogmark & O. Sandberg. Proper coating selection for improved galling performance of forming tool steel, Wear 261, 15-21 (2006).

[Ralls, 1976] Ralls, K., Courtney, T. H., & Wulff, J. (1976). Introduction to materials science and engineering: John Wiley & Sons, Inc. ISBN: 978-0-471-70665-6

[Rao, S.S., 1999], The finite-element method in Engineering: Butterworth-Heinemann.

[Rooij and Schipper 2001] Rooij, M. B. d. & D.J. Schipper. Analysis of Material Transfer from a Soft Workpiece to a Hard Tool: Part II---Experimental Verification of the Proposed Lump Growth Model, Journal of Tribology 123, 474-478 (2001).

[Sandberg, 2004] Sandberg.O., Johansson, B. (2004). Tool steels for blanking and forming – new developments. Recent Advances in Manufacturing & Use of Tools & Dies and Stamping of Steel Sheets. Pp 53-70

[Schuler Handbook, 1998] Schuler – Metal Forming Handbook, Springer, 1998.

[Straffelini 2010] Straffelini, G., Bizzotto, G., & Zanon, V. (2010). Improving the wear resistance of tools for stamping. Wear, 269(9–10), 693697.

[Thomason, 1998] Thomason, P. (1998). A view of ductile-fracture modelling. Fatigue & Fracture of Engineering Materials & Structures, 21(9), 1105-1122.

[Uddeholm and SSAB 2008] Uddeholm & SSAB. Tooling Solutions for Advanced High Strength Steels, Selection Guidelines, (2008).

[Vaziri, 2010] Vaziri, M., Salimi, M., & Mashayekhi, M. (2010). A new calibration method for ductile fracture models as chip separation criteria in machining. Simulation Modelling Practice and Theory, 18(9), 1286-1296.

[Wiedenmann et al, 2009] Wiedenmann, R., Sartkulvanich, P., & Altan, T. (2009). Finite element analysis on the effect of sheared edge quality in blanking upon hole expansion of advanced high strength steel. IDDRG 2009 International Conference, June 2009.

[Wierzbicki, 2005] Wierzbicki, T., Bao, Y., Lee, Y.-W., & Bai, Y. (2005). Calibration and evaluation of seven fracture models. International Journal of Mechanical Sciences, 47(4–5), 719-743.

[Valentine Kanyanta 2014], Aaron Dormeb, Neal Murphy b, Alojz Invankovic " *Impact fatigue fracture of polycrystalline diamond compact (PDC) cutters and the effect of microstructure.*

[J.J.Hernández2006] . Franco, M. Estrems, F Faura . *Modelling and experimental analysis of the effects of tool wear on form errors in stainless steel blanking.*

[Jiansheng Lia,2017], Wen Yueb, c,∗, Wenbo Qinb, Qingzhong Maoa, Bo Gaoa, Yusheng Lia. *Effect of quenching processes on microstructures and tribological behaviors of polycrystalline diamond compact (PCD/WC-Co) in annealing treatment.*

[Hongli Houa, Huiping Lia2017],, Lianfang Hea, Bingtao *Tangb. Analysis of phase transformation and blanking accuracy of B1500HS steel during hot blanking.*

[Kai Wang · Tomasz Wierzbicki 2015] *Experimental and numerical study on the plane-strain blanking process on an AHSS sheet.*

[Emad Al-Momani, Ibrahim Rawabdeh 2008] *An Application of Finite Element Method and Design of Experiments in the Optimization of Sheet Metal Blanking Process.*

[Ridha Hamblia2000,] , Alain Potironb. *Finite element modeling of sheet-metal blanking operations with experimental varication*

[Sunil Goyal2009], V. Karthik', K.V. Kasiviswanathan, M. Valsan, K. Bhanu Sankara Rao, Baldev Raj. *Finite element analysis of shear punch testing and experimental validation.*

https://www.ionbond.com/coating-services/cutting-tools/

https://www.ionbond.com/coating-services/forming-molding-tools/coating-portfolio/

INDEX

Material No	Designation	
1.2379	DIN	X155CrVMo 121
	AISI	D2
	UNI	X 155 CrVMo121 KU

Resume

Name: Mahmod Saleh Mahmod Gomah

Phone: +218913789873

E-mail: samadmssamad @gmail.com

Date of Birth: 25-5-1974

Marital Status: Married

Address: Bani Waleed University, Bani Waleed / Libya

Nationality: Libyan

Education

- BSc in College of Engneering Tecnology - Janzour -Libya 1997-1998.
- MSc in Faculty of Engineering -Tripoli University 2005-2006.

Language

- Excellent oral and written communication skills in Arabic and good in English.

Personal Profile

- Mechanical and Materials Science
- Professional user in ABAQUS software.
- Professional user in solidworks software.
- Computer literate with experience in Microsoft Office and Windows applications
- Productive independent worker and an effective team player.
- Responsible, resourceful, and reliable.